ISSN 1732-9353
eISSN 2543-7496

# Scientific Review

## Engineering and Environmental Sciences

# Przegląd Naukowy

## Inżynieria i Kształtowanie Środowiska

Vol. 29 (3) 2020 Nr 89

Quarterly – Kwartalnik

SCIENTIFIC REVIEW
**ENGINEERING AND ENVIRONMENTAL SCIENCES**
Kwartalnik / Quarterly



Lista recenzentów jest publikowana w ostatnim numerze danego rocznika i na stronie http://iks_pn.sggw.pl
The list of reviewers is published in the last issue of the volume and on the http://iks_pn.sggw.pl

ADRES REDAKCJI / EDITORIAL OFFICE ADDRESS
Wydział Budownictwa i Inżynierii Środowiska SGGW
ul. Nowoursynowska 159, 02-776 Warszawa
tel. (22) 59 35 248, 59 35 240
email: iks_pn@sggw.edu.pl
http://iks_pn.sggw.pl

ISSN 1732-9353
e-ISSN 2543-7496

Wydawnictwo drukowane jest pierwotną wersją Przeglądu Naukowego Inżynieria i Kształtowanie Środowiska

---

„Przegląd Naukowy Inżynieria i Kształtowanie Środowiska" jest indeksowane w bazach: AGRO(Poznań), Biblioteka Nauki, CrossRef, DOAJ, E-publikacje Nauki Polskiej, Google Scholar, Index Copernicus, INFONA, POL-Index, SCOPUS, SIGŻ(CBR)

# Scientific Review

## Engineering and Environmental Sciences

# Przegląd Naukowy

## Inżynieria i Kształtowanie Środowiska

**Vol. 29 (3) 2020 Nr 89**

## Spis treści
## *Contents*

**PRACE ORYGINALNE**
***Original papers***

Opracowanie redakcyjne – Anna Dołomisiewicz, Krystyna Piotrowska

ISSN 1732-9353 eISSN 2543-7496

Druk: ZAPOL sp.j., al. Piastów 42, 71-062 Szczecin

# PRACE ORYGINALNE
# ORIGINAL PAPERS

Scientific Review – Engineering and Environmental Sciences (2020), 29 (3), 275–288
Sci. Rev. Eng. Env. Sci. (2020), 29 (3)
Przegląd Naukowy – Inżynieria i Kształtowanie Środowiska (2020), 29 (3), 275–288
Prz. Nauk. Inż. Kszt. Środ. (2020), 29 (3)
http://iks.pn.sggw.pl
DOI 10.22630/PNIKS.2020.29.3.23

**Elvis ŽIC[1], Patrik BANKO[1], Luka LEŠNIK[2]**

[1]University of Rijeka, Faculty of Civil Engineering
[2]University of Maribor, Faculty of Mechanical Engineering

# Hydraulic analysis of gate valve using computational fluid dynamics (CFD)

**Key words:** gate valve, hydrodynamic analysis, CFD, Ansys Workbench software package

## Introduction

The water supply network consists of a number of interdependent elements, one of which is a gate valve. They represent machine elements commonly used to control fluid flow because they provide positive seal at high liquid and gas pressures (Fig. 1). They are used in various industries such as refineries, petrochemical plants, power stations, hydroelectric power plants, nuclear power plants, etc. High flow velocities with partial opening of the valve can lead to erosion of its walls, vibrations and noise (Banko, 2019). They are most commonly used for drinking water and wastewater in the temperature range from –20 to +70°C and can withstand flow velocities of up to 5 $m \cdot s^{-1}$ and pressures of up to 16 bar. Their main disadvantage is the large required number of turns of the valve opening/closing handwheel.

During the opening or closing of the gate valves, considerable forces are exerted on the valve construction due to the leakage of the flow. The hydrodynamic forces caused by the high flow velocities under the gate valve result in a vertical force downwards. As the gate valve opens, the velocities increase non-linearly in relation to the degree of opening. Most flow changes occur near the valve at a relatively high flow velocity and cause wear on the valve walls and bearings. High flow velocities in partially opened valves can cause erosion of the valve discs and the bearings themselves, and vibrations can cause damage to the partially opened disc (Quimby, 2007). When the gate valve is lowered to reduce the flow (e.g. by closing), the pressure on the lower surface of the valve decreases due to the high flow velocity,

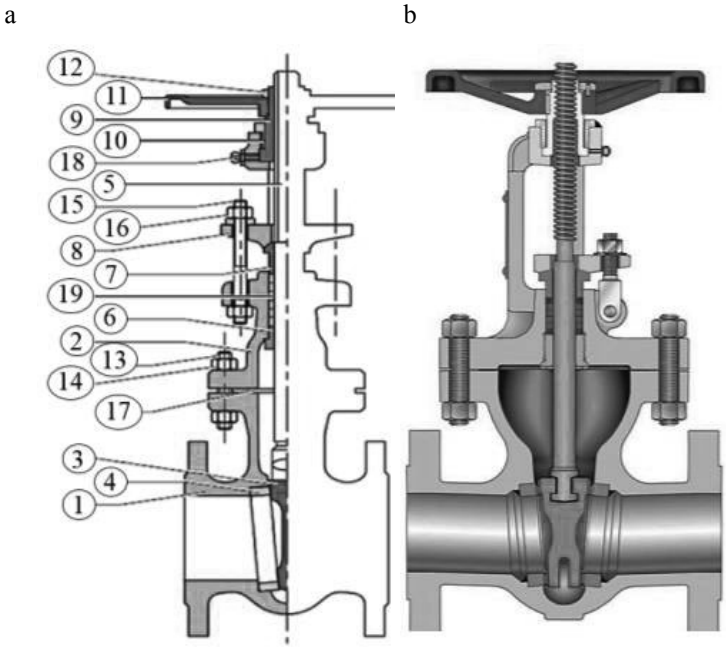


FIGURE 1. Gate valve: a – cross-section (1 – body, 2 – bonnet, 3 – solid wedge, 4 – body seats, 5 – stem, 6 – back seat, 7 – gland follower, 8 – gland flange, 9 – stem nut, 10 – yoke nut, 11 – handwheel, 12 – handwheel nut, 13 – stud bolts, 14 – nuts, 15 – stud bolts, 16 – nuts, 17 – bonnet gasket, 18 – lubricator, 19 – packing); b – model with solid wedge (Banko, 2019)

while the pressure on the upper surface of the valve changes only slightly relative to the static regime. The aim of this paper is to apply computational fluid dynamics (CFD) to gain insights into the physical quantities for gate valve models within a pipe at characteristic opening degrees. By comparing the results of models with different degrees of opening of the gate valve, a more accurate and better quality of the observed pipeline components can be guaranteed.

## Previous research

Numerous studies have been carried out on gate valves, only some of which are listed below. Jatkar and Dhanwe (2013) carry out stress analyses on critical components of gate valves using the FEA technique. The modelling of valve components was performed in the CATIA V5R17 software and analysed with the FEM method in the ANSYS--11 software. The validation of the software results is analytically supported by a stress analysis using the classical theory of solid mechanics. Patil and Gambhire (2014) provide a basic methodology for the design of gate valve bodies using a CAD technology where structural FEM analysis is applied at maximum operating pressure. The work involved static, dynamic, thermal, harmonic and electromagnetic analyses on a valve using CATIA and Ansys Fluent software. The work of Wang (2014) is based on the CAD/CAE

system. The influence of factors such as fluid flow, flow velocity, wall thickness of the valve body and transverse installation was investigated in the paper. Pujari and Joshi (2016) carried out the analysis and optimization of the design of gate valve bodies using the FEA technique and stress analysis. Katkar, Kulkarni, Patil and Katkar (2017) analysed the critical components of a gate valve. The paper gives a detailed overview of the different techniques used in the design of gate valves (developed in CATIA software) and the analysis in the ANSYS Workbench software package using the FEM technique.

## Application of numerical models

For the calculation and hydraulic analysis in this paper the Ansys CFX 19.1 and Ansys Fluent 19.1 software within the Ansys Workbench software package was used (Ansys CFX 15.0, 2015, Žic, 2019). The following part describes the design of a numerical model of a gate valve using the Ansys CFX 19.1 software and the definition of the water supply pipe and the valve around which the fluid flows. The water supply pipe and the 3D geometric model of the gate valve were created in the AutoCAD 2016 software for a starting position of 20% pipe closure. The water supply pipe has a diameter of 100 mm, while the thickness of the pipe and valve flange is 1 mm. Defining and importing the pipe system geometry is done in the SpaceClaim and DesignModeler software packages within the software Ansys Workbench package (Banko, 2019). For the initial model with a 20% of the valve opening a pipe length of 820 mm was taken (300 mm in front of the valve and 520 mm behind the valve), because the changes are larger and longer in the span behind the gate valve. The DesignModeler software was used to generate the network model of the gate valve. After mesh generation, it is necessary to check the quality of the numerical mesh to ensure that a meaningful result is obtained during processing (Žic, 2019). It is also necessary to define all the contour elements of the future model (e.g. inlet and outlet profile, pipe walls, valve, etc.). The network consists of 101,205 nodes and 502,984 elements. In addition to checking the quality of the numerical grid, the quality of the elements was also checked by checking the aspect ratios for the triangle, prism and tetrahedron, the Jacobian ratio or "Jacobian", the twist factor, the characteristic length of the element, etc. For processing, it is necessary to define physical parameters for a given numerical model/submodel, including the definition of the input variables and their values, the definition of a model type, the definition of the dynamic and kinematic viscosity and the initial and boundary conditions. A single-phase problem is selected, which means that only one fluid is defined in the problem (water at 25°C). For the hydrodynamic analysis, a stationary flow regime with a reference pressure of 101,325 Pa without heat transfer within the model and the so-called $k$–ε turbulence model with standard wall function was chosen. The first variable ($k$) represents the turbulent kinetic energy and the second transport variable ($\varepsilon$) refers to the dissipation rate of the turbulent kinetic energy. The transport equation for $k$ is

described by the expression (1) and the transport equation for $\varepsilon$ by the expression (2) (Ansys CFX 15.0, 2015):

$$\rho\frac{Dk}{Dt}=\mu_t\left(\frac{\partial U_j}{\partial x_i}+\frac{\partial U_i}{\partial x_j}\right)\frac{\partial U_j}{\partial x_i}+ +\frac{\partial}{\partial x_i}\left\{(\mu+\mu_t/\sigma_k)\frac{\partial k}{\partial x_i}\right\}-\rho\varepsilon+G_b-Y_M+S_k \quad (1)$$

$$\rho\frac{D\varepsilon}{Dt}=C_{1\varepsilon}\left(\frac{\varepsilon}{k}\right)\left[\mu_t\left(\frac{\partial U_j}{\partial x_i}+\frac{\partial U_i}{\partial x_j}\right)\frac{\partial U_j}{\partial x_i}+C_{3\varepsilon}G_b\right]+ +\frac{\partial}{\partial x_i}\left\{(\mu+\mu_t/\sigma_\varepsilon)\frac{\partial \varepsilon}{\partial x_i}\right\}-C_{2\varepsilon}\rho\left(\frac{\varepsilon^2}{k}\right)+S_\varepsilon \quad (2)$$

The turbulent viscosity $\mu_t$ is defined by the expression $\mu_t=\rho C_\mu\frac{k^2}{\varepsilon}$ where $\rho$ is the density of the liquid. The velocities $U_i$ and $U_j$ define the velocities in the longitudinal and transverse cross section of the flow. The coefficients $\sigma_k$, $\sigma_b$, $C_{1\varepsilon}$, $C_{2\varepsilon}$, $C_{3\varepsilon}$ and $C_\mu$ are the empirically defined constants. With the marks $G_b$, $Y_M$, $S_k$ and $S_\varepsilon$ within the expressions (1) and (2) are presented the values of the variables with which we can model the turbulence. The compressibility effects are denoted by $Y_M$, the buoyancy force by $G_b$ and user-defined sources by $S_k$ and $S_\varepsilon$. The compressibility effects are mainly due to large changes in the properties and characteristics of the fluid. Their influence is described by the coefficients $\beta_c$ and $\beta^*_c$ as a function of the Mach number by the following expressions (Decaix & Goncalvès da Silva, 2013):

$$\beta_c^*=\beta^*(1+\xi^*F(M_t)) \quad (3)$$

$$\beta_c=\beta-\beta^*\xi^*F(M_t) \quad (4)$$

$$F(M_t)=(M_t^2-M_{t0}^2)H(M_t-M_{t0}) \quad (5)$$

for the values $M_{t0}$ = 0.25 and $\xi^*$ = 1.5. An initial inlet flow velocity of 1.0 m·s$^{-1}$ is defined for the inlet profile on the surface of the entire inlet profile, while a relative pressure of 0 Pa is defined on the outlet profile. This means that at the last profile of the water supply pipe the pressure is equal to the pressure outside the pipe (atmospheric pressure). In the post-processing part of the numerical modelling, arbitrary transverse and longitudinal profiles are selected, on the basis of which changes of certain physical quantities within the obtained model can be represented. The gate valve was analysed by four positions: 20, 40, 60 and 80% of the valve closed. For each of these submodels a hydrodynamic analysis of the fluid flow around the valve at an inflow velocity of 1.0 and 1.5 m·s$^{-1}$ was performed.

## Hydrodynamic analysis and research results

The processed variants were compared for each physical quantity, namely flow velocity ($v$), relative pressure ($p$) and turbulence kinetic energy ($k$). Each of the physical quantities is calculated using the same eight transverse (Fig. 2) and nine longitudinal profiles. The transverse profiles are arranged in such a way that the first one is halfway between the start of the pipe and the valve, the second one directly in front of the valve, the fourth profile runs through the middle of the valve, the next three profiles are di-

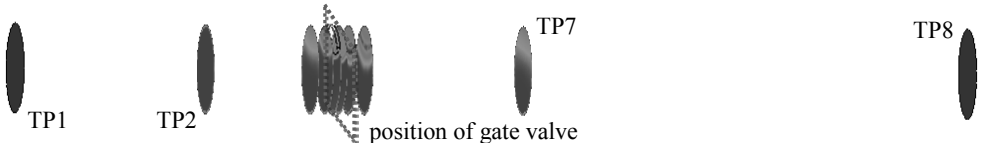


FIGURE 2. Arrangement of the transverse profiles (TP) in relation to the gate valve

rectly behind the valve and the last one halfway between the valve and the end of the pipe. The longitudinal profiles are positioned so that the middle fifth profile is in the middle of the pipe and the four longitudinal profiles are symmetrically arranged at equal distances on both sides.

## Fluid flow velocity

Figure 3 shows a longitudinal view of the gate valve model at various degrees of opening based on the 150 streamlines. The first four models show models with an inlet velocity of 1.0 $m \cdot s^{-1}$ and the last four models with an inlet velocity of 1.5 $m \cdot s^{-1}$.

The figure shows that a vortex flow is observed in the area behind the gate valve at 80% closure, which is a consequence of the abrupt narrowing of the flow cross-section under the valve, which also causes the greatest increase in flow velocity (red colour in Fig. 3). The streamlines of each model are shown at local values, i.e. the colours are not universal and are not the same on each of the models, therefore the flow velocities on the model cannot be compared with each other depending on the colour tones, but only individually (the legends given in Fig. 3 refer to a gate valve with a

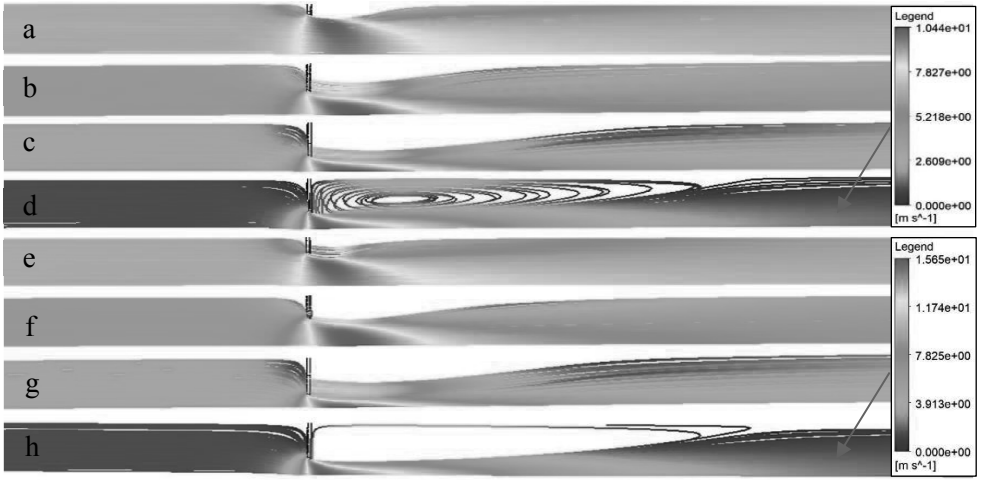


FIGURE 3. Model view of gate valves with streamlines: a – model with 20% gate closure (inlet velocity $v$ = 1 $m \cdot s^{-1}$); b – 40% closure ($v$ = 1 $m \cdot s^{-1}$); c – 60% closure ($v$ = 1 $m \cdot s^{-1}$); d – 80% closure ($v$ = 1 $m \cdot s^{-1}$); e – 20% closure ($v$ = 1.5 $m \cdot s^{-1}$); f – 40% closure ($v$ = 1.5 $m \cdot s^{-1}$); g – 60% closure ($v$ = 1.5 $m \cdot s^{-1}$); h – 80% closure ($v$ = 1.5 $m \cdot s^{-1}$)

valve closing degree of 80% at velocities of 1.0 and 1.5 m·s$^{-1}$). The maximum, minimum and average values of flow velocities for each of the submodels and both inlet flow velocities are shown in Table 1. The average and maximum flow velocities within the model increase exponentially as a function of the percentage closure of the gate valve. The increment percentages coincide with the second decimal place and are 115.5% from 20 to 40% closed, 133% from 40 to 60% closed and 175% from 60 to 80% closed valve for the average values. The percentages for increasing the maximum values of the flow velocities are in the same order: 162, 175 and 240%. Table 2 shows the maximum (bold values) and average values of flow velocities for all positions of valve closure with inlet velocities of 1.0 and 1.5 m·s$^{-1}$ up to eight transverse profiles (Fig. 2). The positions of the largest maximum and average flow velocity values vary depending on the percentage of valve closure.

velocity of 1.0 m·s$^{-1}$ the average valve flow velocity is 1.03 m·s$^{-1}$, for models with 40% closure 1.40 m·s$^{-1}$, with 60% closure 2.39 m·s$^{-1}$ and with 80% closure the value is 6.50 m·s$^{-1}$. The maximum flow velocity of 10.4 m·s$^{-1}$ occurs at the fifth profile (directly behind the valve) for models with an inlet velocity of 1.0 m·s$^{-1}$ and 15.6 m·s$^{-1}$ for models with an inlet velocity of 1.5 m·s$^{-1}$. Maximum flow velocities with lower valve closure occur at a greater distance behind the valve, while models with a higher valve closing percentage have maximum values of flow velocity closer to the valve due to the abrupt narrowing of the flow area. The nine longitudinal profiles are defined at regular intervals, starting from the centre of the pipe towards the edges (the centre of the fifth profile intersects the centre of the valve, seen perpendicular to the valve). They show most clearly the change in flow velocity along the pipe and the transient flow velocity from the beginning of the pipe system through

TABLE 1. View of the maximum, minimum and average values of the flow velocities [m·s$^{-1}$] for each of the gate valve models

| Percentage of gate valve closure [%] | $v$ = 1.0 m·s$^{-1}$ | | | $v$ = 1.5 m·s$^{-1}$ | | |
|---|---|---|---|---|---|---|
| | max | min | avg | max | min | avg |
| 20 | 1.564 | 0.007 | 1.035 | 2.337 | 0.021 | 1.553 |
| 40 | 2.533 | 0.003 | 1.195 | 3.797 | 0.004 | 1.795 |
| 60 | 4.415 | 0.004 | 1.594 | 6.633 | 0.003 | 2.390 |
| 80 | 10.585 | 0.002 | 2.780 | 15.884 | 0.004 | 4.220 |

It is also noticeable that the values of maximum and average flow velocities for all profiles in the immediate vicinity of the valve increase exponentially with the percentage of closure. For models with 20% closure and an inlet flow

the valve to the recovery of the flow velocity at a certain distance behind the valve. Table 3 shows the maximum and average flow velocities for all positions of valve closure with inlet velocities of 1.0 and 1.5 m·s$^{-1}$ for nine randomly selected

TABLE 2. View of the maximum and average values of the flow velocities [m·s$^{-1}$] at a gate valve on the corresponding transverse profiles

| Cross section profile | 20% valve closure | | 40% valve closure | | 60% valve closure | | 80% valve closure | |
|---|---|---|---|---|---|---|---|---|
| | max | avg | max | avg | max | avg | max | avg |
| 1 | 1.03 | 1.00 | 1.03 | 0.99 | 1.03 | 0.99 | 1.03 | 0.99 |
| 2 | 1.15 | 0.99 | 1.37 | 1.02 | 1.72 | 1.08 | 2.34 | 1.14 |
| 3 | 1.29 | 1.01 | 1.77 | 1.25 | 2.76 | 1.64 | 5.99 | 2.40 |
| 4 | 1.45 | 1.03 | 2.13 | 1.40 | 3.75 | **2.39** | 9.93 | **6.49** |
| 5 | 1.53 | 1.02 | 2.28 | 1.20 | 4.03 | 1.59 | **10.40** | 2.68 |
| 6 | **1.56** | **1.17** | 2.43 | 1.40 | 4.26 | 1.80 | 10.34 | 2.62 |
| 7 | 1.51 | 1.16 | **2.53** | **1.57** | **4.41** | 1.97 | 9.84 | 2.81 |
| 8 | 1.16 | 0.98 | 1.59 | 0.97 | 2.51 | 1.14 | 4.78 | 2.04 |
| Cross section profile | 20% valve closure | | 40% valve closure | | 60% valve closure | | 80% valve closure | |
| | max | avg | max | avg | max | avg | max | avg |
| 1 | 1.54 | 1.49 | 1.54 | 1.48 | 1.54 | 1.48 | 1.54 | 1.48 |
| 2 | 1.73 | 1.49 | 2.05 | 1.54 | 2.59 | 1.62 | 3.51 | 1.72 |
| 3 | 1.92 | 1.51 | 2.64 | 1.87 | 4.13 | 2.46 | 8.99 | 3.60 |
| 4 | 2.17 | 1.54 | 3.20 | 2.10 | 5.63 | **3.58** | 14.91 | **9.75** |
| 5 | 2.28 | 1.51 | 3.43 | 1.80 | 6.04 | 2.39 | **15.59** | 4.02 |
| 6 | **2.34** | **1.73** | 3.65 | 2.12 | 6.39 | 2.71 | 15.50 | 3.93 |
| 7 | 2.26 | 1.72 | **3.79** | **2.37** | **6.63** | 2.96 | 14.76 | 4.22 |
| 8 | 1.74 | 1.48 | 2.39 | 1.46 | 3.79 | 1.71 | 7.14 | 3.02 |

longitudinal profiles. The maximum average flow velocities on the defined longitudinal profiles are 1.79 m·s$^{-1}$ for the model with an inflow velocity of 1.0 and 2.67 m·s$^{-1}$ for the model with an inflow velocity of 1.5 m·s$^{-1}$. Figure 4a shows

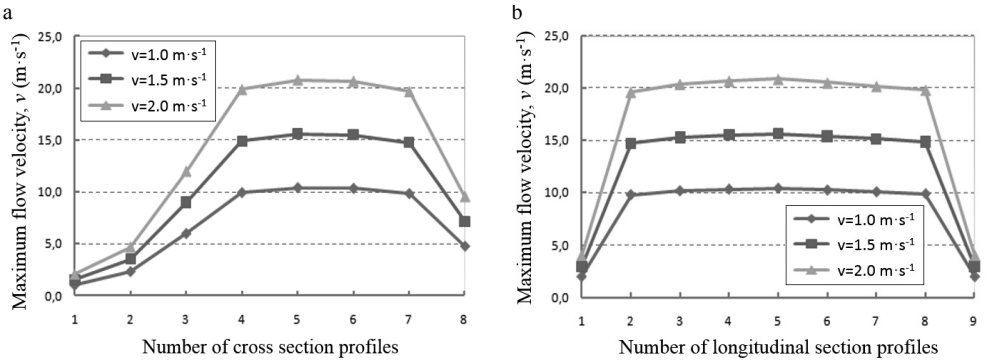


FIGURE 4. Graphical view of the maximum flow velocities for a gate valve model with 80% closure based on transverse profiles (a) and longitudinal profiles (b)

TABLE 3. View of the maximum and average values of flow velocities [m·s$^{-1}$] at a gate valve at the corresponding longitudinal profiles

| Longitudinal profile | 20% valve closure | | 40% valve closure | | 60% valve closure | | 80% valve closure | |
|---|---|---|---|---|---|---|---|---|
| | max | avg | max | avg | max | avg | max | avg |
| 1 | 1.561 | 1.015 | 2.378 | 1.019 | 3.806 | 0.994 | 2.021 | 0.976 |
| 2 | 1.559 | 1.002 | 2.522 | 1.027 | 4.160 | 1.110 | 9.816 | 1.325 |
| 3 | 1.549 | 0.982 | **2.532** | 1.040 | 4.356 | 1.195 | 10.198 | 1.635 |
| 4 | 1.551 | 0.981 | 2.529 | 1.042 | 4.383 | 1.208 | 10.347 | 1.702 |
| 5 | 1.549 | 0.981 | 2.529 | **1.052** | **4.413** | **1.243** | **10.437** | **1.787** |
| 6 | 1.545 | 0.981 | 2.528 | 1.044 | 4.390 | 1.213 | 10.264 | 1.700 |
| 7 | 1.547 | 0.986 | 1.527 | 1.035 | 4.333 | 1.182 | 10.098 | 1.566 |
| 8 | 1.553 | 1.002 | 2.521 | 1.027 | 4.160 | 1.116 | 9.911 | 1.337 |
| 9 | **1.563** | **1.016** | 2.405 | 1.026 | 3.946 | 0.997 | 2.022 | 0.971 |
| Longitudinal profile | 20% valve closure | | 40% valve closure | | 60% valve closure | | 80% valve closure | |
| | max | avg | max | avg | max | avg | max | avg |
| 1 | 2.333 | 1.529 | 3.584 | 1.541 | 5.712 | 1.497 | 2.963 | 1.453 |
| 2 | 2.326 | 1.505 | 3.787 | 1.546 | 6.245 | 1.668 | 14.730 | 1.970 |
| 3 | 2.309 | 1.472 | **3.796** | 1.562 | 6.540 | 1.793 | 15.295 | 2.438 |
| 4 | 2.311 | 1.470 | 3.793 | 1.565 | 6.582 | 1.813 | 15.517 | 2.541 |
| 5 | 2.308 | 1.469 | 3.788 | **1.578** | **6.627** | **1.864** | **15.650** | **2.670** |
| 6 | 2.302 | 1.470 | 3.792 | 1.565 | 6.592 | 1.819 | 15.390 | 2.541 |
| 7 | 2.306 | 1.479 | 3.792 | 1.553 | 6.506 | 1.773 | 15.146 | 2.339 |
| 8 | 2.318 | 1.506 | 3.788 | 1.542 | 6.248 | 1.674 | 14.871 | 1.998 |
| 9 | **2.336** | **1.530** | 3.617 | 1.539 | 5.918 | 1.498 | 2.987 | 1.456 |

a graphical representation of the flow velocities for a gate valve model with 80% closure at an inflow velocity of 2.0 m·s$^{-1}$, compared with the same model with an inflow velocity of 1.0 and 1.5 m·s$^{-1}$. The maximum velocity value on the fifth profile at an inlet velocity of 2.0 m·s$^{-1}$ is 20.80 m·s$^{-1}$. Figure 4b shows the values of maximum flow velocities per longitudinal profile for the model with 80% valve closure for inlet velocities of 1.0, 1.5 and 2.0 m·s$^{-1}$.

## Relative pressure

The maximum, minimum and average values of relative pressures [Pa] for all submodels of gate valves based on the $k$–ε turbulent model are shown in Table 4. The maximum, minimum and average relative pressure values increase exponentially when the valve is closed. The average relative pressure of a valve 80% closed is approximately 75 times higher than in the case of a valve 20%

TABLE 4. View of maximum, minimum and average relative pressures [Pa] for each of the gate valve submodels

| Percentage of gate valve closure [%] | $v = 1.0$ m·s$^{-1}$ | | | $v = 1.5$ m·s$^{-1}$ | | |
|---|---|---|---|---|---|---|
| | max | min | avg | max | min | avg |
| 20 | 895 | –1 053 | 171 | 1 983 | –2 501 | 355 |
| 40 | 1 989 | –2 689 | 407 | 4 433 | –6 057 | 886 |
| 60 | 7 223 | –8 209 | 1 897 | 16 195 | –18 347 | 4 228 |
| 80 | 56 948 | –46 156 | 12 890 | 127 831 | –103 401 | 29 080 |

closed. The values to be analysed when dimensioning the valve as a function of pressure are maximum and minimum pressures, since extreme maximum and minimum pressures can cause the pipe itself to expand or twist, which can lead to its damage and cracking. The upper row in Figure 5 shows the changes in relative pressures at the first four transverse profiles (a), b), (c) and (d) and the bottom row shows the changes in relative pressures at the last four transverse profiles (e), (f), (g) and (h) for the gate valve submodel at 80% closed (at 1.0 m·s$^{-1}$).

Table 5 shows the maximum, minimum and average values of the relative pressures at the transverse profiles for all submodels of gate valves and both inlet velocities. The highest relative pressures and the lowest negative pressures occur at both inlet flow velocity variants for the same profiles. The maximum relative pressure values are 56,942 Pa for the inlet velocity of 1.0 m·s$^{-1}$ and 127,817 Pa for the inlet velocity of 1.5 m·s$^{-1}$, which occur for partial models with 80% valve closure on the third profile 7 cm in front of the disc surface of gate valve, seen in the direction of flow. The lowest negative pressures also occur in submodels with 80% valve closure on the fourth profile, which is located at the back of the valve disc.

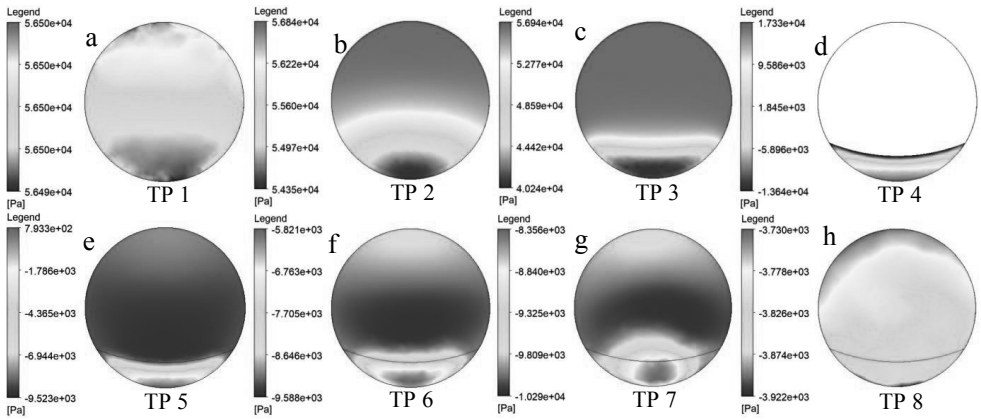


FIGURE 5. Distribution of the relative pressures on transverse profiles of gate valve submodels with 80% of valve closure and inflow velocity of 1.0 m·s$^{-1}$

TABLE 5. The view of maximum, minimum and average values of the relative pressures [Pa] at the transverse profiles TP1 to TP8 in gate valve model

| Cross section profile | $v = 1.0$ m·s$^{-1}$ | | | | | | | | | | | |
|---|---|---|---|---|---|---|---|---|---|---|---|---|
| | 20% valve closure | | | 40% valve closure | | | 60% valve closure | | | 80% valve closure | | |
| | max | min | avg | max | min | avg | max | min | avg | max | min | avg |
| 1 | 443 | **439** | **441** | 1 538 | **1 534** | **1 536** | 6 773 | **6 769** | **6 671** | **56 499** | **56 495** | **56 497** |
| 2 | 665 | 261 | 403 | 1 836 | 1 076 | 1 446 | 7 103 | 5 769 | 6 583 | 56 844 | 54 647 | 56 160 |
| 3 | **870** | 123 | –367 | **1 978** | 517 | 1 137 | **7 216** | 3 526 | 5 546 | 56 942 | 40 241 | 52 472 |
| 4 | 48 | –58.2 | –230 | 178 | –1 548 | –791 | 1 834 | –3 759 | –1 782 | 17 326 | **–13 637** | –3 976 |
| 5 | –21 | –623 | –343 | –185 | –1 430 | –1 035 | 141 | –3 221 | –2 530 | 793 | –9 522 | –7 905 |
| 6 | –110 | **–838** | **–443** | –674 | –1 602 | –1 272 | –1 736 | –2 412 | –2 970 | –5 821 | –9 588 | –8 699 |
| 7 | **–174** | –591 | –373 | **–1 185** | **–1 844** | **–1 589** | **–3 098** | **–3 822** | **–3 579** | **–8 856** | –10 293 | **–9 819** |
| 8 | 97 | 90 | 94 | –39 | –68 | –54 | –669 | –735 | –69 | –3 730 | –3 922 | –3 807 |
| Cross section profile | $v = 1.5$ m·s$^{-1}$ | | | | | | | | | | | |
| | 20% valve closure | | | 40% valve closure | | | 60% valve closure | | | 80% valve closure | | |
| | max | min | avg | max | min | avg | max | min | avg | max | min | avg |
| 1 | 951 | **944** | **949** | 3 406 | **3 398** | **3 402** | 15 170 | **15 160** | **15 165** | 126 880 | **126 850** | **126 850** |
| 2 | 1 459 | 552 | 869 | 4 084 | 2 375 | 3 208 | 15 919 | 12 920 | 14 750 | 127 593 | 121 977 | 126 100 |
| 3 | **1 924** | 245 | 789 | **4 407** | 1 119 | 2 492 | **16 178** | 7 837 | 12 420 | **127 817** | 90 249 | 117 820 |
| 4 | 81 | –1 377 | –568 | 335 | –3 549 | –1 827 | 4 067 | –8 558 | –40 71 | 38 779 | **–30 978** | –9 124 |
| 5 | –74 | –1 435 | –804 | –461 | –3 254 | –2 375 | –259 | –7 321 | –5 755 | 1 715 | –21 557 | –17 870 |
| 6 | –269 | **–1 830** | **–993** | –1 563 | –3 682 | –2 925 | –3 962 | –7 750 | –6 749 | –13 093 | –21 718 | –19 650 |
| 7 | **–415** | –1 298 | –843 | **–2 698** | **–4 244** | **–3 636** | **–7 016** | **–8 658** | **–8 111** | **–18 727** | –23 214 | **–22 110** |
| 8 | 188 | 171 | 180 | –188 | –122 | –154 | –1 538 | –1 686 | –1 599 | –8 267 | –8 721 | –8 446 |

Cavitation can occur on the part of the pipe behind the gate valve due to negative pressures. The highest average relative pressures are much higher in submodels with higher closure percentages (60 and 80%) than 20% closure valve. The value of the highest average relative pressure at 80% closed valve is almost 120 times higher than the 20% closed valve submodel. As the inlet velocity and the valve closure percentage increase, an additional increase in relative pressures can be expected up to a certain closure percentage when the maximum pressure value decreases from that of the previous valve closure percentage. For processed submodels, the maximum absolute pressure to be expected within the pipeline is 2.29 bar at 80% closure and an inlet velocity of 1.5 $m \cdot s^{-1}$, which is a fully acceptable pressure for water pipes. The maximum relative pressure for both flow velocities occur at the middle profile and have values of 56,948 Pa for the inlet velocity of 1.0 $m \cdot s^{-1}$ and 127,831 Pa for the inlet velocity of 1.5 $m \cdot s^{-1}$ (submodel with 80% of valve closure). The highest pressures occur in the vicinity of the second and penultimate longitudinal profile, which are 15 mm from the pipe wall.

## Turbulent kinetic energy

In fluid dynamics, the turbulent kinetic energy – TKE ($k$) is a measure of the kinetic energy per unit mass associated with eddy currents in turbulent flows. According to the RANS equations (Reynolds-averaged Navier–Stokes equations), the turbulent kinetic energy can be calculated according to the turbulence model. It is generally calculated as half the sum of the variance (the square of the standard deviations) of the velocity components. Figure 6 shows the values of the turbulent kinetic energy on the cross profiles of the submodels at 80% valve closure and an inflow velocity of 1.5 $m \cdot s^{-1}$. The upper part of Figure 6 shows three profiles in front of valve (a), b), (c) and one at valve (d), and the lower part of the figure shows profiles (e), (f), (g), (h), which are located behind the gate valve. The figure shows that the maximum values of the turbulent kinetic energy occur at the valve itself and beyond, extending from the bottom of the valve wall to the upper half of the pipe along the flow behind the valve. The maximum value that appears is 2.66 $m^2 \cdot s^{-2}$ on the last cross-sectional profile. The maximum value of the turbulent kinetic energy of 5.52 $m^2 \cdot s^{-2}$ does not appear on any user-defined profile, but directly behind the last profile ($h$). Table 6 shows the maximum (values in bold), minimum and average values of the turbulent kinetic energy [$m^2 \cdot s^{-2}$] on the transverse profiles for all numerical submodels and both input velocities of 1.0 and 1.5 $m \cdot s^{-1}$.

With the increase of the valve closure degree, the maximum values of the turbulent kinetic energy move further away from the valve. This is due to the increase in the variations in flow velocities caused by moving away from the valve in submodels with a smaller closing degree compared to a larger closing degree (e.g. 60% of the valve closing degree). For this reason, the maximum values for submodels with higher closure percentages occur behind the last user-defined cross-section profile in the direction of water flow.

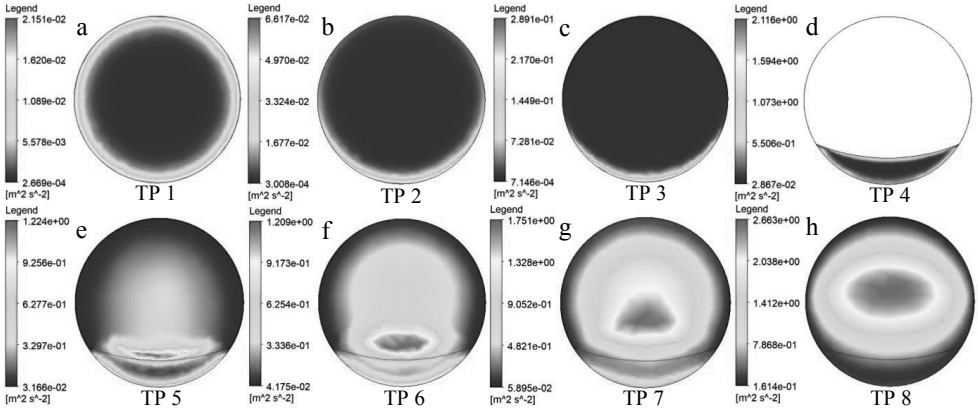


FIGURE 6. Distribution of turbulent kinetic energy at transverse profiles of a gate valve submodel with 80% of valve closure and an inlet flow velocity of 1.5 $m \cdot s^{-1}$

## Conclusions

In this paper a hydraulic analysis of gate valve models was performed using the commercial softwares Ansys CFX 19.1 and Ansys Fluent 19.1. The analyses were performed for 4° of opening of the gate valve with inlet velocities of 1.0 and 1.5 $m \cdot s^{-1}$. After the hydrodynamic analysis it was found that all models show vortices in the area behind the gate valve, especially at smaller opening degrees. The appearance of the vortex and its movement along the pipe is clearly visible on the given central longitudinal profiles of the pipe system. In the case of the gate valve with 40% closing degree and an inlet flow velocity of 1.0 $m \cdot s^{-1}$, the maximum velocity occurring is 2.53 $m \cdot s^{-1}$, whereas for the same model and an inlet flow velocity of 1.5 $m \cdot s^{-1}$ it is 3.80 $m \cdot s^{-1}$. The analysis shows that maximum values of velocities, pressures and other physical quantities occur in models with a lower valve opening degree. The maximum values of the physical quantities in the analysed models occur mainly in the valve area or behind it. This paper shows that the implementation of hydrodynamic analysis is possible for different forms of valve geometry. Correct numerical modelling through CFD technology allows the obtained results to be used to improve the valve characteristics in its design and operation.

### Acknowledgements

This paper is the result of a project on the Development of Research Infrastructure at the University Campus in Rijeka (RC.2.2.06-0001), co-funded by the European Regional Development Fund (ERDF) and the Ministry of Science and Education of the Rep. of Croatia.

TABLE 6. The view of the maximum, minimum and average values of turbulent kinetic energy [$m^2 \cdot s^{-2}$] on the transverse profiles TP1 to TP8 of a gate valve

| Cross section profile | $v = 1.0$ m·s$^{-1}$ | | | | | | | | | | | |
|---|---|---|---|---|---|---|---|---|---|---|---|---|
| | 20% valve closure | | | 40% valve closure | | | 60% valve closure | | | 80% valve closure | | |
| | max | min | avg | max | min | avg | max | min | avg | max | min | avg |
| 1 | 0.01144 | 0.00014 | 0.00311 | 0.01051 | 0.00014 | 0.00314 | 0.01081 | 0.00014 | 0.00313 | 0.01089 | 0.00014 | 0.00314 |
| 2 | 0.01356 | 0.00010 | 0.00308 | 0.01716 | 0.00011 | 0.00322 | 0.02147 | 0.00012 | 0.00350 | 0.03406 | 0.00014 | 0.00378 |
| 3 | 0.01497 | 0.00011 | 0.00243 | 0.02404 | 0.00016 | 0.00273 | 0.04333 | 0.00034 | 0.00384 | 0.14914 | 0.00033 | 0.00949 |
| 4 | 0.02208 | 0.00011 | **0.00565** | 0.05912 | 0.00022 | 0.01691 | 0.16759 | 0.00092 | 0.03915 | 0.88934 | 0.01319 | 0.21620 |
| 5 | 0.01968 | 0.00013 | 0.00347 | 0.05966 | 0.00033 | 0.01707 | 0.13125 | 0.00206 | 0.03468 | 0.53885 | 0.01338 | 0.10860 |
| 6 | 0.02064 | 0.00015 | 0.00482 | 0.09068 | 0.00094 | 0.02597 | 0.17000 | 0.00644 | 0.05021 | 0.53124 | 0.01730 | 0.13810 |
| 7 | **0.02233** | **0.00021** | 0.00503 | **0.18801** | 0.00256 | **0.04415** | **0.29017** | 0.01401 | **0.08991** | 0.69996 | 0.02282 | 0.20790 |
| 8 | 0.01337 | 0.00012 | 0.00317 | 0.03227 | **0.00321** | 0.01127 | 0.20445 | **0.01421** | 0.06462 | **1.14978** | **0.06886** | **0.35820** |
| Cross section profile | $v = 1.5$ m·s$^{-1}$ | | | | | | | | | | | |
| | 20% valve closure | | | 40% valve closure | | | 60% valve closure | | | 80% valve closure | | |
| | max | min | avg | max | min | avg | max | min | avg | max | min | avg |
| 1 | 0.02268 | 0.00027 | 0.00623 | 0.02073 | 0.00027 | 0.00628 | 0.02135 | 0.00027 | 0.00626 | 0.02151 | 0.00027 | 0.00628 |
| 2 | 0.02666 | 0.00021 | 0.00617 | 0.03358 | 0.00024 | 0.00642 | 0.04186 | 0.00027 | 0.00698 | 0.06617 | 0.00030 | 0.00751 |
| 3 | 0.02969 | 0.00023 | 0.00489 | 0.04692 | 0.00035 | 0.00546 | 0.08415 | 0.00074 | 0.00762 | 0.28910 | 0.00071 | 0.01871 |
| 4 | 0.06786 | 0.00025 | 0.01495 | 0.12699 | 0.00048 | 0.03366 | 0.33137 | 0.00200 | 0.08358 | 2.11641 | 0.02867 | 0.47990 |
| 5 | 0.06669 | 0.00028 | 0.01783 | 0.13641 | 0.00070 | 0.03853 | 0.30955 | 0.00449 | 0.08088 | 1.22364 | 0.03166 | 0.26990 |
| 6 | **0.13371** | 0.00040 | 0.02447 | 0.19733 | 0.00206 | 0.05792 | 0.40030 | 0.01428 | 0.11610 | 1.20911 | 0.04175 | 0.34190 |
| 7 | 0.12998 | 0.00075 | **0.02473** | **0.40703** | 0.00555 | **0.09827** | **0.68619** | **0.03434** | **0.21010** | 1.75139 | 0.05895 | 0.52140 |
| 8 | 0.02658 | **0.00087** | 0.00666 | 0.07491 | **0.00718** | 0.02506 | 0.47935 | 0.03283 | 0.15270 | **2.66295** | **0.16141** | **0.84520** |

## References


Ansys CFX 15.0 (2015). *Manual.* Southpointe, Canonsburg: ANSYS Inc.

Banko, P. (2019). *Hydraulic analysis of gate and butterfly valves using Computational Fluid Dynamics* (graduate thesis). University of Rijeka, Rijeka.

Decaix, J. & Goncalvès da Silva, E. (2013). Compressible effects modelling in turbulent cavitating flows. *European Journal of Mechanics – B/Fluids*, *39*, 11-31.

Jatkar, K.H. & Dhanwe, S.S. (2013). Finite Element Analysis of Gate Valve. *Asian Review of Mechanical Engineering*, *2*(1), 44-49.

Katkar, N.Y., Kulkarni, R.S., Patil, P.A. & Katkar, S.E. (2017). A review on design and analysis of gate valve using various computer aided techniques. *International Journal for Innovative Research in Science and Technology*, *3*(10), 218-220.

Patil, P.B. & Gambhire, V.R. (2014). Structural analysis of gate valve body using FEA. *International Journal of Engineering Research & Technology*, *3*(6), 1815-1818.

Pujari, A.A. & Joshi, G.S. (2016). Analysis and design optimization of 8''- 600# gate valve body using FEA and stress analysis. *International Journal of Research in Engineering and Technology*, *4*(2), 440-443.

Quimby, B. (2007). *Hydrodynamic loads.* Retrieved from: https://www.bgstructuralengineering.com/BGASCE7/BGASCE7006/BGASCE70604.htm

Wang, D. (2014). Research on CAD/CAE system of gate valve based on UG. *Applied Mechanics and Materials*, *541-542*, 618-621.

Žic, E. (2019). *3rd Summer School of Computational Fluid Dynamics* (materials from lectures). Novi Sad: Faculty of Technical Sciences in Novi Sad.


## Summary


**Hydraulic analysis of gate valve using computational fluid dynamics (CFD).** As a very important element of most water supply systems, valves are exposed to the effects of strong hydrodynamic forces. When exposed to large physical quantities, the valve and piping can be damaged, which could endanger the performance of a water supply system. This is the main reason why it is necessary to foresee and determine the maximum values of velocity, pressure and other physical quantities that can occur in the system under certain conditions. Predicting extreme conditions allows us to correctly size the valve for the expected conditions to which the valve might be exposed, which is also the main objective of this paper. One of the methods for predicting and determining extreme values on a valve is to perform a simulation with computational fluid dynamics (CFD). This is exactly the method used in the preparation of this paper with the aim of gaining insight into the physical magnitudes for models of gate valves positioned inside a pipe under characteristic degrees of valve closure. The Ansys CFX 19.1 and Ansys Fluent 19.1 software was used to simulate the hydrodynamic analysis and obtain the required results. The hydrodynamic analysis was performed for four opening degrees of gate valve.



**Authors' address:**
Elvis Žic
(https://orcid.org/0000-0002-5626-8394)
University of Rijeka
Faculty of Civil Engineering
Radmile Matejčić, 3, 51000, Rijeka
Croatia
e-mail: elvis.zic@uniri.hr

Scientific Review – Engineering and Environmental Sciences (2020), 29 (3), 289–297
Sci. Rev. Eng. Env. Sci. (2020), 29 (3)
Przegląd Naukowy – Inżynieria i Kształtowanie Środowiska (2020), 29 (3), 289–297
Prz. Nauk. Inż. Kszt. Środ. (2020), 29 (3)
http://iks.pn.sggw.pl
DOI 10.22630/PNIKS.2020.29.3.24

**Eva SINGOVSZKA, Magdalena BALINTOVA**
Technical University of Kosice, Faculty of Civil Engineering

# Year over year comparison of sediment quality in the rivers of Eastern Slovakia

**Key words:** bottom sediment, potential ecological risk assessment, heavy metals

## Introduction

Trace metals entering the river originate from either natural or anthropogenic sources (Bem, Gallorini, Rizzio & Krzemin, 2003; Wong, Li, Zhang, Qi & Peng, 2003; Adaikpoh, Nwejai & Ogala, 2005; Akoto, Bruce & Darko 2008). In unaffected environments, the concentration of most metals is very low and is typically derived from mineralogy and the weathering processes (Karbassi, Monavari, Nabi Bidhendi, Nouri & Nematpour, 2008). The main anthropogenic sources of heavy metal contamination are due to mining, disposal of untreated and partially treated effluents containing toxic metals, as well as metal chelates from different industries and the indiscriminate use of heavy metal – containing fertilizer and pesticides in agriculture fields (Hatje, Bidone & Maddock, 1998; Nouri, Mahvi, Jahed & Babaei, 2008). Metals enter river water from mining areas through various means such as mine discharge, runoff, chemical weathering of rocks and soils, wet and dry fallout of atmospheric particulate matter (Macklin et al., 2003; Bird et al., 2003; Kraft, Tumpling & Zachman, 2006; Singh et al., 2008; Venugopal et al., 2009). The mine water, runoff from abandoned watersheds and associated industrial discharges are the major source of heavy metal contamination, total dissolved solid and low pH of streams in mining area (US EPA, 1998; Mohanty, Misra & Nayak, 2001; Cravotta, 2008; Shahtaheri, Abdollahi, Golbabaei, Rahimi-Froshani & Ghamari, 2008).

The anthropological influences (i.e. urban, industrial and agricultural activities) as well as the natural processes (i.e. changes in precipitation amounts, erosion and weathering of crustal materials) degrade surface water quality and impair its use for drinking, industrial, agricultural, recreational and other purposes. Due to spatial and temporal variations in water chemistry, a monitoring program

that provides a representative and reliable estimation of the quality of surface waters has become an important necessity. Consequently, comprehensive monitoring programs that include frequent water sampling at numerous sites and include a full analysis of a large number of physicochemical parameters designed for the proper management of water quality in surface waters are required.

Potential ecological risk index (PERI), proposed by Hakanson (1980), is used as a quick and practical tool for environmental assessment, obtaining as results the pollution classification of areas and the identification of the toxic substances of interest, supporting actions for pollution control of limnic aquatic systems. Potential ecological risk index provides a fast and simple quantitative value for PER of a given contamination situation. This model, despite being formulated in 1980s and for limnic systems, has an organized structure based on simple algorithms, including the most important environmental parameters for an ecological risk assessment, and also includes the mathematical relationships between them.

## Material and methods

### Study area

Hornad belongs to Danube river basin. Area of Hornad is 4,414 km$^2$. In the basin is 27.6% of arable land, 15.7% of other agricultural land, 47.4% of forests, 2.7% shrubs and grasses and 6.6% is other land. There is 164 surface water bodies while 162 are in the category of the flowing waters/rivers and two are in the category of standing waters/reservoirs. Ten groundwater bodies exist in the basin while one is in quaternary sediment, two is geothermal waters and seven are in pre-quaternary rocks. Hornad has 11 transverse structures without fishpass in operation. From the point of view of environmental loads, there are 11 high-risk localities which have been identified in the river basin. Diffuse pollution is from agriculture and municipalities without sewerage. The upper stretch of Hornad to Spišská Nová Ves is in good ecological status while the lower stretch is changed to poor status. From the Ružín Water Reservoir, Hornad achieves moderate ecological status. According to chemical status assessment, Hornad is in good status. Fifty six water bodies (34%) are failing to achieve good ecological status in Hornad river basin. The water body of intergranular ground waters of quaternary alluviums of Hornad river basin achieves poor chemical status (pollution from the point and diffuse sources) and poor quantitative status identified on the base of long-term decrease of groundwater levels. The water body of pre-quaternary rocks is in good status – quantitative and chemical (SEA, 2015).

Poprad is in Vistula river basin district and is the only Slovak river that drains their waters into Baltic Sea. It sources in High Tatras over Popradské Lake. It flows to the southeast direction up to city of Svit. The river mouths into Dunajec from the right side, in Poland, river km 117.00. It drains the area of 1,890 km$^2$. There are 83 surface water bodies all in the category of the flowing waters/rivers. Five groundwater bodies exist in the basin while one is in quaternary sediment, one is geothermal

waters and three are in pre-quaternary rocks. Poprad has 27 transverse structures without fishpass in operation. Significant industrial and other pollution sources are: Chemosvit Energochem, a.s., Svit, Whirlpool Slovakia, s.r.o., Poprad, screw factory Exim, Stará Ľubovňa, Východoslovenské stavebné hmoty a.s (closed in 2013). From the point of view of environmental loads, there are 17 high-risk localities which have been identified in the river basin. Diffuse pollution is from agriculture and municipalities without sewerage (Ondruš, 1991).

Laborec is a river in Eastern Slovakia that flows through the districts of Medzilaborce, Humenné, and Michalovce in Košice Region, and Prešov Region. The river drains the Laborec Highlands. Tributaries of Laborec include Uh which joins Laborec near the city of Drahňov in Michalovce District, and Cirocha. Laborec itself is a tributary, flowing into Latorica. Catchment area of Ižkovce hydrometric profile at Laborec is 4,364 km$^2$ and it is situated at 94.36 m a.s.l. (SEA, 2015).

## Sampling materials

Sediment was sampled according to standard ISO 5667-6 which outlines the principles and design of sampling programs and manipulation, as well as the preservation of samples. Monitoring was carried out in the 2017–2018. The samples of sediment were air-dried and ground using a planetary mill to a fraction of 0.063 mm. The chemical composition of sediments was determined by means of X-ray fluorescence (XRF) using SPECTRO iQ II (Ametek, Germany, 2000). Sediment samples were prepared as pressed tablets with a diameter of 32 mm by mixing 5 g of sediment and 1 g of dilution material (Hoechs Wax C Micropowder – M-HWC-C38H76N2O2) and compressing them at a pressure of 0.1 MPa·m$^{-2}$. The mean total concentrations of 8 heavy metals in sediment of sediments samples are presented in Table 1.

Results of XRF analysis of sediments were compared with the limited values according to the Slovak Act 188/2003

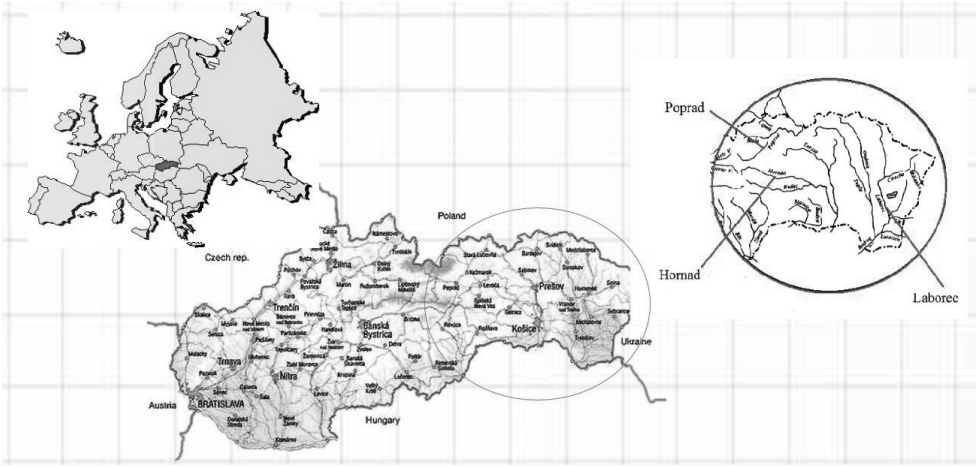


FIGURE 1. Situation of three investigation rivers in Eastern Slovakia

TABLE 1. Results of chemical analyses of sediment from the rivers of Eastern Slovakia in 2017–2018

| Year | River | Sampling point | As | Cd | Cr | Cu | Hg | Ni | Pb | Zn |
|---|---|---|---|---|---|---|---|---|---|---|
| | | | mg·kg$^{-1}$ | | | | | | | |
| 2017 | Hornád | S1 | 14.9 | < 5.1 | 35.8 | 110.3 | < 2 | 59.4 | < 2 | 167.0 |
| | | S3 | 82.3 | < 5.1 | 141.2 | 233.0 | < 2 | 130.5 | 37.9 | 360.4 |
| | | S4 | < 1 | < 5.1 | 169.9 | 108.4 | < 2 | 45.2 | 51.1 | 177.4 |
| | | S5 | 12.6 | < 5.1 | 189.9 | 188.0 | < 2 | 64.6 | < 2 | 202.7 |
| | Laborec | S1 | < 1 | < 5.1 | 52.6 | 18.4 | < 2 | 51.7 | < 2 | 36.3 |
| | | S2 | < 1 | < 5.1 | 28.1 | 30.1 | < 2 | 66.5 | < 2 | 51.7 |
| | | S3 | < 1 | < 5.1 | 36.6 | 35.8 | < 2 | 54.0 | < 2 | 33.7 |
| | | S4 | 1.3 | < 5.1 | 28.0 | 38.0 | < 2 | 64.6 | < 2 | 61.1 |
| | Poprad | S1 | < 1 | < 5.1 | 124.7 | 51.6 | < 2 | 65.7 | < 2 | 100.4 |
| | | S2 | < 1 | < 5.1 | 28.7 | 24.7 | < 2 | 50.3 | < 2 | 58.1 |
| | | S3 | < 1 | < 5.1 | 56.9 | 2.9 | < 2 | 35.5 | < 2 | 118.6 |
| | | S4 | < 1 | < 5.1 | 38.5 | 5.6 | < 2 | 20.0 | < 2 | 105.6 |
| 2018 | Hornád | S1 | < 1 | < 5.1 | 122.0 | 36.2 | < 2 | 39.4 | < 2 | 85.6 |
| | | S2 | < 1 | < 5.1 | 28.7 | 29.4 | < 2 | 40.3 | 2.5 | 179.7 |
| | | S3 | < 1 | < 5.1 | 34.1 | 27.5 | < 2 | 37.4 | < 2 | 55.9 |
| | | S4 | < 1 | < 5.1 | 50.9 | 62.9 | < 2 | 33.9 | < 2 | 71.2 |
| | Laborec | S1 | < 1 | < 5.1 | 5.0 | 8.4 | < 2 | 19.7 | < 2 | < 1 |
| | | S2 | < 1 | < 5.1 | 5.0 | 10.1 | 2.2 | 17.7 | < 2 | < 1 |
| | | S3 | < 1 | < 5.1 | 5.0 | 1.5 | < 2 | 13.4 | < 2 | < 1 |
| | | S4 | < 1 | < 5.1 | 5.0 | 10.7 | < 2 | 15.5 | < 2 | < 1 |
| | Poprad | S1 | < 1 | < 5.1 | 5.0 | 8.1 | < 2 | 2.2 | < 2 | 122.7 |
| | | S2 | < 1 | < 5.1 | 44.7 | 14.9 | < 2 | 20.9 | < 2 | 39.4 |
| | | S3 | < 1 | < 5.1 | 5.0 | 32.7 | < 2 | 34.5 | < 2 | 49.5 |
| | | S4 | < 1 | < 5.1 | 5.0 | 11.5 | < 2 | 2.0 | < 2 | 71.0 |
| × | | | Limits | | | | | | | |
| | | | 20 | 10 | 1 000 | 1 000 | 10 | 300 | 750 | 2 500 |

Coll. of Laws on the application of treated sludge and bottom sediments to fields. It can be stated that limit values comparing with Slovak legislation were not exceeding in all sediment samples in rivers in Eastern Slovakia.

## Potential ecological risk index (PERI)

In this research, potential ecological risk index (PERI) proposed by Hakanson (1980) was used to evaluate the potential ecological risk of heavy metals. This method comprehensively considers the synergy, toxic level, concentration of the

heavy metals and ecological sensitivity of heavy metals (Nabholz, 1991; Singh, Sharma, Agrawal & Marshall, 2010; Ouay et al., 2013). Potential ecological risk index is formed by three basic modules: degree of contamination ($C_d$), toxic-response factor ($T_r$) and potential ecological risk factor ($E_R$). According to this method, the potential ecological risk index of a single element ($E^i_R$) and comprehensive potential ecological risk index ($RI$) can be calculated via the following equations:

$$C_f^i = \frac{C_i}{C_n^i} \tag{1}$$

where $C_i$ is the mean concentration of an individual metal examined and $C_n{}^i$ is the background concentration of the individual metal. In this work, background concentrations of contents of selected elements in sediments unaffected by mining activities in the assessment area were used (Table 3). Index $C_f^i$ is the single-element one. The sum of contamination factors for all examined metals represents the contamination degree ($C_d$) of the environment:

$$C_d = \sum_{i=1}^{n} C_f^i \tag{2}$$

Indicator $E_r{}^i$ is the potential ecological risk index of an individual metal. It is calculated by

$$E_r^i = C_f^i \cdot T_r^i \tag{3}$$

where $T_r{}^i$ is the toxic response factor provided by Hakanson (1980). Indicator $R^i$ is the potential ecological risk index, which is the sum of $E_r{}^i$:

$$R^i = \sum_{i=1}^{n} E_r^i \tag{4}$$

Hakanson defined five categories of $E_r{}^i$ and four categories of $R^i$, as shown in Table 2.

TABLE 2. Risk grades indexes and grades of potential ecological risk of heavy metal pollution

| $E^i_r$ | Risk grade | $R^i$ | Risk grade |
|---|---|---|---|
| $E^i_r < 40$ | low | $R^i < 150$ | low |
| $40 \le E^i_r < 80$ | moderate | $150 \le R^i < 300$ | moderate |
| $80 \le E^i_r < 160$ | considerable | $300 \le R^i < 600$ | considerable |
| $160 \le E^i_r < 320$ | high | $R^i \ge 600$ | very high |
| $E^i_r \ge 320$ | very high | × | |

## Results and discussion

Based on the monitoring data of sediment quality in the study area, a quantitative analysis of heavy-metal pollution in sediment was conducted using the method of PERI. The results based on potential ecological risk index show that the quality of sediment in 2018 is better than 2017. The worst result were obtained for Hornad in 2017. Significant improvement were occurred at the sampling point S2 in Hornad in 2018. The best results were determined for Laborec in 2018.

TABLE 3. Statistical results of potential ecological risk index of a single element (ER) and comprehensive potential ecological risk index (PERI) for rivers of Eastern Slovakia in 2017–2018

| Year | River | Sampling point | $E_r$ | | | | | | | | $R^i$ | Risk grade |
|---|---|---|---|---|---|---|---|---|---|---|---|---|
| | | | As | Cd | Cr | Cu | Hg | Ni | Pb | Zn | | |
| 2017 | Hornad | S1 | 149 | 30 | 2.95 | 20.13 | 40 | 11.98 | 5 | 4.32 | 263.36 | moderate |
| | | S2 | 823 | 30 | 11.62 | 42.52 | 40 | 26.31 | 94.75 | 9.31 | 1 077.51 | very high |
| | | S3 | 10 | 30 | 13.98 | 19.79 | 40 | 9.11 | 127.75 | 4.54 | 255.21 | moderate |
| | | S4 | 126 | 30 | 15.63 | 34.31 | 40 | 13.02 | 5 | 5.24 | 269.19 | moderate |
| | Poprad | S1 | 10 | 30 | 2 | 255 | 40 | 5.05 | 5 | 25.8 | 372.85 | considerable |
| | | S2 | 10 | 30 | 6.86 | 218.35 | 40 | 6.15 | 5 | 22.5 | 338.86 | considerable |
| | | S3 | 10 | 30 | 4.18 | 455 | 40 | 7.45 | 5 | 24.7 | 576.33 | considerable |
| | | S4 | 10 | 30 | 5.28 | 320 | 40 | 5.10 | 5 | 30.0 | 445.38 | considerable |
| | Laborec | S1 | 10 | 30 | 49.88 | 99.73 | 40 | 5 | 100.4 | 38.08 | 497.34 | considerable |
| | | S2 | 10 | 30 | 11.48 | 47.50 | 40 | 5 | 58.1 | 38.08 | 325.91 | considerable |
| | | S3 | 10 | 30 | 2.0 | 12.12 | 40 | 5 | 148.2 | 38.08 | 335.27 | considerable |
| | | S4 | 10 | 30 | 22.76 | 5.58 | 40 | 5 | 118.6 | 38.08 | 301.59 | considerable |
| 2018 | Hornad | S1 | 10 | 30 | 11.4 | 20.13 | 40 | 11.45 | 5 | 3.95 | 111.8 | low |
| | | S2 | 10 | 30 | 9.3 | 42.52 | 40 | 0.64 | 6.25 | 8.36 | 116.06 | low |
| | | S3 | 10 | 30 | 8.7 | 19.79 | 40 | 0.54 | 5 | 2.6 | 107.15 | low |
| | | S4 | 10 | 30 | 39.8 | 34.31 | 80 | 0.39 | 10 | 6.62 | 196.12 | moderate |
| | Poprad | S1 | 10 | 30 | 0 | 9.4 | 40 | 5 | 5 | 9.02 | 108.92 | low |
| | | S2 | 10 | 30 | 0 | 17.35 | 40 | 52.25 | 5 | 2.9 | 147.5 | low |
| | | S3 | 10 | 30 | 0 | 38 | 40 | 86.25 | 5 | 3.64 | 212.89 | moderate |
| | | S4 | 10 | 30 | 0 | 13.35 | 40 | 5.00 | 5 | 5.22 | 108.57 | low |
| | Laborec | S1 | 10 | 30 | 2 | 42 | 40 | 8.21 | 5 | 1 | 138.21 | low |
| | | S2 | 10 | 5.8 | 2 | 50.5 | 40 | 7.375 | 5 | 1 | 121.67 | low |
| | | S3 | 10 | 30 | 2 | 7.5 | 40 | 5.585 | 5 | 1 | 101.09 | low |
| | | S4 | 10 | 30 | 2 | 53.5 | 40 | 6.46 | 5 | 1 | 147.96 | low |

## Conclusions

Environmental risk in the water catchments are closely related to the quality and quantity of water flows in the catchment and the quality is one of the most important indicators of risk in the river basin. The monitoring and evaluation of water quality have a permanent place in the process of risk management. The possibility of minimizing the negative impact on the environment presents the assessment and management of environmental risks by using different methodologies. Methodology for assessing environmental risks in the basin presents a risk characterization for the particular conditions of water flows. The results represent the basis for risk management in the river basin, whose task is to ensure the sustainability of water bodies.

Different calculation methods on the basis of different algorithms might lead to a discrepancy of the pollution assessment when they are used to assess the quality of sediment. So it is of great importance to select a suitable method to assess sediment quality for decision making and spatial planning. Pollution indices is a powerful tool for processing, analysing, and conveying environmental information to decision makers, managers, technicians and the public. Potential ecological risk index is based exclusively on chemical parameters of sediments because sediment data show mean integrated values in time, with higher stability than water column parameters; sediments are easily sampled at field work; sediment samples are more representative for time and space scales and analytical data are easily obtained, especially because sediments present high concentrations of contaminants, decreasing the possible errors due to detection limits of the applied analytical method. The results show on the basis on potential ecological risk index that the quality of sediment in 2018 is better than 2017.


### Acknowledgements

This work has been supported by the Slovak Grant Agency for Science (Grant No 1/0419/19).


## References


Adaikpoh, E.O., Nwajei, G.E. & Ogala, J.E. (2005). Heavy metals concentrations in coal and sediments from river Ekulu in Enugu, Coal City of Nigeria. *Journal of Applied Sciences and Environmental Management*, *9*(3), 5-8.

Akoto, O., Bruce, T.N. & Darko, G. (2008). Heavy metals pollution profiles in streams serving the Owabi reservoir. *African Journal of Environmental Science and Technology*, *2*(11), 354-359.

Bem, H., Gallorini, M., Rizzio, E. & Krzemin, S.M. (2003). Comparative studies on the concentrations of some elements in the urban air particulate matter in Lodz City of Poland and in Milan, Italy. *Environmental International*, *29*(4), 423-428. doi 10.1016/S0160-4120(02)00190-3

Bird, G., Brewer, P., Macklin, M., Balteanu, D., Driga, B., Serban, M. & Zaharia, S. (2003). The solid state partitioning of contaminant metals and As in river channel sediments of the mining affected Tisa drainage basin, northwestern Romania and eastern Hungary. *Applied Geochemistry*, *18*(10), 1583-1595.

Cravotta, A.C. (2008). Dissolved metals and associated constituents in abandoned coal-mine discharges, Pennsylvania, USA. Part 1: constituent quantities and correlations. *Applied Geochemistry*, *23*(2), 166-202.

Hakanson, L. (1980). An ecological risk index for aquatic pollution control. A sedimentological approach. *Water Research*, *14*(8), 975-1001.

Hatje, V., Bidone, E.D. & Maddock, J.L. (1998). Estimation of the natural and anthropogenic components of heavy metal fluxes in fresh water Sinos river, Rio Grande do Sul state. South Brazil. *Environmental Technology*, *19*(5), 483-487.

ISO 5667-6-2005. Water quality. Sampling. Part 6: Guidance on sampling of rivers and streams.

Karbassi, A.R., Monavari, S.M., Nabi Bidhendi, G.R., Nouri, J. & Nematpour, K. (2008). Metal pollution assessment of sediment and water in the Shur River. *Environmental Monitoring and Assessment*, *147*(1-3), 107-116.

Kraft, C., Tumpling, W. & Zachmann, D.W. (2006). The effects of mining in Northern Romania on the heavy metal distribution in sediments of the rivers Szamos and R. Reza; G. Singh Tisza (Hungary). *Acta Hydrochimica et Hydrobiologic*, *34*(3), 257-264.

Macklin, M.G., Brewer, P.A., Balteanu, D., Coulthard, T.J., Driga, B., Howard, A.J. & Zaharia, S. (2003). The long term fate and environmental significance of contaminant metals released by the January and March 2000 mining tailings dam failure in Maramures County, upper Tisa basin, Romania. *Applied Geochemistry*, *18*(2), 241-257.

Mohanty, J.K., Misra, S.K. & Nayak, B.B. (2001). Sequential leaching of trace elements in coal: a case study from Talcher coalfield, Orissa. *Journal of the Geological Society of India*, *58*(5), 441-447.

Nabholz, J.V. (1991). Environmental hazard and risk assessment under the United States Toxic Substances Control. *Science of the Total Environment*, *109*, 649-665.

Nouri, J., Mahvi, A.H., Jahed, G.R. & Babaei, A.A. (2008). Regional distribution pattern of groundwater heavy metals resulting from agricultural activities. *Environmental Geology*, *55*(6), 1337-1343.

Ondruš, Š. (1991). *Ešte raz o pôvode tatranskej rieky Poprad* [*Once again about the origin of Tatra River Poprad*]. Bratislava: Veda, Vydavateľstvo Slovenskej akadémie vied.

Ouay, F., Pelfrene, A., Planque, J., Fourrier, H., Richard, A., Roussel, H. & Girondelot, B. (2013). Assessment of potential health risk for inhabitants living near a former lead smelter. Part 1: metal concentrations in soils, agricultural crops, and home-grown vegetables. *Environmental Monitoring Assessment*, *185*(5), 3665-3680.

Shahtaheri, S.J., Abdollahi, M., Golbabaei, F., Rahimi- Froshani, A. & Ghamari, F. (2008). Monitoring of mandelic acid as a biomarker of environmental and occupational exposures to styrene. *International Journal of Environmental Research*, *2*(2), 169-176.

Singh, A.K., Mondal, G.C., Kumar, S., Singh, T.B., Tewary, B.K. & Sinha, A. (2008). Major ion chemistry, weathering processes and water quality assessment in upper catchment of Damodar River basin, India. *Environmental Geology*, *54*(4), 745-758.

Singh, A., Sharma, R.K., Agrawal, M. & Marshall, F.M. (2010). Health risk assessment of heavy metals via dietary intake of foodstuffs from the wastewater irrigated site of a dry tropical area of India. *Food and Chemical Toxicology*, *48*(2), 611-619.

Slovak Act. No 188/2003 Coll. of Laws on the application of treated sludge and bottom sediments to fields.

Slovak Environmental Agency [SEA] (2015). *Introduction. Pilot Project PiP1: Hornád/ /Hernád, Integrated Revitalisation of the Hornád/Hernád River Valley*. Banská Bystrica: Slovak Environmental Agency.

United States Environmental Protection Association [US EPA] (1998). *Guidelines for ecological risk assessment.* Washington, DC: US EPA.

Venugopal, T., Giridharan, L. & Jayaprakash, M. (2009). Characterization and risk assessment studies of bed sediments of River Adyar-An application of speciation study. *International Journal of Environmental Research*, *3*(4), 581-598.

Wong, C.S.C., Li, X.D., Zhang, G., Qi, S.H. & Peng, X.Z. (2003). Atmospheric deposition of heavy metals in the Pearl River Delta, China. *Atmospheric Environment*, *37*(6), 767-776.

## Summary

**Year over year comparison of sediment quality in the rivers of Eastern Slovakia.** Quality is one of the most important

risk indicators in river basins. Therefore, monitoring and evaluating water and sediment quality has a very important role in process of risk management. The aim of the monitoring is provide for the sustainability of water bodies and these results are the basis for the risk management in the river catchment area. Hornad, Laborec and Poprad are the rivers in Eastern Slovakia. Hornad and Laborec belongs to basin of Danube and Poprad belongs to basin of Vistula. Sediment sampling was carried out according to ISO 5667-6. Monitoring was carried out in the spring on 2017–2018. The chemical composition of sediments was determined by means of X-ray fluorescence (XRF) using SPECTRO iQ II (Ametek, Germany, 2000). The results of sediment quality evaluated by method PERI revealed that the quality of sediment in 2018 was better than 2017. Results of XRF analysis of sediments were compared with the limited values according to the Slovak Act 188/2003 Coll. of Laws on the application of treated sludge and bottom sediments to fields. It can be state that limit values comparing with Slovak legislation were not exceeding in all sediment samples in rivers in Eastern Slovakia. Based on the monitoring data of sediment quality in the study area, a quantitative analysis of heavy-metal pollution in sediment was conducted using the method of potential ecological risk index (PERI) which is method for evaluate the potential ecological risk of heavy metals. It is based exclusively on chemical parameters of sediments because sediment data show mean integrated values in time, with higher stability than water column parameters; sediments are easily sampled at field work; sediment samples are more representative for time and space scales and analytical data are easily obtained, especially because sediments present high concentrations of contaminants, decreasing the possible errors due to detection limits of the applied analytical method. This method comprehensively considers the synergy, toxic level, concentration of the heavy metals and ecological sensitivity of heavy metals. Potential ecological risk index can be obtained using three basic modules: degree of contamination (*CD*), toxic-response factor (*TR*) and potential ecological risk factor (*ER*). The results show on the basis on potential ecological risk index that the quality of sediment in 2018 is better than 2017. The worst result shows Hornad in 2017. Significant improvement occurred at the sampling point S2 in Hornad in 2018. The best results show Laborec in 2018. The results show on the basis on potential ecological risk index that quality of sediment in 2018 is better than 2017.

**Authors' address:**
Eva Singovszka
Technical University of Kosice
Faculty of Civil Engineering
Institute of Environmental Engineering
Vysokoskolska 4, 042 00, Kosice
Slovakia
e-mail: eva.singovszka@tuke.sk

Scientific Review – Engineering and Environmental Sciences (2020), 29 (3), 298–307
Sci. Rev. Eng. Env. Sci. (2020), 29 (3)
Przegląd Naukowy – Inżynieria i Kształtowanie Środowiska (2020), 29 (3), 298–307
Prz. Nauk. Inż. Kszt. Środ. (2020), 29 (3)
http://iks.pn.sggw.pl
DOI 10.22630/PNIKS.2020.29.3.25

**Stanisław MAJER**

West Pomeranian University of Technology in Szczecin, Faculty of Civil and Environmental Engineering

# Flow coefficient of the aggregates as a parameter characterizing the suitability of non-cohesive soils for earthworks

**Key words:** flow coefficient of the aggregates, uniformity coefficient

## Introduction

The introduction of European standards for the assessment of construction aggregates over 20 years ago provided a number of new testing methods previously non-existing in Poland. One of them is the flow coefficient of aggregates, popularly known as aggregate angularity. The method of determination is given in PN-EN 933-6:2014 standard, which defines the method of determining the coefficient for coarse aggregates with grain sizes between 4 and 20 mm and fine aggregates with grain sizes below 2 mm. This test is particularly important when designing mineral–asphalt mixtures (Mitchell, 2001). Aggregate angularity, particularly for fine aggregates, is the main factor influencing the workability of mixtures (Little, Button, Jayawickrama & Hudson, 2003). In the 1980s in the USA and France, it was proven that the angularity of an aggregate affects the stability and rutting resistance of mixtures (Topal & Sengoz, 2005). It is desirable to include angular fine aggregates in the composition. Rounded grains, especially natural sand, can lead to rutting of the mixture. The problem of grain angularity is also considered in concrete design (Quiroga & Fowler, 2004).

The shape of grains is a complex characteristics, determined by three parameters: sphericity, angularity and surface micro texture. The shape of grains affects the compaction of non-cohesive soils (Szerakowska, 2018). The problems of grain shape influence on parameters of non-cohesive soils in Poland was studied by (Parylak, 2000; Mamok, 2006; Chmielewski, 2008; Zięba, 2013).

The coefficient of uniformity ($C_U$) is still regarded as one of the basic parameters characterizing the aggregates/soils

intended for embankment construction. This parameter describes the shape of the grain-size curve. Since the 1970s the requirements for subsoil for road surface constructions in Poland are given in typical surface catalogues and include (Judycki et al., 2014a; Judycki et al., 2014b):

– non-swelling of the soil,
– $CBR \geq 10$ (after four days of water saturation); since 2014 also secondary modulus $E_2 \geq 80$ MPa,
– compaction in accordance with current standards or/and guidelines.

Non-swelling of the soil depends on the content of the dust and clay fraction and their activity – the sand equivalent (SE). In earthworks, the parameter relating to the ability to carry loads without excessive deformation is the bearing ratio or secondary modulus ($E_2$) determined with static load plate test (VSS). The value of the bearing ratio for non-cohesive soils depends mainly on the angle of repose.

The angle of repose depends on many factors, among others, the shape, roundness of the grain and the compaction (Hansen, Lundgren, Beuck & Rönfeldt, 2013). The influence of various factors on the angle of repose is determined by the Lundgren formula (Glazer, 1985):

$$\phi = 36° + \phi_1 + \phi_2 + \phi_3 + \phi_4 \quad (1)$$

where:
$\phi_1$ – grain shape –5° for round aggregates; +1° for angular (range 7°),
$\phi_2$ – dimensions of grains 0° for sands do +2° for coarse (range 3°),
$\phi_3$ – degree of compaction from –3° for $C_U < 5$ to +3° for $C_U \geq 15$ (range 7°),
$\phi_4$ – density index from –6° for loose soils to +6° for compacted soils (range 13°).

The shape of the grains can cancel out the impact of grading on the angle of repose.

The paper attempts to determine if there is a strong correlation between the California bearing ratio (*CBR*) and flow coefficient of the aggregates. The strength of the correlation with other parameters determining the suitability of soil/aggregates for earthworks was evaluated. Among others those parameters were: effective grain size, coefficient of uniformity ($C_U$), curvature coefficient ($C_C$) and dry density of solid particles.

## Determination of flow coefficient of aggregates

In the United States, the angularity of the aggregate is determined in accordance with AASHTO T 304 standard or ASTM C 1252. The porosity of the loose rock material passing through a standard 30 ml funnel into a cylinder is determined. In France, the test is carried out on the basis of AFNOR P18-564 standard. The time in seconds of flow (pouring) of a certain amount of aggregate through the funnel was determined as a measure of the angularity of the aggregate. Similar approach can be seen in comparative viscometers such as Engler's. The comparison of the results for above mentioned methods can be found in the study (Aschenbrener, 1994).

The same principle as in France is adopted in BS EN 933-6 standard. The flow rate of fine aggregate is determined on a 0.063/2 mm fraction. The laboratory sample is washed, dried and then reduced to reference test portion with $M_1$ mass according to the formula:

$$M_1 = \left( 1{,}000 \frac{\rho_p}{2.70} \pm 2 \right) \quad (2)$$

where:
$\rho_p$ – pre-dried particle density (EN 1097--6) [Mg·m$^{-3}$],
2.70 – constant, the density of reference material in dried state [Mg·m$^{-3}$].

A polycarbonate funnel with a 12 mm hole is used to test the 0/2 mm aggregates. The flow time ($E_{csi}$) is measured with a stopwatch with an accuracy of 0.1 s. Five runs are made. The aggregate flow time ($E_{cs}$) is calculated from the formula:

$$E_{sc} = E_{csm} + (E_{RS} - E_{cse}) \quad (3)$$

where:
$E_{csm}$ – average flow time [s],
$E_{RS}$ – flow time for reference material 32 s,
$E_{cse}$ – flow time for the reference test portion (30–34 s).

The apparatus for determining the flow time is extremely simple and includes a tripod polycarbonate funnel and a measuring cylinder. The bulk density of the aggregate in the measuring funnel and the measuring cylinder has a significant influence on the obtained results. This problem has been solved by using an additional cylinder with a shutter – Figure 1.

## Additional tests

Simultaneously while preparing the sample for determination of the flow coefficient of fine aggregates it is also possible to determine the grading curve of the soil. As the PN-B--04481:1988 standard was withdrawn in 2015, while the ISO/TS 17892-4:2004 technical specification was replaced in 2017 by the PN-EN ISO 17892-4:2017-01 standard, the grain composition was determined in accordance with the PN-EN 933-1:2012 standard.

The second test necessary to conduct the flow time of fine aggregates is the density determination by pycnometric method. The determination is carried out according to PN-EN 1097-6:2013 standard. Density of pre-dried grains is defined as the ratio of mass of the sample in

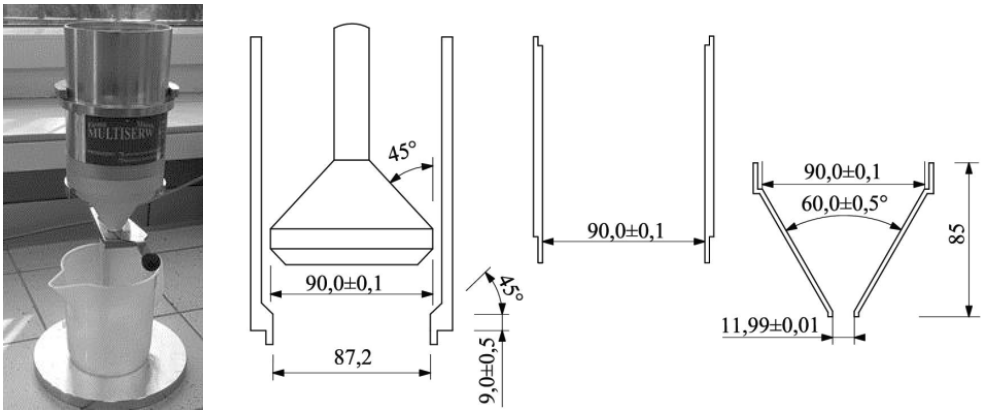


FIGURE 1. Aparatus required for the determination on the flow coefificent of fine aggragate

dry state to the volume it occupies in water. The mass is determined by weighing the sample in saturated state, surface--dried and then re-weighing. The volume is determined by weighing.

Two samples must be prepared for testing. The weight of the samples shall not be less than that given in Table 1. The first step is to wash the sample to get rid of clogged grains and to discard grains that remain on the 31.5 mm sieve and pass through the 0.063 mm sieve. The sample shall then be dried in the oven at 110 ±5°C. After drying, the aggregate shall be cooled to ambient temperature. The next step is to get a net weight $M_1$ of a setup with a known volume $V$ (Fig. 2) and put the sample in to determine the total weight of the setup $M_2$. The pycnometer is then filled with water ($T$ = 22 ±3°C) up to about 30 mm below the line at the neck. In order to remove the air, the sample is mixed with a glass rod. Afterwards, the pycnometer is filled with water up to 20 mm below the measuring line and placed in a water bath ($T$ = 22 ±3°C) for 1 h. It is important that the level in the water bath reaches 20 mm below the neck of the pycnometer. After one hour, the pycnometer should be taken out of the bath, the outer surface should be dried and then weighed

TABLE 1. Minimum mass of samples for density testing by pycnometer method

| Upper ($D$) aggregate size [mm] | Minimum mass of test specimen [kg] |
|---|---|
| 31.5 | 1.5 |
| 16 | 1.0 |
| 8 | 0.5 |
| ≥ 4 | 0.25 |

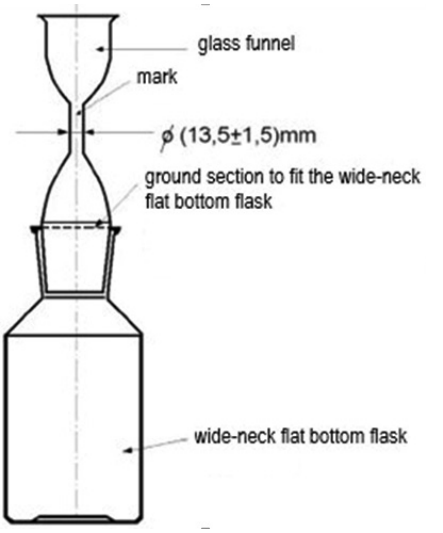


FIGURE 2. Pycnometer for determining the density of aggregates

to obtain $M_3$. After the test, calculate the density using the formula:

$$\rho_p = \frac{(M_2 - M_1)}{V - \dfrac{(M_3 - M_2)}{\rho_w}} \tag{4}$$

where:
$\rho_p$ – pre-dried grain density [Mg·m$^{-3}$],
$M_1$ – mass of pycnometer [g],
$M_2$ – mass of pycnometer with a sample [g],
$M_3$ – mass of pycnometer with a sample and water [g],
$V$ – pycnometer volume [mm$^3$].
$\rho_w$ – water density at set temperature [Mg·m$^{-3}$].

The density shall be determined to an accuracy of 0.001 Mg·m$^{-3}$. The accepted difference between two samples shall not exceed 0.019 Mg·m$^{-3}$. The final result is given as the average of two values with an accuracy of 0.01 Mg·m$^{-3}$.

As part of the research program, the *CBR* was additionally determined according to the procedure given in the PN-S-02205:1998 standard. The Proctor's test was included to determine the maximum dry density of solid particles ($\rho_{ds}$).

## Test materials

The research was carried out on 19 soils (Nos 1–19 in Table 2) from the area of north-western Poland, four washed and sieved sands (20–23) and seven crushed aggregates (24, 29 – basalt, 25, 30 – granite, 26 – greywacke, 27 – granodiorite, 28 – amphibolite). The materials were categorized in accordance with the PN-EN 14688-2:2018 standard. Majority of the studied soils were evenly and gap-graded, only a few sands with gravel and one coarse sand (10) could be categorized as medium-graded. As predicted, washed and sieved aggregates (20–23) were single-graded, while crushed sands were medium-graded or, as in case of 26, gap-graded. All the soils studied in terms of *CBR* values met the requirements for the construction of road embankments and other structural layers. Natural sands are characterized by $E_{cs}$ of 24 to 35 with an average value of 28, while crushed sands are characterized by $E_{cs}$ of 35 to 45 with an average of 40. The aggregates and soils were listed by the *CBR* values (Table 2).

TABLE 2. Soil and aggregates parameters taken for testing

| No | Type | $C_C$ [-] | $C_U$ [-] | $d_{10}$ [mm] | $d_{30}$ [mm] | $d_{60}$ [mm] | $\rho_{ds}$ [Mg·m$^{-3}$] | $\rho_p$ [Mg·m$^{-3}$] | *CBR* [%] | $E_{sc}$ [s] |
|---|---|---|---|---|---|---|---|---|---|---|
| 23 | MSa | 0.9 | 2.1 | 0.25 | 0.34 | 0.53 | 1.76 | 2.66 | 14 | 29 |
| 1 | FSa | 1.0 | 1.8 | 0.15 | 0.20 | 0.27 | 1.70 | 2.64 | 15 | 25 |
| 16 | FSa | 0.9 | 2.6 | 0.11 | 0.16 | 0.28 | 1.65 | 2.62 | 15 | 25 |
| 19 | MSa | 1.1 | 2.2 | 0.10 | 0.14 | 0.21 | 1.76 | 2.65 | 15 | 27 |
| 3 | MSa | 0.9 | 2.0 | 0.25 | 0.34 | 0.50 | 1.81 | 2.66 | 16 | 24 |
| 4 | FSa | 1.0 | 2.2 | 0.09 | 0.14 | 0.20 | 1.69 | 2.65 | 16 | 26 |
| 22 | MSa | 0.9 | 2.3 | 0.25 | 0.36 | 0.58 | 1.81 | 2.55 | 16 | 27 |
| 6 | FSa | 1.0 | 2.0 | 0.10 | 0.14 | 0.19 | 1.70 | 2.66 | 17 | 27 |
| 21 | MSa | 0.9 | 1.9 | 0.26 | 0.34 | 0.49 | 1.77 | 2.65 | 17 | 28 |
| 20 | MSa | 1.0 | 2.4 | 0.19 | 0.30 | 0.47 | 1.79 | 2.65 | 19 | 27 |
| 5 | MSa | 1.0 | 2.4 | 0.12 | 0.19 | 0.30 | 1.72 | 2.65 | 20 | 26 |
| 8 | MSa | 0.9 | 3.0 | 0.21 | 0.34 | 0.61 | 2.03 | 2.64 | 20 | 27 |
| 7 | MSa | 0.9 | 2.4 | 0.21 | 0.32 | 0.51 | 1.76 | 2.67 | 21 | 25 |
| 9 | MSa | 0.9 | 3.3 | 0.19 | 0.31 | 0.61 | 1.79 | 2.66 | 21 | 27 |
| 11 | MSa | 0.9 | 2.3 | 0.22 | 0.32 | 0.49 | 1.76 | 2.67 | 21 | 25 |
| 18 | grSa | 0.7 | 4.9 | 0.32 | 0.58 | 1.56 | 1.86 | 2.65 | 21 | 30 |
| 14 | MSa | 0.9 | 2.2 | 0.16 | 0.23 | 0.35 | 1.71 | 2.66 | 22 | 25 |
| 15 | MSa | 1.1 | 3.4 | 0.13 | 0.25 | 0.45 | 1.79 | 2.63 | 22 | 25 |

TABLE 2 cont.

| No | Type | $C_C$ [-] | $C_U$ [-] | $d_{10}$ [mm] | $d_{30}$ [mm] | $d_{60}$ [mm] | $\rho_{ds}$ [Mg·m$^{-3}$] | $\rho_p$ [Mg·m$^{-3}$] | *CBR* [%] | $E_{sc}$ [s] |
|---|---|---|---|---|---|---|---|---|---|---|
| 25 | CSa | 1.1 | 6.7 | 0.10 | 0.23 | 0.67 | 1.92 | 2.68 | 24 | 35 |
| 10 | CSa | 0.9 | 4.5 | 0.18 | 0.35 | 0.81 | 1.78 | 2.69 | 25 | 32 |
| 13 | grSa | 0.7 | 6.5 | 0.16 | 0.36 | 1.07 | 1.96 | 2.70 | 25 | 32 |
| 12 | grSa | 0.6 | 8.6 | 0.16 | 0.35 | 1.38 | 2.00 | 2.69 | 27 | 35 |
| 28 | CSa | 1.0 | 10.1 | 0.09 | 0.24 | 0.91 | 2.08 | 2.86 | 27 | 37 |
| 2 | grSa | 0.4 | 8.9 | 0.15 | 0.29 | 1.33 | 1.95 | 2.67 | 29 | 34 |
| 29 | CSa | 1.2 | 6.2 | 0.17 | 0.48 | 1.08 | 2.08 | 3.09 | 30 | 40 |
| 17 | grSa | 0.8 | 4.9 | 0.18 | 0.36 | 0.88 | 1.99 | 2.64 | 31 | 35 |
| 27 | CSa | 1.5 | 9.3 | 0.13 | 0.35 | 1.21 | 1.97 | 2.64 | 33 | 41 |
| 30 | CSa | 1.0 | 7.7 | 0.14 | 0.40 | 1.09 | 1.81 | 2.65 | 34 | 39 |
| 26 | CSa | 0.8 | 4.8 | 0.26 | 0.44 | 1.26 | 1.97 | 2.73 | 35 | 42 |
| 24 | CSa | 1.7 | 7.1 | 0.17 | 0.37 | 1.20 | 2.23 | 3.13 | 42 | 45 |

## Analysis of the relationship between the flow time and other parameters

The correlation between the parameters describing the grading curve, i.e. $C_U$ and $C_C$, and the *CBR* and volumetric density of the dry density of soils was analysed. The correlations were analysed for soils and aggregates together. Pearson coefficient of linear correlation was used to measure the relationship. Table 3 presents the obtained coefficient values for relations between selected parameters. Analysing the obtained dependencies, it should be stated first of all that the $C_C$ does not show any relation with the *CBR* or flow coefficient. For soils only there is a negative relation while for soils and aggregates together, no relation at all.

TABLE 3. Impact of individual stakeholder groups on the study contract (own studies)

| Parameter | Correlation coefficient | |
|---|---|---|
| | *CBR* | $E_{cs}$ |
| $C_U$ | 0.76 | 0.81 |
| $C_C$ | 0.29 | 0.33 |
| $d_{30}$ | 0.48 | 0.48 |
| $d_{60}$ | 0.76 | 0.78 |
| $E_{cs}$ | 0.90 | – |
| $\rho_{d\,max}$ | 0.77 | 0.80 |

However, as predicted, the $C_U$ shows much better dependence. The flow coefficient shows the highest values of dependence in relation to the coefficient of uniformity but also to the *CBR*. This indicates the potential of this simple study. Figures 3–5 present the correlation between major parameters and the confidence interval.

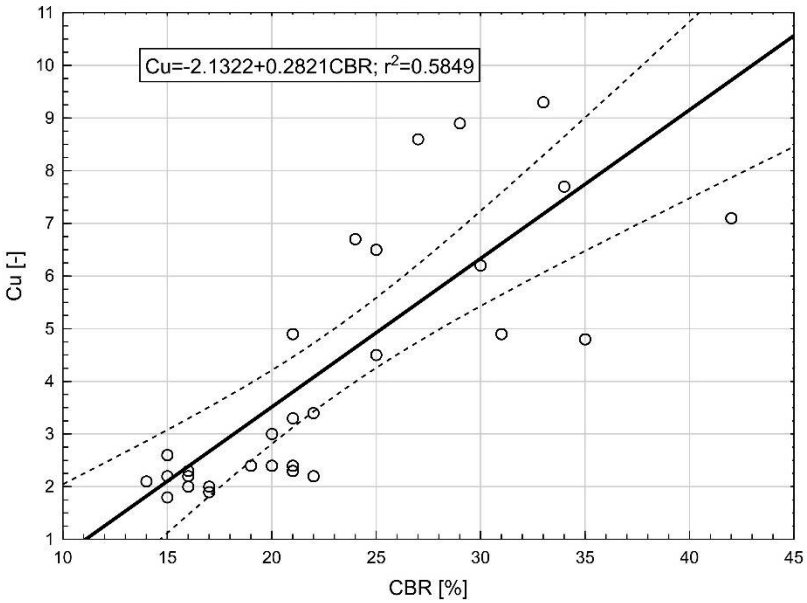


FIGURE 3. The relationship between the uniformity coefficient and *CBR*

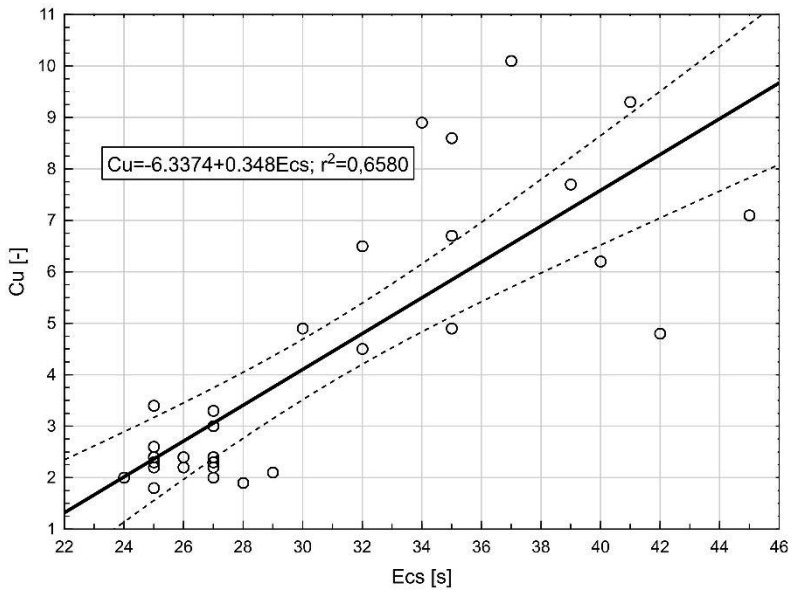


FIGURE 4. The relationship between the uniformity coefficient and flow coefficient of the aggregates

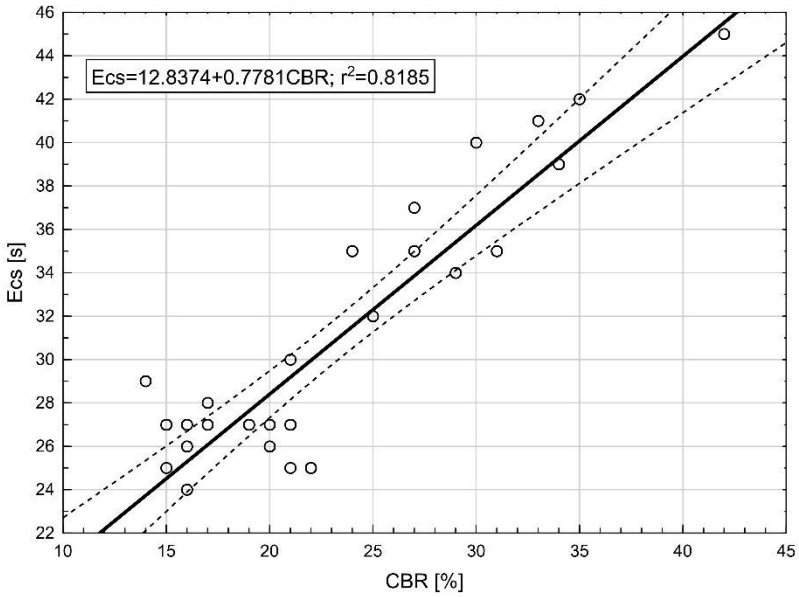


FIGURE 5. The relationship between the flow coefficient of the aggregates and *CBR*

## Recapitulation

The study tried to determine the correlation between the flow coefficient $E_{cs}$ and California bearing ratio as well as other parameters describing the non-cohesive soils. It was proven that for studied soils and aggregates the flow coefficient had the strongest correlation to the bearing ratio, which in the author's opinion is the most basic parameter for assessing the suitability of soils and aggregates for embankment's construction. Determination of soils and aggregates suitability based mainly on the coefficient of uniformity is improper. This can lead to exclusion of materials which can be safely used as subsoils for road construction. From tested materials all of them met the requirements of minimal *CBR*, some met the requirements for improved subgrade and freezing depth ($\geq 20$, $\geq 25$).

Flow coefficient of aggregates can be tested in a simple way and can be performed in parallel with screen analysis, assuming a density of $\rho_p = 2.65$ Mg·m$^{-3}$ for quartz sands. Natural sands were characterized by $E_{cs}$ flow coefficient from 24 to 35 with the mean value of 28, while crushed sands were characterized by $E_{cs}$ from 35 to 45 with the mean value of 40. However, analysing the results of the research it should be stated that for the same value of flow coefficient, e.g. 25, 27, there is a variability of *CBR* in the range of 15–22 and 15–21, respectively. Of course, this indicates that the flow coefficient is a rather simplified measure and detailed analyses of grain shape should be carried out using more precise methods and parameters, e.g. general shape index proposed by Parylak (2000).

## References


AASHTO T 304 (2017). *Standard method of test for uncompacted void content of fine aggregate*. Washington: American Association of State and Highway Transportation Officials.

AFNOR P18-564 (1990). *Determination du coefficient d'écoulement des sables* [*Determination of the flow coefficient of sands*]. Paris: PR Industrie.

Aschenbrener, T. (1994). *Implementation of a Fine Aggregate Angularity Test (Final Report CDOT-DTD-R-94-6)*. Denver: Colorado Department of Transportation.

ASTM C1252 (2017). *Standard test methods for uncompacted void content of fine aggregate (as influenced by particle shape, surface texture, and grading)*. West Conshohocken, PA: American Society for Testing and Materials.

Chmielewski, M. (2008). *Badania nad wpływem cech kształtu cząstek gruntów niespoistych na wybrane parametry ściśliwości* [*The studies on the influence of non-cohesive soil particle shape on the selected compressibility parameters*]. Wrocław: Uniwersytet Przyrodniczy we Wrocławiu.

EN 1097-6:2013. Tests for mechanical and physical properties of aggregates. Determination of particle density and water absorption.

Glazer, Z. (1985). *Mechanika gruntów* [*Soil mechanics*]. Warszawa: Wydawnictwa Geologiczne.

Hansen, J.B., Lundgren, H., Beuck, O. & Rönfeldt, L. (2013). *Hauptprobleme der Bodenmechanik* [*Problems in soil mechanics*]. Berlin: Springer.

ISO/TS 17892-4:2004. Geotechnical investigation and testing. Laboratory testing of soil. Part 4: Determination of particle size distribution.

Judycki, J., Jaskuła, P., Pszczoła, M., Alenowicz, J., Dołżycki, B., Jaczewski, M., Ryś, D. & Stiness, M. (2014b). *Katalog typowych konstrukcji podatnych i półsztywnych nawierzchni* [*Catalogue of typical semi-rigid and flexible pavements*]. Warszawa: Generalna Dyrekcja Dróg Krajowych i Autostrad.

Judycki, J., Jaskuła, P., Pszczoła, M., Ryś, D., Jaczewski, M., Alenowicz, J., Dołżycki, B. & Stiness, M. (2014a). *Analizy i projektowanie konstrukcji nawierzchni podatnych i półsztywnych* [*Analyses and design of semi-rigid and flexible pavements*]. Warszawa: Wydawnictwa Komunikacji i Łączności.

Little, D., Button, J., Jayawickrama, P. & Hudson, B. (2003). *Quantify shape, angularity and surface texture of aggregates using image analysis and study their effect on performance*. Austin: Texas Transportation Institute.

Mamok, B. (2006). *Wpływ zagęszczenia i nieregularności kształtu cząstek drobnoziarnistych gruntów niespoistych na wartości kąta tarcia wewnętrznego* [*The influence of the compaction and shape irregularities of fine-grained non-cphesive soils on the values of internal friction angle*]. Wrocław: Uniwersytet Przyrodniczy we Wrocławiu.

Mitchell, T. (ed.) (2001). *Superpave mixture. Design guide*. Washington: U.S. Department of Transport, Federal Highway Administration.

Parylak, K. (2000). Charakterystyka kształtu cząstek drobnoziarnistych gruntów niespoistych i jej znaczenie w ocenie wytrzymałości [Characteristics of particle shape of fine-graded cohesionless soils and its significance in strength assessment]. *Zeszyty Naukowe Politechniki Śląskiej*, *90*, 3-130.

PKN-EN ISO 14688-2:2018. Rozpoznanie i badania geotechniczne. Oznaczanie i klasyfikowanie gruntów. Część 2: Zasady klasyfikowania [Geotechnical investigation and testing. Identification and classification of soil. Part 2: Principles for a classification].

PN-B-04481:1988. Grunty budowlane. Badania próbek gruntu [Construction soils. Testing of soil samples].

PN-EN 1097-6:2013. Badania mechanicznych i fizycznych właściwości kruszyw. Część 6: Oznaczanie gęstości ziarn i nasiąkliwości [Tests for mechanical and physical properties of aggregates. Part 6: Determination of particle density and water absorption].

PN-EN 933-1:2012. Badania geometrycznych właściwości kruszyw. Część 1: Oznaczanie składu ziarnowego. Metoda przesiewania [Tests for geometrical properties of aggregates. Part 1: Determination of particle size distribution. Sieving method].

PN-EN 933-6:2014. Badania geometrycznych właściwości kruszyw. Część 6: Ocena właściwości powierzchni [Tests for geometrical properties of aggregates. Part 6: Assessment of surface characteristics].

PN-EN ISO 17892-4:2017-01. Rozpoznanie i badania geotechniczne. Badania laboratoryjne gruntów. Część 4: Badanie uziarnienia gruntów [Geotechnical investigation and testing. Laboratory testing of soil. Part 4: Determination of particle size distribution].

PN-S-02205:1998. Drogi samochodowe. Roboty ziemne. Wymagania i badania [Car roads. Earthworks. Requirements and tests].

Quiroga, P.N. & Fowler, D.W. (2004). *The effects of aggregates characteristics on the performance of Portland cement concrete*. Austin: International Center for Aggregates Research, The University of Texas.

Szerakowska, S. (2018). *Ocena parametrów kształtu ziaren i ich wpływu na zagęszczalność gruntów niespoistych* [*Asessment of grain shape parameters and their influence on the compactability of non-cohesive soils*]. Białystok: Politechnika Białostocka.

Topal, A. & Sengoz, B. (2005). Determination of fine aggregate angularity in relation with the resistance to rutting of hot-mix asphalt. *Construction and Building Materials*, *19*(2), 155–163. https://doi.org/10.1016/j.conbuildmat.2004.05.004

Zięba, Z. (2013). *Wpływ cech kształtu cząstek drobnoziarnistych gruntów niespoistych na ich wodoprzepuszczalność* [*Influence of particle shape of fine-grained soils on their permeability*]. Wrocław: Politechnika Wrocławska.

## Summary

**Flow coefficient of the aggregates as a parameter characterizing the suitability of non-cohesive soils for earthworks.** The article presents the results of the flow coefficient of aggregate for 30 sands and aggregates. The introduction of European standards for the assessment of construction aggregates over 20 years ago introduced a number of new testing methods not previously used in Poland. One of them is the flow coefficient of aggregate, popularly called aggregate angularity. The method of determination is given in the standard PN-EN 933-6:2014. This standard defines the method of determining the index for coarse aggregates with grain sizes between 4 and 20 mm and fine aggregates with grain sizes below 2 mm. This test is particularly important when designing mineral-asphalt mixtures. Aggregate angularity, particularly in fine aggregates, is the main factor influencing the workability of mixtures. The flow time through the apparatus depends on the degree of roundness and form of the grain. The study determined the relationship between the flow coefficient of aggregate and *CBR* in relation to the uniformity coefficient. This indicator is still considered to be one of the main parameters that affect the suitability of non-cohesive soils in earthworks. It was proven that $E_{cs}$ is more dependent on *CBR* than $C_U$.

**Authors' address:**
Stanisław Majer
(https://orcid.org/0000-0003-2476-1982)
Zachodniopomorski Uniwersytet Technologiczny w Szczecinie
Wydział Budownictwa i Inżynierii Środowiska
Katedra Dróg i Mostów
al. Piastów 50a, 71-310 Szczecin
Poland
e-mail: majer@zut.edu.pl

Scientific Review – Engineering and Environmental Sciences (2020), 29 (3), 308–318
Sci. Rev. Eng. Env. Sci. (2020), 29 (3)
Przegląd Naukowy – Inżynieria i Kształtowanie Środowiska (2020), 29 (3), 308–318
Prz. Nauk. Inż. Kszt. Środ. (2020), 29 (3)
http://iks.pn.sggw.pl
DOI 10.22630/PNIKS.2020.29.3.26

**Kazimierz GWIZDAŁA, Paweł WIĘCŁAWSKI**

Gdansk University of Technology, Faculty of Civil and Environmental Engineering

# Displacement piles – classification and new methods for the calculation of bearing capacity

**Key words:** displacement pile, bearing capacity, load–settlement, pile foundation, Eurocode 7

## Introduction

When we are paying great attention to ecology in the broadest sense of the word, we should strive to use technology that will be environmentally friendly and have a minimal impact on the environment.

Deep foundation solutions are of particular importance, as they are in any case interference with the environment and the natural ground. The classic division of pile foundations includes:

– ready-made, prefabricated piles, prepared in advance, inserted into the ground using various techniques, e.g. wooden, reinforced concrete, steel and plastic piles;
– piles made in the ground, e.g. drilled, driven in with an extractor pipe, screwed in without a casing pipe (Gwizdała, 2010).

The classification of piles used so far is being modified due to the manufacturing technology. Today, displacement piles are increasingly used. As an additional element there are constantly appearing new materials used for pile construction. Another aspect is existence of the methods for calculating the load capacity and settlement of piles. Since 2010, after the introduction of the PN-EN:1997-1:2008 standard, it was necessary to change the approaches used so far based on years of experience and tradition. The old methods have been improved by defining coefficients allowing to extrapolate the settlement curve from the range of critical values to limit values.

To a large extent these are empirical procedures. The main determinant in the process of designing and then verifying the load capacity of piles has become the determination of the force that causes settlements equal to 10% of the pile diameter.

## Classification of displacement piles

Displacement piles is a group of technologies whose main idea is to install or make piles without excavating the ground. In accordance with this definition, contained in PN-EN:1997-1:2008 standard, the displacement piles should be considered as hammered in, pressed in, vibrated and executed with the use of spreading drills (Fig. 1).

- easy adaptation of the current length to local soil conditions;
- possibility of ongoing control by measuring the momentum and verifying the depth into the ground;
- possibility of ongoing control using dynamic formulas and dynamic tests;
- possibility of making inclined piles in a large inclination range.

Wide use of prefabricated piles is possible thanks to a wide range of cross-sections, from 20 × 20 to 45 × 45 cm every 5 cm, respectively, and different lengths (Gwizdała, 2010).

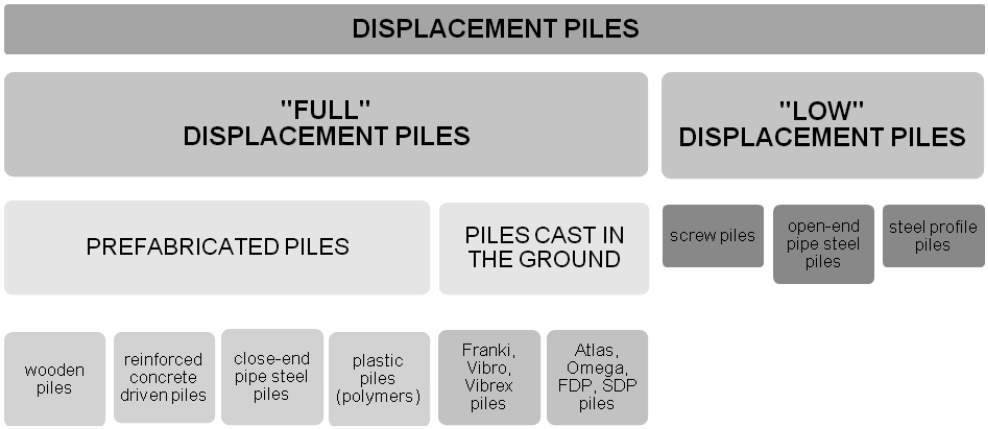


FIGURE 1. Classification of displacement piles

## Prefabricated reinforced concrete driven piles

Prefabricated reinforced concrete driven piles are known and used in various types of construction in Poland for many years. Their use is determined by the following advantages:

- execution speed, from 200 to 350 m piles per day using piling machine;
- considerable pile length, using combined piles up to 50 m;

## Pipe steel piles

Steel piles are most often used in hydrotechnical construction, marine and bridge construction. Made of closed or open steel pipes with diameters from 400 to 2,500 mm. Recently, they have very often been used to build offshore wind turbines foundation as monopiles


FIGURE 2. Types of piles: a – prefabricated reinforced concrete piles (photo by K. Gwizdała); b – pipe piles (photo by K. Gwizdała); c – steel profile piles (©Thyssen Krupp); d – wooden piles (photo by K. Gwizdała); e – plastic piles (©Akerpol.pl); f – disc screw pile (©sw.birmiss.com)

with diameters of up to several meters (Fig. 2).

**Steel profile piles, combined elements**

Sometimes there ate used steel piles from sheet piling walls and sections. Combined piles can transmit vertical forces, but above all significant bending moments. These solutions have been successfully used for many years on the Polish coast for hydrotechnical and marine construction.

**Wooden piles**

Wooden piles are the oldest type of displacement piles. Properly applied, they are an economic and safe way of founding objects, as evidenced by the numerous historic buildings founded on piles. The advantages of wooden piles include:

– low material cost;
– durability in optimal conditions over 100 years (under water);
– resistance to stray currents;
– do not require corrosion protection;
– are driven using typical pile driver equipment.

**Plastic piles**

In the face of growing environmental concerns, new products made of recycled plastic or vinyl are appearing on the market. Among these products are also piles and sheet piles. The advantage of the material is that it can be processed with standard tools for wood and metal.

The material from which they are made is characterised:

– waterproofing;
– resistance to rotting and corrosion;
– no reaction with water and soil;
– resistance to chemicals, salt and sea water.

**Screw piles**

The technology consists in screwing a pipe with a screw-shaped spiral into the ground. To make it, pipes with high resistance to torsional moments caused by significant forces needed to sink are required. Another solution in this subgroup are disc-shaped bolt piles, designed to carry low loads, consisting of perches and spiral carriers. The advantage of this design is the possibility of increasing the length of piles by adding more segments. The load-bearing capacity of the pile can be increased by injecting it through a rod. The piles reach a load capacity of up to 500 kN.

**Vibro, Vibrex and Franki piles**

Vibro, Vibro-Fundex, Vibrex piles are fully displacement piles made in the ground, without bringing the ground to the surface. The most commonly used shank diameters are 457 and 508 mm, the diameter of the lost steel base is larger and ranges from 500 to 700 mm. Enlarged diameter of the steel shoe causes that we get immediately a pile with an extended base (Fig. 3a). Pulling the pipe out with a vibrator compacts the concrete and ensures that the pile shaft is well connected to the ground. Vibro--Fundex piles are characterized by very favourable characteristics, i.e. high load capacity for small settlements. Franki piles are one of the oldest deep foundation techniques. After some modifications, this technology is still used today with great success. The diameter of a steel pipe usually ranges from 500 to 600 mm, length from 12 to 20 m. The steel pipe is driven into the interior with a dry concrete plug using a free fall tup insert. Knockout of the cork with a rammer causes the formation of an enlarged base (Fig. 3b), and successive lifting of the steel pipe using a winch with simultaneous concrete filling – forming a sideway well connected with the surrounding ground (Gwizdała, 2010).

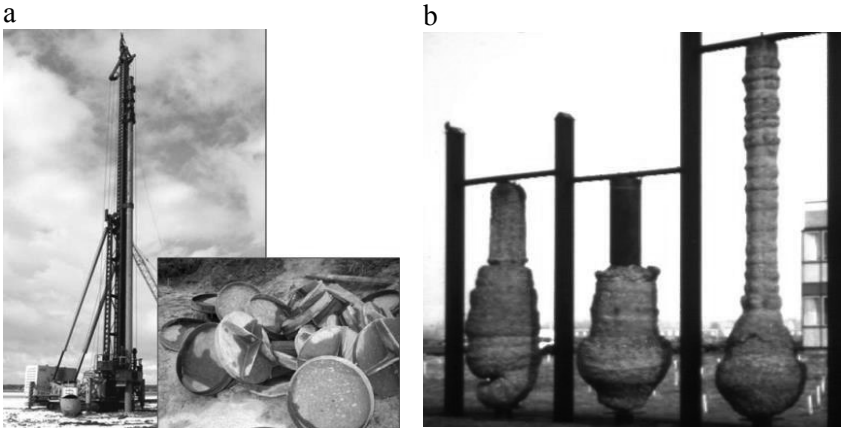


FIGURE 3. a – execution of the Vibro pile and steel base (photo by K. Gwizdała); b – Franki piles (photo by K. Gwizdała)

**Atlas, Omega, FDP, SDP piles**

A subgroup of displacement piles made by means of augers of special construction and geometry. The drill is immersed in the ground without a casing pipe and excavation of ground material to the surface (Fig. 4). Moving the soil horizontally to the sides and vertically and diagonally at the base causes the soil to compact in the immediate vicinity of the pile, increase in the horizontal pressure component and generate pore water pressure in the soil. Pile diameters usually range from 400 to 600 mm and length up to 30 m. The piles are characterized by high load capacity and small settlements, however, they require drilling machines with a sufficiently high torque (Gwizdała, 2010).

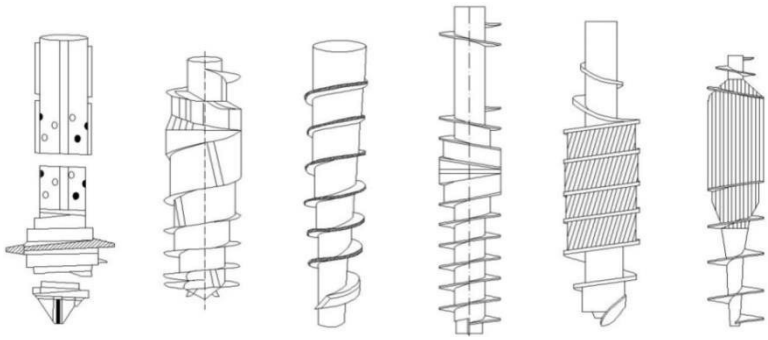

FIGURE 4. Drills of screw displacement piles (Gwizdała, 2013)

## Capacity of displacement piles

According to the PN-EN 1997--1:2008 standard, we distinguish four methods of designing pile foundations based on:

- the static load test results (SPLT);
- empirical or analytical calculation methods;
- the results of a dynamic test (DLT);
- observations of the behaviour of comparable pile foundations.

## Interpretation methods for static load tests

The only reliable source of verification is the static test load carried out for subsidence and limit-bearing capacities, or to the extent that it allows for their precise determination. In the literature you can find proposals for methods of extrapolation of incomplete *Q*–*s* curves, which enable the estimation of settlement limits and pile-bearing capacity (Gwizdała, 2013). They do not take into account such factors as: the way the piles are made; the roughness and stiffness of the pile shaft, but only the general trend of the *Q*–*s* curve. The most popular methods of curve extrapolation from a static survey include: PN-83/B--02482 standard, Gwizdała, Brinch-Hansen, Chin, Davisson (Gwizdała, 2013;

Więcławski, 2018), Meyer–Kowalow (Meyer & Szmechel, 2012) method and many more.

In tests carried out on prefabricated reinforced concrete, pipe, wood and plastic piles, which have a smooth surface and a regular base surface, "full" settlement curves are obtained. In this case, the conventional ultimate limit resistance can be read directly from the graph or extrapolated to this value without fear of major error. As a verification, a pile drive analysis (PDA) can also be used. This is not the case with piles formed in the ground by means of vibrators, which compacts the ground around the sidewalk and with an extended base, as is the case with Vibro, Vibrex and Franki technology.

The scattering of the minimum to maximum load limit value obtained by means of different methods of interpreting static loads for Vibro piles is almost 50%. Recently, Więcławski (2018) proposed an empirical method based on more than a hundred real curves from test loads for this technology. The condition for the application of the method is the quasi-linear character of the settlement curve resulting from the location of the pile base in non-cohesive soils, mainly compacted medium and fine sands.

In standard test loads, the result is a settlement curve and this is sufficient to verify the load capacity of the pile. However, a common procedure is to determine the load distributions for each part of the pile. Various extensometer or fiber optic systems are used for this purpose for all pile technologies. Research of this nature for displacement piles, both precast reinforced concrete and ground-based, driven and screwed, was popularized by Krasiński (Krasiński, 2012; Gwizdała, 2013; Gwizdała & Krasiński, 2013).

In his research Krasiński used a neostrain system, in the form of a chain of string extensometers mounted in canals inside the pile. The results of the test beyond the total settlement curve are the friction curves at the side of the pile depending on the depth and the resistance curve at the base of the pile. Friction on the sidewalk is taken into account in the test, depending on the ground layer.

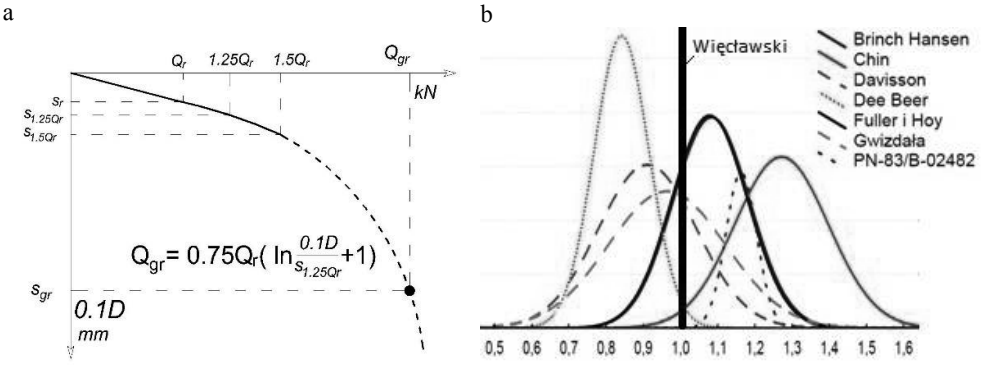


FIGURE 5. a – the Więcławski method of limiting load capacity based on extrapolation of the settlement curve for Vibro piles; b – distributions of the limit load value obtained with different methods in relation to the values from the Więcławski method (Więcławski, 2018)

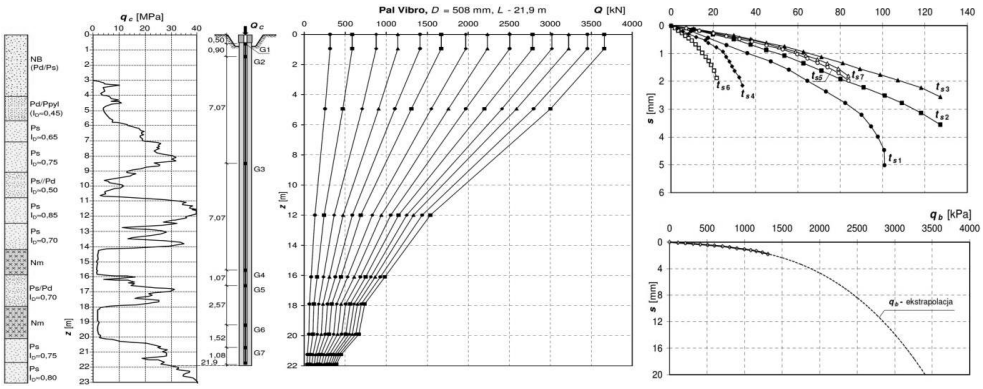


FIGURE 6. Interpretation of the static test load with resistance distribution along the side surface and under the pile base using the neostrain system (Gwizdała et al., 2013)

## Analytical methods for determining the value of bearing capacity

Assessing the load capacity and settlement of a single pile in complex geotechnical conditions is a very difficult engineering task. They're determined on a basis:

- calculations made on the basis of soil tests;
- correlations, empirical or semi-empirical methods based on field tests and static load test results;
- methods based on transformation functions, determined analytically or in model tests;
- finite element methods (FEM), boundary element methods (MEB) or other matrix solutions.

More and more rarely, methods of determining the geotechnical parameters of the subsoil on the basis of statistical methods and the so called B method popular in Poland are used. For design, we use the soil parameters from in-situ tests with high efficiency, among which the CPT results are the most important. On the basis of the probe measurements, we can apply direct methods and estimate the load capacity of the piles. The standard PN-EN 1997-1:2008 does not impose a calculation method, it proposes to use for example the methods from the old German standards DIN 1054, the Schmertmann method, the Dutch method of DeRuiter and Beringen (Gwizdała, 2010; Gwizdała, Brzozowski & Więcławski, 2010). The only condition is the application of an appropriate calculation approach, which involves the selection of appropriate correlation and safety factors.

The French method of Bustamante and Giasenelli – LCPC and the Gwizdała and Stęczniewski method have been used in Poland for years. The popularity of the latter results from the definition of individual relationships for local conditions and the detailed classification of the layout of the subsoil layers, hence a specific scheme is used for the calculations. An additional advantage is that we take into account the technology of mak-

ing piles, for Vibro we have individual load capacity coefficients (Gwizdała & Stęczniewski, 2004; Gwizdała, 2010).

$$q_{bu} = \psi_1 \cdot \overline{q}_c \,,\; q_{sui} = \frac{\overline{q}_{csi}}{\psi_{2i}} \tag{1}$$

where:
$q_{bu}$ – unitary limiting resistance under the base of the pile,
$\overline{q}_c$ – average resistance under the probe cone at the base of the pile,
$q_{sui}$ – unitary limiting resistance at the pile side within the $i$-th calculation layer,
$\overline{q}_{csi}$ – averaged resistance under the probe cone within the layer.
$P_A$ = 1.0 MPa.

The prediction of the full load–settlement characteristics is reliable. Such a solution is provided by methods based on a hyperbolic model of the settlement curve, adopted mainly in transformation functions, and a complex, linear-exposure model, which reflects with great accuracy the interaction of the ground with displacement piles. The transformation functions have great practical applications. They allow for non-linear load–sitting relationships. Functions are used to describe the relationship between the resistance at the side of the pile and displacement ($t$–$z$ curve) and the relationship between the resistance under the base of the pile and its displacement ($q$–$z$ curve). In the literature there are many items containing the description of transformation functions, among others Gwizdała, Vijayvergiya, Van Impe, Randalph and Wroth or Hirayama (Gwizdała, 2010). Analytical methods are most often combined with transformational functions. On the basis of the classical approaches, the values of the side and base resistance are determined, and using the appropriate function $t$–$z$ and $q$–$z$, the possible course of the settlement curve is determined for the calculated limit resistance and accepted limit settlements (Gwizdała & Krasiński, 2016).

$$q_b = q_{b;f}\left(\frac{s_b}{z_f}\right)^{\beta} \quad \text{for } q_b \le q_{b;f}$$

$$q_s = q_{s;\max}\left(\frac{s_s}{z_v}\right)^{\alpha} \quad \text{for } q_s \le q_{s;\max} \tag{2}$$

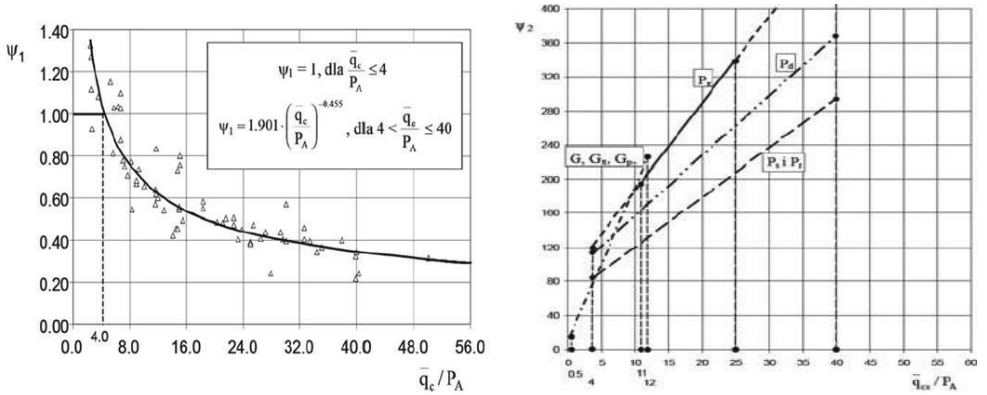


FIGURE 7. Capacity coefficients for Vibro piles in the Gwizdała–Stęczniewski method (Gwizdała, 2013)

where:
$\alpha$, $\beta$ – function exponent,
$z_v$ – pile sidewall displacement at which maximum soil friction is mobilized $q_{s;\max}$,
$z_f$ – displacement of the pile base at which boundary soil resistance is mobilized $q_{b;f}$ under the base.

TABLE 1. Proposed parameters of transformation functions

| Specification | $z_v$ | $\alpha$ | $z_f$ | $\beta$ |
|---|---|---|---|---|
| Driver precast concrete piles | 0.01$D$ | 0.50 | 0.05$D$ | 0.25 |
| Vibro piles | 0.01$D$ | 0.25 | 0.05$D$ | 0.25 |
| SDP, SDC, CMC | 10 mm | 0.38 | 0.1$D$ | 0.38 |

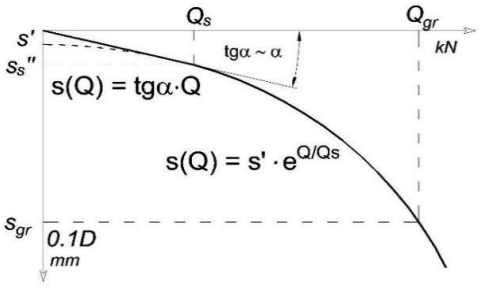


FIGURE 8. Idea of the Więcławski method and correlations to determine the settlement curve for Vibro piles in medium sands (Więcławski, 2016)

The philosophy of direct determination of the settlement curve based on CPT test results is particularly useful for the purpose of optimal design and use of the load-bearing capacity of piles.

This is opposed to the proposal of the Więcławski empirical direct method for Vibro piles. The main assumption of the method is a two-phase load–setting characteristic. This means that there is initially a linear displacement which includes the mobilisation of resistance at the side of the pile and then a non-linear displacement as a result of exceeding the boundary friction and mobilisation of resistance under the base of the pile.

$$\frac{s''}{Q_s} = 2D\left\{0.022\left[\frac{q_{c,avg}\cdot L}{2L_{gn}}\right]^{-D}\right\} \qquad (3)$$

$$s' = 1.17\ln\left(\frac{s''}{Q_s}\right) + 8.91 \text{ (for MSa)}$$

where:
$Q_s$ – load initiating the elasto-plastic phase of the pile–soil interaction for settlement $s_s''$,
$D$ – piles diameter,
$q_{c,avg}$ – average resistance $q_c$ from *CPT*,
$L$ – piles length,
$L_{gn}$ – depth of the pile base in medium sand,
$s'$ – initial point of non-linear load––settlement function for $Q$ = 0 kN.

The above dependencies (3) are of universal character for Vibro piles made in soils stratified with a base in medium sands throughout Poland (Więcławski, 2016). Detailed guidelines and relationships for other conditions are presented in the author's work. An important aspect is that the method can be adapted to specific local conditions. An example is the adaptation of the method to the geotechnical conditions prevailing in coastal areas in sea ports in Gdynia and Szczecin (Więcławski, 2019).

The method is characterized by high accuracy comparable to the methods of interpretation of static and dynamic test loads.

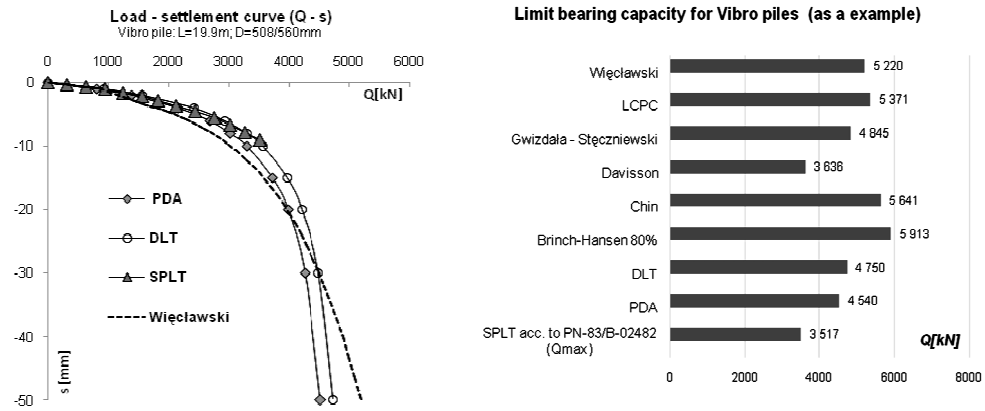


FIGURE 9. Summary of the results of the limit load capacity obtained on the basis of analytical methods and field tests for Vibro pile: $L$ = 19.9 m, $D$ = 508/560 mm (Gwizdała, 2013)

## Conclusions

The displacement piles allow for rational and economic execution of deep foundation in any soil conditions (Biliszczuk, 2019). It's affecting it:

– greater control of the piling process than in the case of drilled piles;
– immediately after piling, the next works can be started, without waiting for the concrete to set, which generally speeds up the foundation works;
– the displacement piles technology does not require excavation, storage or removal of soil from the excavated material, which is cumbersome in the case of drilled piles and weak-bearing soil (especially in built-up areas).

Recent calculation methods make it possible to precisely assess the interaction between piles and the ground centre. The trend of forecasting the full characteristics of the $Q$–$s$ pile affects the development of design methods, the main criterion of which is settling. This approach allows the full potential of the pile structure to be exploited for load-bearing purposes. Displacement piles are able to carry significant vertical and horizontal loads, which are influenced by changes in the state of stress in the ground, resulting from their technology.

## References

Biliszczuk, J. (2019). *Ekologia czy ekonomia? Aspekt decydujący o zastosowaniu pali przemieszczeniowych do posadowienia obiektów mostowych* [*Ecology or economy? The aspect determining the use of displacement piles for the foundations of bridge structures*]. Wrocław: Dolnośląskie Wydawnictwo Edukacyjne.

Gwizdała, K. (2010). *Fundamenty palowe, technologie i obliczenia* [*Pile foundations, technologies and calculations*]. Warszawa: Wydawnictwo Naukowe PWN.

Gwizdała, K. (2013). *Fundamenty palowe. Badania i zastosowanie* [*Pile foundations. Testing and application*]. Warszawa: Wydawnictwo Naukowe PWN.

Gwizdała, K., Brzozowski, T. & Więcławski, P. (2010). Calculation aspects used in Eurocode 7 for pile foundation. In *From Research to*

*Design in European Practice*, Bratislava, Slovak Republic, 2-4 June 2020.

Gwizdała, K. & Krasiński, A. (2013). Bearing capacity of displacement piles in layered soils with highly diverse strength parameters. In *Proceedings of the 18th International Conference on Soil Mechanics and Geotechnical Engineering* (pp. 2-5).

Gwizdała, K. & Krasiński, A. (2016). Fundamenty palowe, obliczenia z zastosowaniem zasad Eurokodu 7 i doświadczeń krajowych [Pile foundations, calculations according to Eurocode 7 rules and local experiences]. *Acta Scientiarum Polonorum. Architectura*, *15*(2), 3-22.

Gwizdała, K. & Stęczniewski, M. (2004). Obliczanie nośności i osiadań pali Vibro na podstawie sondowania sondą statyczną [Estimation of bearing capacity and settlement of Vibro-piles based on cone penetration test (CPT)]. *Inżynieria i Budownictwo*, *60*(6), 328-331.

Krasiński, A. (2012). Proposal for calculating the bearing capacity of screw displacement piles in non-cohesive soils based on CPT results. *Studia Geotechnica et Mechanica*, *24*(4), 41-50.

Meyer, Z. & Szmechel, G. (2012). Metoda interpretacji testów statycznych obciążeń pali prefabrykowanych [Interpretation method of static pile test]. *Zeszyty Naukowe Politechniki Rzeszowskiej. Budownictwo i Inżynieria Środowiska*, *59(3/4)*, 57-64.

PN-83/B-02482. Fundamenty budowlane. Nośność pali i fundamentów palowych [Building foundations. Bearing capacity of piles and pile foundations].

PN-EN 1997-1:2008. Eurokod 7: Projektowanie geotechniczne. Część 1: Zasady ogólne [Eurocode 7: Geotechnical design. Part 1: General principles].

PN-EN 1997-2:2008. Eurokod 7: Projektowanie geotechniczne. Część 2: Rozpoznanie i badania podłoża gruntowego [Eurocode 7: Geotechnical design. Part 2: Identification and soil tests].

Więcławski, P. (2016). *Methodology for estimating settlement of Vibro piles based on CPT*. Gdańsk: Gdansk University of Technology.

Więcławski, P. (2018). Metoda szacowania nośności granicznych pali Vibro na podstawie quasi-liniowych krzywych osiadania [The method of estimating the ultimate load capacity of Vibro piles on the basis of quasi-linear settlement curves]. *Inżynieria Morska i Geotechnika*, *6*, 410-416.

Więcławski, P. (2019). The application of phenomenological methodology for designing pile foundation in port structures. *Polish Maritime Research*, *1*(2019), 49-54.

## Summary

**Displacement piles – classification and new methods for the calculation of bearing capacity.** The paper presents technological changes concerning not only the method of construction, but also the materials used. Another aspect is the methods of calculating the load-bearing capacity and settlement of piles. With acceptance for use the PN-EN:1997-1:2008 standard in 2010, it was necessary to change the approaches applied that based on many years of experience and tradition. The best method in this case is to forecast the full load-settlement characteristics. On the basis of the collected data, a comparative analysis of particular displacement piles technologies was made. The usefulness of individual methods of load-bearing capacity calculation depending on the pile technology was determined.

**Authors' address:**
Paweł Więcławski
(https://orcid.org/0000-0002-8681-7083)
Politechnika Gdańska
Wydział Inżynierii Lądowej i Środowiska
ul. Narutowicza 11/12, 80-233 Gdańsk
Poland
e-mail: pawwiecl@pg.edu.pl

Scientific Review – Engineering and Environmental Sciences (2020), 29 (3), 319–331
Sci. Rev. Eng. Env. Sci. (2020), 29 (3)
Przegląd Naukowy – Inżynieria i Kształtowanie Środowiska (2020), 29 (3), 319–331
Prz. Nauk. Inż. Kszt. Środ. (2020), 29 (3)
http://iks.pn.sggw.pl
DOI 10.22630/PNIKS.2020.29.3.27

**Azealdeen Salih Al-JAWADI, Yousra Taha ABDUL BAQI, Ali Mohammed SULAIMAN**

Mosul University, Dams and Water Resources Research Center

# Qualifying the geotechnical and hydrological characteristic of the Bandawaya stream valley – Northern Iraq

**Key words:** geotechnical characteristics, hydrology, Bandawaya, dam, stream valley, Northern Iraq

## Introduction

Hydrological systems are critically important for maintaining vital water supplies, which alarmingly deplete every day. Suitable structures are necessary to maintain permanent or seasonal vapor surface runoff or basic flow. This water is used for improving soil moisture availability, recharge the groundwater, circumvent extreme runoff, and assistance in flood control in the inferior catchment. Such structures are responsive, depending on these parameters, to variations in geotechnical and hydrological parameters through the intact rock properties, discontinuities features, location, slopes of land, type of soil, rainfall and land cover.

Bandawaya village is about 40 km northwest city of Mosul, beside the village a permanently flowing stream, the stream formed from Duhok mountain in the north passing the village and later pouring in Mosul dam reservoir, as shown in Figure 1. The good amount of water flowing in the stream is from runoff in the rainy season and/or from springs in even dry season (summer), as shown in Figure 2A. At the middle length of this stream the cross-section of the valley is contracted at the plunges of Alquosh and Dahkan anticlines. This contraction is the study area, and looks a good place for dam construction from the first view.

Geomorphologically, the region of the meandering stream valley generally extends from north to south. The high of the west bank is approximately 120 m, and the east bank is approximately 80 m (Fig. 2B).

The topographical, hydrological, and geological parameters should be well given in the advancement of site selection for the performance of the dam safety guarantee. The seven sections of the

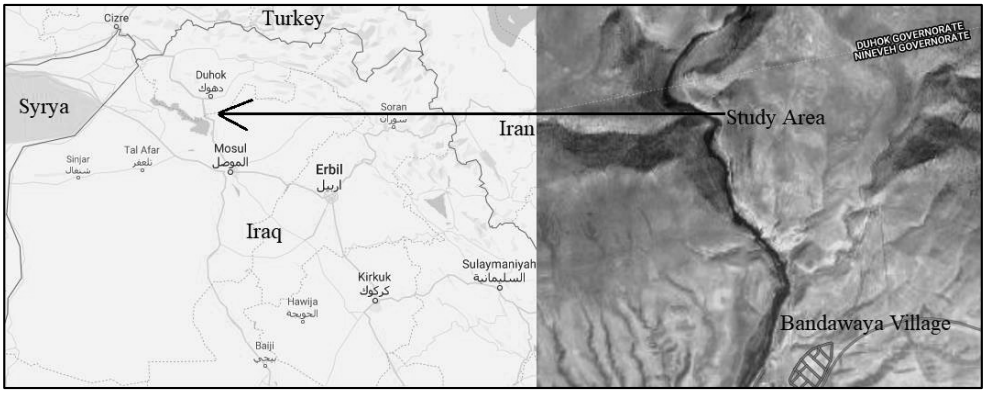


FIGURE 1. The location of the study area with the stream spilling in Mosul dam reservoir

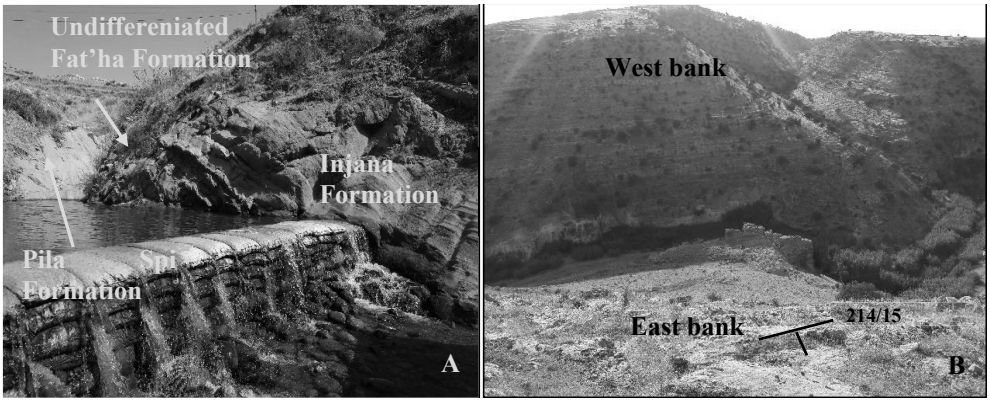


FIGURE 2. Bandawaya stream valley: A – water quantity in the summer season (photo by Azealdeen Al-Jawadi, 03.08.2018); B – view of proposed site dam

code of practice will be applied to the qualification of the site (BS 5930, 2009). These sections include primary factors, ground studies, field observations, laboratory experiments, soil and rock descriptions, reports, and interpretations (BS 5930, 2009). Khan (1992) explained that small barriers are built over existing rivers for the processing and storage of the rivers from the catchment. In the 1992 environmental restoration of degrade areas, the 13.5-meter high earthen dam installed in the undulating region of the Relmajra village – the Nawashahar District was studied, with a potential for introducing a region of approximately 25 ha of additional irrigation to that dam (Samra, Bansal, Sikka, Mittal & Agnihotri, 1995).

The objective of this study is to qualify and evaluate the geotechnical and hydrological characteristics of the Bandawaya stream valley, since water behind this dam can be restricted and used in agriculture and energy production. Furthermore, aimed to conserve the excellent water quality and good quantity in this valley and not allo-

wed it to spill into Mosul dam reservoir, the access to the goal is constructing a dam in the gorge of Bandawaya.

## Geological setting

The study area is the gorge of Bandawaya in a stream valley between the two plunges; western Alquosh anticline and eastern Dahkan anticline (Fig. 3). Single plunge anticlines are both Alquosh and Dahkan. For Pila Spi Formation (Middle--Upper Eocene), the lithology of limestone, dolomitic limestone, or dolomite is dominant for the stream valley and sometimes for the formations Fat'ha (Middle Miocene) and Injana (Upper Miocene), marl, sandstone, and claystone (Jassim & Goff, 2006). Slope deposits are mildly cemented; rock fragments, sand, and silt, surround both anticlines and create deposits in the valley (Fig. 3). Structurally, a horizontal bed plane parallel to the mainstream valley trend represents the bedding strike, and beds dipping from 10 to 15° to the east bank (Fig. 2). Tectonically, the study area is located in the Mosul High of Chemchemal – Butmah sub-zone within the Low Folded Zone that comprises of a wide, low amplitude, gentle folding series (Fouad, 2015). Tectonically, in the Mosul High sub-zone of Chemchemal – Butmah, in the Low Folded Zone, the study area is comprised of a wide, low amplitude, gentle folding range.

## Methodology

### Geotechnical studies

The field geotechnical study is including define rock type, strength, and weathering, discontinuity attitude, persistence, spacing, openness, filling materials, and ends. For the protection of dams and the stability of the area around the dam and reservoir, geological documentation is important (Szafarczyk, 2019). Rock types vary between limestone, dolomitic limestone, dolomite, and somewhere marly limestone. The uniaxial compressive strength is estimated by using Schmidt hammer type N, which be better than L type to determine the strength based on weathering grade (Basu, Celestino & Bortolucci, 2009). Weathering classifies into five categories, from micro fresh state to completely decomposed state (ISRM, 1980; Williamson & Kuhn, 1988; Hoek & Bray, 2005; Basu et al., 2009; BS 5930, 2009; Cabria, 2015). Numerous weathering and weathering indices have been

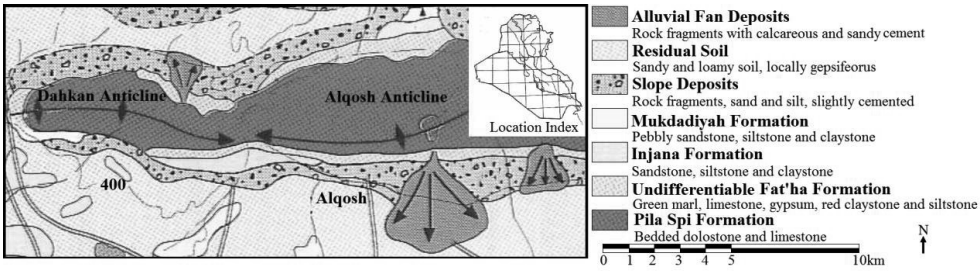


FIGURE 3. Geological map of the study area (Sissakian & Fouad, 2015)

developed for quantifying the consequence of weathering for engineering properties of rocks. The geotechnical investigation for discontinuities is comprising discontinuity attitude that scaled by Silva compass for bedding planes, major two systematic sets of joints, and a random set of joints. Persistence, spacing, and openness are measured by scale tape for each set of discontinuities. Due to the importance of filling materials, they are classified into stronger and weaker than host rock; their types are clay, soil, rock fragments, and calcite. Finally, the ends of discontinuities are not visible unless at the boundaries of outcrop that covered by soil. Consequently, geotechnical parameters have been selected in detail for the proposed site of the dam. These previous parameters help the engineers to evaluate the rock mass according to the most of classification systems such as Q-System, rock mass rating (RMR), geological strength index (GSI), and rock mass index (RMi).

### Hydrological studies

The methodology proposed is based on site selection criteria. The favorate site for any dam is a position where a wide valley with high walls lead to a small canyon, with stubborn walls, which leads to a reduction of earthwork and cost. The location is prepared through visual interpretation of satellite images (LANDSAT 8, 2013) data. Digital elevation model (DEM) has been prepared based on the Shuttle Radar Topography Mission (SRTM) with 30-meter resolution data from the United States Geological Survey (USGS). The DEM data is used for extracting the watershed boundary. The delineation of the watershed boundary, catchment area, generating slope drainage pattern and stream ordering based on Strahler method, etc. all were carried out using Arc Gis Ver. 10 software. The morphological and areal data prepared from the Watershed Modeling System (WMS) Ver. 7.1 software. Depending on the data available length and height of the proposed dam were determined. Also area of the reservoir, the volume of storage verse fixed interval elevation at specific dam height was determined. The shape of the reservoir formed upstream the proposed dam carried out by Global Mapper Ver. 13 software.

## Results and discussion

### Geotechnical results

Since the rocks in the study area carbonate, so the strength is forecasting high. The uniaxial compressive strength of these rocks is ranged between 49 and 103 MPa that classified strong in general (Hoek, Marinos & Benissi, 1998; Marinos & Hoek, 2000). The higher compressive strength rocks; more than 65 MPa are cited in grade fresh and slightly weathered, while the others classified as moderately to highly weathered (Table 1). There are good relations between the strength and degree of weathering (Basu et al., 2009). For any engineering project, discontinuity characteristics are an important geotechnical investigation. Spacing and orientation are reflecting the block size and shape. In the study area, the block size ranges 0.5–5.25 and the shape is regular, i.e. cubic and orthogonal. These characteristics are reflecting a good rock quality designation (RQD) that is very good for dam sites; it is fore-

cast permeability and shear strength (Rastegarnia et al., 2019). Values of RQD are calculated from the volumetric joints count ($J_v$) values (Palmstrom, 1982). Using of modified blockiness evaluation method shows that rock mass is classified as slight-blockiness (Chen, Yin & Niu, 2018). The mainly worldwide classification systems used are Q-System, RMR, GSI, and RMi, which are published by Barton, Lien and Lunde (1974), Bieniawski (1989), Palmstrom (1995), and Marinos and Hoek (2000). All these systems estimate the rock mass quality quantitatively and estimate the sufficient support of rock mass (Palmstrom, 2009). For various engineering projects, rock mass classification systems have been used to understand the conditions and determine the rock mass quality (Singh & Thakur, 2019). The general classification of the site is good: Q = 35.8, RMR = 69.3, GSI = 71.4, and RMi = 7.3 (Table 1), which means a high value of rock mass compressive strength ($\sigma_{cm}$). There are some zones with low thickness classify as fair, these zones can be treat before construction. According to representative elementary volume (REV), the consequence of these small zones to the rock mass characteristics is neglected as the scale of the dam site (Xia, Zheng & Yu, 2016; Wang, 2017). However, the presence of this weak zone and its thickness, which does not exceed 10 cm, may affect the upper rock beds and reduce their strength, as illustrated in Figure 4. Therefore, it is recommended to treat such beds with real treatment before starting any construction work because their impact extends to several meters as shown in zone B in Figure 4. For the Daniel-Johnson dam in Canada, the structural faults, particularly joints, of the rock mass, needed severe attention during the construction of the dam. These surveys used to determine the classification of rock masses to allow the evaluation of the quality of rock mass and the measurement of joint openings. When an RMR

TABLE 1. Geotechnical characteristics of the dam site

| Bed | Lithology | Thickness [cm] | Degree of weathering* | Unit weight [kN·m$^{-3}$] | Estimated UCS** [MPa] | Rock mass classification | | | |
|---|---|---|---|---|---|---|---|---|---|
| | | | | | | Q | RMR | GSI | RMi |
| 1 | Dol. Lst. | 120 | III | 22.87 | 56.8 | 38 | 73 | 68 | 7 |
| 2 | Dol. Lst. | 60 | III | 23.03 | 61.7 | 38 | 75 | 69 | 6 |
| 3 | Dol. Lst. | 40 | III | 23.41 | 67.5 | 39 | 75 | 71 | 7 |
| 4 | Dol. Lst. | 60 | II | 23.24 | 77.9 | 40 | 75 | 71 | 7 |
| 5 | Dol. Lst. | 60 | IV | 22.53 | 52.4 | 34 | 68 | 65 | 8 |
| 6 | Dol. Lst. | 40 | IV | 22.33 | 58.0 | 34 | 67 | 62 | 7 |
| 7 | Dol. Lst. | 40 | IV | 22.34 | 58.2 | 34 | 68 | 60 | 6 |
| 8 | Dol. Lst. | 80 | II | 22.27 | 65.3 | 38 | 66 | 62 | 7 |
| 9 | Dol. Lst. | 70 | II | 22.26 | 67.5 | 38 | 63 | 68 | 8 |
| 10 | Mar. Lst. | 10 | III | 22.12 | 50.3 | 34 | 62 | 67 | 0.8 |
| 11 | Dol. Lst. | 100 | IV | 23.01 | 63.5 | 36 | 65 | 70 | 8 |
| 12 | Dol. Lst. | 100 | III | 22.89 | 65.1 | 35 | 63 | 73 | 9 |

TABLE 1 cont.

| Bed | Lithology | Thickness [cm] | Degree of weathering* | Unit weight [kN·m$^{-3}$] | Estimated UCS** [MPa] | Rock mass classification | | | |
|---|---|---|---|---|---|---|---|---|---|
| | | | | | | Q | RMR | GSI | RMi |
| 13 | Dol. Lst. | 60 | III | 22.76 | 60.2 | 38 | 62 | 78 | 8 |
| 14 | Dol. Lst. | 100 | I | 23.74 | 71.7 | 41 | 70 | 79 | 8 |
| 15 | Dol. Lst. | 100 | I | 23.43 | 76.1 | 41 | 71 | 82 | 10 |
| 16 | Dol. Lst. | 60 | I | 23.91 | 70.2 | 40 | 68 | 79 | 7 |
| 17 | Bre. Lst. | 70 | IV | 21.32 | 48.7 | 22 | 55 | 54 | 0.8 |
| 18 | Dol. Lst. | 1 000 | II | 22.01 | 68.6 | 38 | 66 | 72 | 7 |
| 19 | Dol. Lst. | 70 | III | 22.74 | 62.8 | 34 | 65 | 73 | 8 |
| 20 | Dol. Lst. | 70 | IV | 22.32 | 62.7 | 36 | 65 | 69 | 6 |
| 21 | Dol. Lst. | 70 | III | 22.96 | 62.9 | 36 | 65 | 63 | 6 |
| 22 | Dol. Lst. | 70 | III | 22.31 | 62.7 | 36 | 63 | 60 | 5 |
| 23 | Dol. | 200 | I | 23.89 | 103.1 | 43 | 82 | 87 | 15 |
| 24 | Dol. Lst. | 170 | I | 22.95 | 72.5 | 40 | 81 | 83 | 11 |
| 25 | Dol. Lst. | 100 | I | 22.73 | 69.7 | 40 | 80 | 81 | 6 |
| 26 | Dol. | 200 | I | 23.67 | 98.6 | 40 | 85 | 83 | 12 |
| 27 | Dol. | 200 | I | 23.77 | 74.7 | 39 | 79 | 81 | 9 |
| 28 | Mar. Lst. | 150 | IV | 22.81 | 58.7 | 36 | 64 | 68 | 6 |
| Total thickness | | 3 470 | mean | 22.84 | 66.7 | 35.8 | 69.3 | 71.4 | 7.3 |

*Classification according to ISRM (1980), Williamson and Kuhn (1988), Hoek and Bray (2005), Basu et al. (2009), BS 5930 (2009), Cabria (2015).
**Estimated from the Schmidt hammer type N.

assessment of the rock mass classification is used, it is possible to suggest certain values for the deformation module of the rock mass (Quirion, 2015). Therefore, good rock mass refers to safe dams.

## Hydrological results

For satellite images of the study area a catchment area was used of the proposed dam from the SRTM DEM and the area of interest (AOI). DEM, drainage pattern, satellite image maps of the study shown in Figures 5, 6 and 7. Important linear and arial parameters and features such as basin area, perimeter, basin length, shape factor, sinuosity factor, etc. have been calculated. The drainage patterns of the watershed are dendritic with fourth-order streams. The details of various morphometric parameters in this study are shown in Table 2. With fourth-order flow stream, the water drainage patterns are dendritic. Table 2 displays the descriptions of the different morphometric parameters for this study.

The maximum and minimum elevation in the watershed 1,336; 431 m a.s.l., respectively, and the watershed covers 115.64 km$^2$. Depending on the site topography and dam height, the accessible

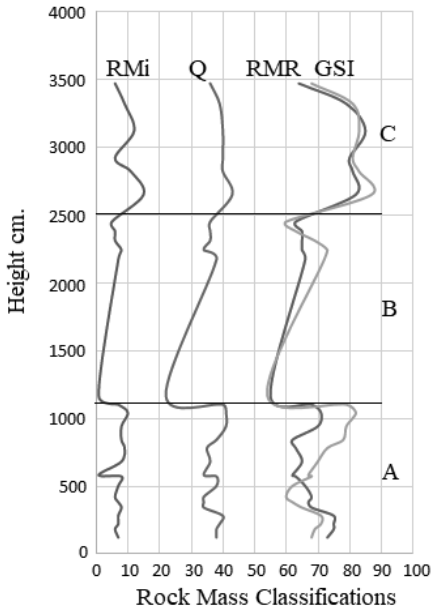


FIGURE 4. Rock mass classification of the proposed dam site

storage capacity of a reservoir depends. At that specific location and the cross--section of the valley, three scenarios were assumed to the dam height 450, 460, 470 m a.s.l., the length of the dam, area of the reservoir upstream the dam, volume of storage at each height are defined as shown in Table 3. These parameters (storage capacity, water spread area at different elevations) are used to generate indexes based on the primary parameters combination. The ratio between the average storage volume (mean *V*) and the mean surface area (mean *A*) at the specific elevation is calculated to determine the index (mean *d*) of the evaporation losses, (0.0104, 0.0107, 0.0089) are the index (mean *d*) at each elevation.

The form of the reservoir, of course, will affect the amount of water lost during the evaporation progression. A narrow and deep reservoir would have slightly less loss of evaporation than a shallow reservoir abroad. The surface area of water and water depth are the major factors associated with the evaporation process. The metrological factors, however, are "e.g. Relative humidity, precipitation density, wind speed and temperature" are mostly the same and have a minor impact. Therefore, in the

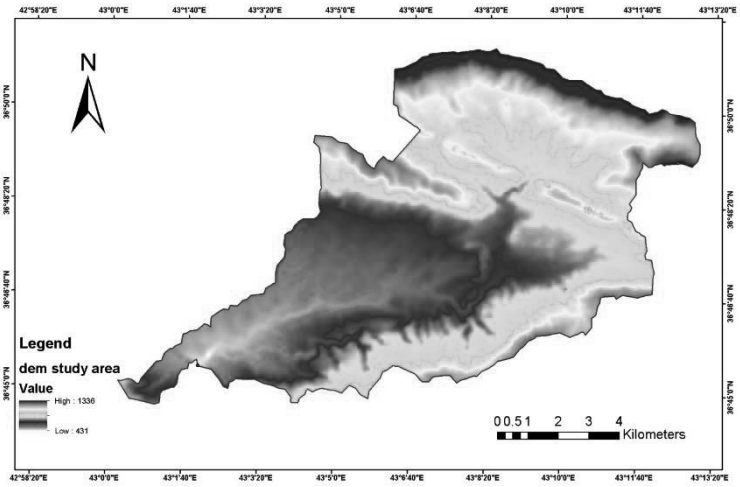


FIGURE 5. The DEM of the study area

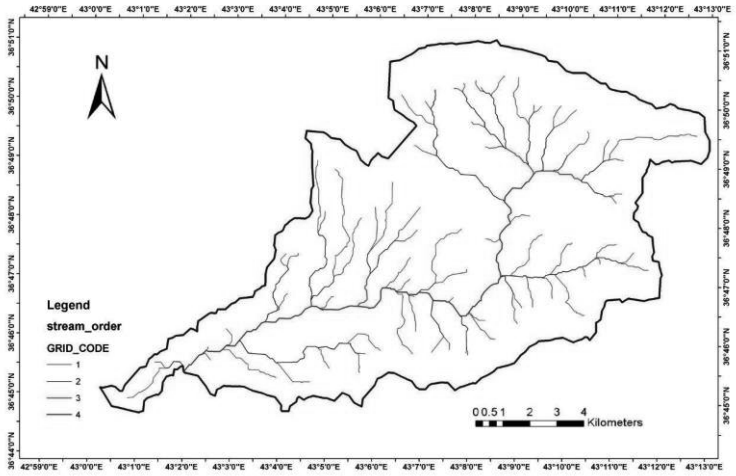


FIGURE 6. The drainage pattern with stream order of study area

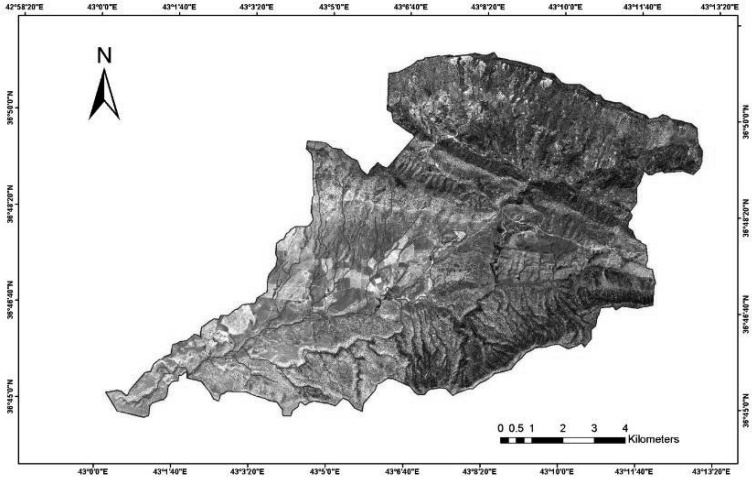


FIGURE 7. The satellite image with the drainage pattern of the study area

TABLE 2. The morphometric and areal characteristics for the proposed dam watershed

| Parameter | Value | Parameter | Value |
|---|---|---|---|
| Basin area | 113.64 $km^2$ | Mean basin elevation | 743.18 m |
| Basin slope | 0.1813 | Max flow distance | 25 027 m |
| Basin lengths | 18 164 m | Max stream length | 23 910 m |
| Perimeter | 78 231 m | Max stream slope | 0.021 $m \cdot m^{-1}$ |
| Shape factor | 2.9 | Distance from centroid to stream | 59.0 m |
| Sinuosity factor | 1.32 | Centroid stream distance | 12 243 m |

TABLE 3. The storage capacity at elevation 450, 460, 470 m a.s.l. for the dam watershed

| No | Dam elevation 450 m a.s.l | | Dam elevation 460 m a.s.l. | | Dam elevation 470 m a.s.l. | |
|---|---|---|---|---|---|---|
| | elevation | storage | elevation | storage | elevation | storage |
| 1 | 438.50 | 0 | 435.50 | 0 | 435.50 | 0 |
| 2 | 439.65 | 54 121.75 | 437.95 | 58 750.58 | 438.95 | 100 766.15 |
| 3 | 440.80 | 86 879.65 | 440.40 | 179 456.32 | 442.40 | 319 745.59 |
| 4 | 441.95 | 126 046.7 | 442.85 | 357 488.39 | 44585 | 638 066.92 |
| 5 | 443.10 | 179 456.32 | 445.30 | 578 248.15 | 449.30 | 1 043 980.03 |
| 6 | 444.25 | 236 782.65 | 447.75 | 856 334.23 | 452.75 | 1 564 901.85 |
| 7 | 445.40 | 306 927.28 | 450.20 | 1 162 905.45 | 456.20 | 2 322 428.28 |
| 8 | 464.55 | 395 587.25 | 452.65 | 1 545 674.39 | 459.65 | 3 315 135.07 |
| 9 | 447.70 | 487 095.73 | 455.10 | 2 053 955.94 | 463.10 | 4 597 678.06 |
| 10 | 448.85 | 585 369.43 | 457.55 | 2 682 409.13 | 466.55 | 6 358 281.65 |
| 11 | 450.00 | 640 764.41 | 460.00 | 3 429 787.74 | 470.00 | 8 590 763.41 |

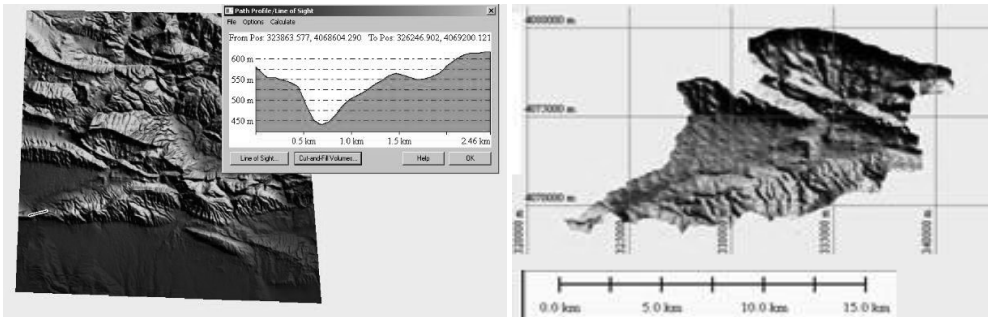


FIGURE 8. The shape of the reservoir formed upstream the proposed dam 470 m with cross section

assessment of the current study, the area of water surface and the depth of water were regarded. The shape of the reservoir formed upstream of the dam at elevation 470 is shown in Figure 8. The important factor affecting the construction of a dam is cost construction, so the earthwork depends on the cross-section and length of the dam, the least length is the best. The length of the proposed dam as measured from contour data is 66, 190, 373 m respectively, the surface area and length of the reservoir also calculated as shown in Table 4.

The important factor affecting the construction of a dam is cost construction, so the earthwork depends on the cross-section and length of the dam, the least length is the best. The length of the proposed dam as measured from contour data is 66, 190, 373 m respectively, the surface area and length of the reservoir also calculated as shown in Table 4.

An important aspect of any hydrological study is the definition of the curve of storage capacity with levels. The storage capacity at dam elevation 450, 460, 470 m is 640,764.41; 3,429,787.74;

TABLE 4. Length of the dam and reservoir with the storage according to the area of the reservoir at different heights

| No | Elevation [m a.s.l.] | Area of reservoir [km$^2$] | Volume of storage [m$^3$] | Dam length [m] | Length of reservoir [km] |
|---|---|---|---|---|---|
| 1 | 450 | 123.6 | 1 286 007 | 66 | 9 09.5 |
| 2 | 460 | 319.8 | 3 429 788 | 190 | 1 150 |
| 3 | 470 | 962.9 | 8 590 763 | 373 | 2 750 |
| 4 | 480 | 1 890 573.6 | – | 469 | 3 238 |
| 5 | 490 | 3 293 661.4 | – | 541 | 4 856 |

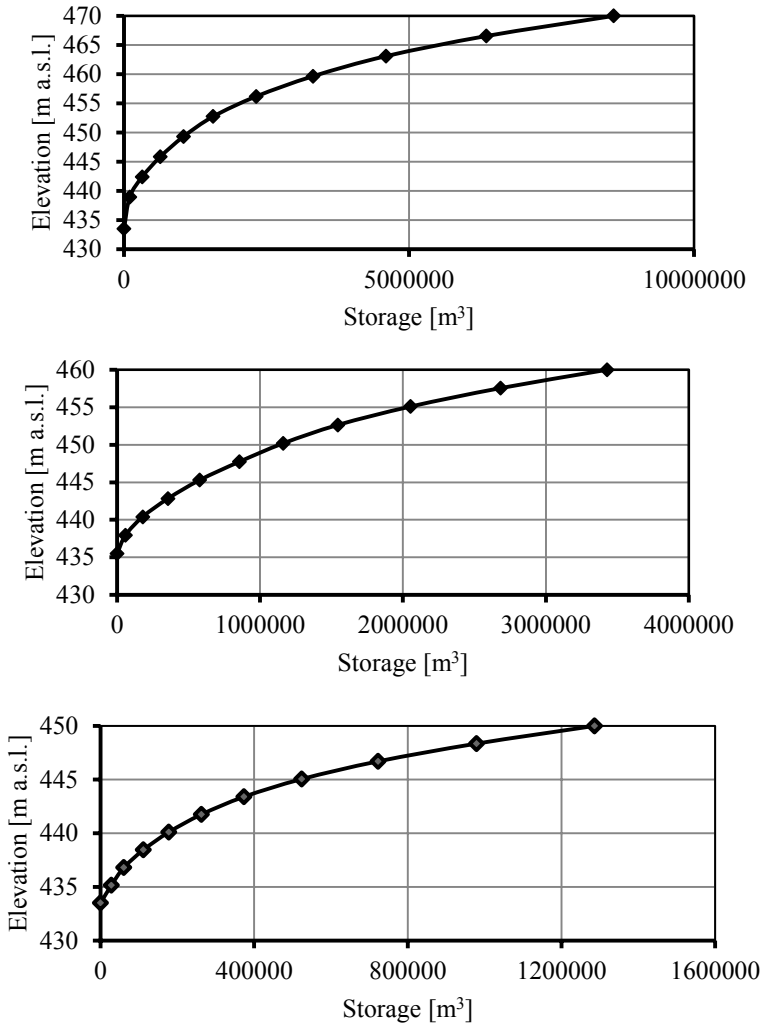


FIGURE 9. Storage at elevations 470, 460, and 450 m a.s.l. respectively

8,590,763.41 $m^3$ respectively, the plotted curves shown in Figure 9. Table 2 shows the storage at equal intervals for each height.

## Conclusions

The proposed dam site is good geotechnically according to the categories of rock mass classification. The stream valley is narrow, meandering with the two significant joints, resulting in high dam stability and low construction costs. The lithology consists of limestone, dolomite, dolomitic limestone, and somewhere marly limestone, with no karstic or caves indication, nevertheless some pores not exceed 5 cm in diameter. For the proposed heights, the basement and the shoulders of the dam are appropriate with a high value of $\sigma_{cm}$. Because of its excellent spacing, close openness and presence of marl and calcite as filling materials between adjacent walls, the water is being little filtrated from the reservoir following the discontinuity features. Finally, the suggested dam site is very significant concerning hydrological and geotechnical characteristics.

According to its distinct engineering requirements, the hydraulic study has shown that the proposed position of the dam is very good. The site is distinguished by its narrow valley, its cliffs and rock hardy heights and the abundance of water that flows all seasons. The site has an important characteristic.The availability of suitable geotechnical and hydraulic resources is one of the difficulties that engineers face in selecting the dam sites, but the current situation is characterized by both.

**Acknowledgements**

Authors of this paper would like to express gratitude to the University of Mosul, Mosul, Iraq for support to complete this work. For much fruitful cooperation on laboratory tests, we thank our colleagues in the Dams and Water Resources Research Center.

## References

Barton, N., Lien, R., & Lunde, J. (1974). Engineering classification of rock masses for the design of tunnel support. *Rock Mechanics Felsmechanik Mécanique Des Roches*, *6*(4), 189-236. https://doi.org/10.1007/BF01239496

Basu, A., Celestino, T.B. & Bortolucci, A.A. (2009). Evaluation of rock mechanical behaviors under uniaxial compression with reference to assessed weathering grades. *Rock Mechanics and Rock Engineering*, *42*(1), 73-93. https://doi.org/10.1007/s00603-008-0170-2

Bieniawski, Z.T. (1989). *Engineering rock mass classifications: a complete manual for engineers and geologists in mining, civil, and petroleum engineering.* New York: John Wiley & Sons.

British Standard 5930 [BS 5930] (2009). *Code of practice for site investigations*. London: British Standards Institution.

Cabria, X.A. (2015). *Effects of weathering in the rock and rock mass properties and the influence of salts in the coastal roadcuts in Saint Vincent and Dominica*. Enschede: University of Twente, Faculty of Geo-Information and Earth Observation (ITC).

Chen, Q., Yin, T. & Niu, W. (2018). Replacing RQD and discontinuity spacing with the modified blockiness index in the rock mass rating system. *Archives of Mining Sciences*, *63*(2), 353-382. https://doi.org/10.24425/122452

Hoek, E. & Bray, J. (2005). *Rock slope engineering. Fourth edition.* London: CRC Press. https://doi.org/10.1201/9781315274980

Hoek, E., Marinos, P. & Benissi, M. (1998). Applicability of the geological strength index (GSI) classification for very weak and sheared rock masses. The case of the Athens Schist Formation. Bulletin of Engineering Geology and the Environment, *57*(2), 151-160. https://doi.org/10.1007/s100640050031

Fouad, S.F. (2015). Tectonic map of Iraq, scale 1 : 1000 000. Iraqi Bulletin of Geology and Mining, *11*(1), 1-7.

International Society for Rock Mechanics [ISRM] (1980). *Basic geotechnical description of rock masses.* Salzburg: ISRM.

Jassim, S.Z. & Goff, J.C. (2006). *Geology of Iraq.* Brno: Dolin, Prague and Moravian Museum.

Khan, M. (1992). Development of surface water resources. In *Rehabilitation of degraded arid ecosystem* (pp. 136-143). Jodhpur: Scientific Publishers.

LANDSAT 8 (2013). *Landsat missions*. Retrieved from: https://www.usgs.gov/land-resources/nli/landsat/landsat-data-access?qt-science_support_page_related_con=0#qt-science_support_page_related_con

Marinos, P. & Hoek, E. (2000). GSI: A geologically friendly tool for rock mass strength estimation. In *ISRM International Symposium*. Salzburg: International Society for Rock Mechanics and Rock Engineering.

Palmstrom, A. (1982). *The volumetric joint count; a useful and simple measure of the degree of rock mass jointing*. International Association of Engineering Geology. Retrieved from: https://eurekamag.com/research/020/473/020473508.php

Palmstrom, A. (1995). *RMi – a rock mass characterization system for rock engineering purposes*. Oslo: University of Oslo.

Palmstrom, A. (2009). Combining the RMR, Q, and RMi classification systems. *Tunnelling and Underground Space Technology*, *24*(4), 491-492. https://doi.org/10.1016/j.tust.2008.12.002

Quirion, M. (2015). Daniel-Johnson multiple arch dam, Québec, Canada-Rock foundation safety assessment. In *13th ISRM International Congress of Rock Mechanics: Montreal, Canada 10-13 May 2015*. Montreal: International Society for Rock Mechanics and Rock Engineering.

Rastegarnia, A., Lashkaripour, G.R., Ghafoori, M. & Farrokhad, S.S. (2019). Assessment of the engineering geological characteristics of the Bazoft dam site, SW Iran. *Quarterly Journal of Engineering Geology and Hydrogeology*, *52*(3), 360-374. https://doi.org/10.1144/qjegh2017-042

Samra, J.S., Bansal, R.C., Sikka, A.K., Mittal, S.P. & Agnihotri, Y. (1995). Resources conservation through watershed management in Shiwalik foothills. *Relmajra Bulletin*, T-28/c-7.

Singh, J. & Thakur, M. (2019). Landslide stability assessment along Panchkula–Morni road, Nahan salient, NW Himalaya, India. *Journal of Earth System Science*, *128*(6), 148. https://doi.org/10.1007/s12040-019-1181-y

Szafarczyk, A. (2019). Stages of geological documentation on the example of landslides located on the slopes of the dam reservoir "Swinna Poreba"(Poland). *E&ES*, *221*(1), 1-8. https://doi.org/10.1088/1755-1315/221/1/012037

Wang, R. (2017). *Study of scale effects of rock quality designation (RQD) measurements using a discrete fracture network approach*. Vancouver: University of British Columbia.

Williamson, D. & Kuhn, C. (1988). *The unified rock classification system. Rock classification systems for engineering purposes*. West Conshohocken, PA: ASTM International.

Xia, L., Zheng, Y. & Yu, Q. (2016). Estimation of the REV size for blockiness of fractured rock masses. *Computers and Geotechnics*, *76*, 83-92.

## Summary

**Qualifying the geotechnical and hydrological characteristic of the Bandawaya stream valley – Northern Iraq.** In northern Iraq, countless non-abuse stream valleys can be used to store water for a variety of purposes; domestic, supplementary irrigation, and recharging groundwater. Bandawaya is one of the stream valleys, which form the first perspective has excellent quality. The location of the suggested dam has been evaluated by hydrological and geotechnical

studies. Geotechnical studies included measurement of all the parameters related to the rock mass classification for evaluation based on four classification systems, which are the Q-System, the rock mass rating (RMR), the geological strength index (GSI), and the rock mass index (RMi). The classification results indicated that the rocks of the valley are good for constructing a dam on them, with some weak zones that may affect the integrity of the dam, which the study recommended treating before starting the construction of the dam. According to preliminary studies on different dam's heights the qualification demonstrates an excellent choice of the site. Four stream orders are recognized, dendritic pattern in the southern part of the watershed, and trellised in the northern part. Three heights assumed to the proposed dam 450, 460, 470 m a.s.l. with 640,764; 3429,787; 8,590,763 $m^3$ storage capacity respectively. According to the Q-System, the RMR, the GSI, and the RMi, the rock mass of the study area is evaluated. The findings illustrate the excellent selection by geotechnical, hydrological, and engineering features of the dam place.

**Authors' address:**
Azealdeen Salih Al-Jawadi
(https://orcid.org/0000-0002-0184-1034)
Mosul University
Dams and Water Resources Research Center
Aljamea Street, 16, 00964, Mosul
Iraq
e-mail: azealdeenaljawadi@uomosul.edu.iq

Yousra Taha Abdul Baqi
(https://orcid.org/0000-0003-0195-9865)
Dams and Water Resources Research Center
– Mosul University – Iraq
Aljamea Street, 16, 00964, Mosul
Iraq
e-mail: yousrataha2017@uomosul.edu.iq

Ali Mohammed Sulaiman
(https://orcid.org/0000-0002-7424-8514)
Dams and Water Resources Research Center
– Mosul University – Iraq
Aljamea Street, 16, 00964, Mosul
Iraq
e-mail: ali_msh2@uomosul.edu.iq

Scientific Review – Engineering and Environmental Sciences (2020), 29 (3), 332–342
Sci. Rev. Eng. Env. Sci. (2020), 29 (3)
Przegląd Naukowy – Inżynieria i Kształtowanie Środowiska (2020), 29 (3), 332–342
Prz. Nauk. Inż. Kszt. Środ. (2020), 29 (3)
http://iks.pn.sggw.pl
DOI 10.22630/PNIKS.2020.29.3.28

**Mohammed Fakhraldeen AHMED**

Mosul University, College of Environmental Sciences and Technology

# The performance assessment of reverse osmosis stations at Al-Mahalabea area

**Key words:** brackishwater, desalination, membrane technology, reverse osmosis, SAW, TOPSIS

## Introduction

Reverse osmosis (RO) is a wide spread technique used to supply potable water from seawater and brackishwater. There are different types of membranes used in RO structure such as; micro porous, symmetric, non-porous symmetric, asymmetric and thin film composite (TFC). Most companies synthesis TFC membranes that have a lot of advantages including durability with long lifetime in spite of sensitivity to chlorine (Bouchareb et al., 2019). Membrane life is an important factor to determine the economic efficiency of RO systems (Metcalf & Eddy et al., 2007). Process of RO has simple design, easy operation, and able to remove organic and inorganic pollutants. Therefore, RO is more environmentally friendly option (Garud, Kore, Kore & Kulkarni, 2011; Al-Hotmani, Al-Obaidi, John, Patel & Mujtaba, 2020). The most disadvantages of RO include the requirement for high pressure and adding of chemicals against scaling and fouling.

A number of researchers have evaluated the performance of RO process based brackishwater desalination as follows.

Makki (2009) studied the performance of RO in Dura – Iraq power station. The study examined RO with TFC membrane constructed as spiral wound module, and concluded that TFC membrane has higher productivity and durability to chemicals with TDS removing percentage reached 96%.

El-Harrak et al. (2013) evaluated the performance of RO process for irrigation purpose in Dokkala – Morocco. The results showed that the performance of RO system decreases after few months. The study included illumination of chlorine and sodium bisulfate for the feed water.

Al-Bayati (2015) outlined the efficiency of five brackish water desalination plants for drinking purpose at Salahaldin province – Iraq. The research

included examination of 17 samples of well water and more than 17 parameters for each sample were analysed. The research concluded that the permeate water were within the permissible standards and the TDS removal percentage reached 98.18%.

Abdel-Fatah, El-Gendi and Ashour (2016) studied a RO system which has flush cycle for the treatment of saline water in Cairo University – Egypt. The study showed that the resulted water has low concentration in TDS which equals to 100 ppm while the feed water concentration exceeds 10,000 ppm.

Al-Jlil (2017) studied the reduction of TDS concentrations from wastewater using Nano Filtration NF and RO in Saudi Arabia. The study found that RO removes mono valent ions such as $Cl^-$ reaching rejection efficiency 94.4 %.

Haider (2017) evaluated the brackishwater at each component of RO system in Buraydah, Qussim – Saudi Arabia during the year 2016. The research used fuzzy AHP to extract the weights of five main variables and fuzzy weighted sum method to evaluate the average monthly performance. The results showed high performance of the system and meets drinking water limits.

Bouchareb et al. (2019) outlined the RO performance which have TFC membrane type (TW30-2540) for desalination brackish water at Alpine region in the north of Algeria. The results showed that this type of membrane has less cost and high rejection efficiency reaches 97% of salts.

The study aims to assess the performance of four RO stations at different sites within Al-Mahalabea area in Nineveh governorate – Iraq. Besides, a ranking of RO stations performance is conducted according to their rejection efficiency (at zero time of operation and after ten weeks of operation) by using the SAW and the TOPSIS techniques, and identifying the higher removal percentage parameters. The collected data of the feed water can be used as a feedback for groundwater quality database for Nineveh governorate.

## Material and methods

### The studied area

The studied area is located about 35 km south west of Mosul city. Its area is about 888 $km^2$. Table 1 illustrates the names of RO stations' sites. Also, the locations of the RO stations can be seen in Figure 1.

### The components of used RO stations

The studied RO system is consisted of the following components; working pressure pump (4 bar), flow rate gage,

TABLE 1. Reverse osmosis stations within the studied area

| RO station | Site name | Longitude | Latitude | Management |
|---|---|---|---|---|
| RO1 | Ain Alwah, | 420°37′08″ | 360°14′16″ | specialized environmental crew |
| RO2 | Misherfa Altaha | 420°48′20″ | 360°05′15″ | specialized environmental crew |
| RO3 | Ghiziel | 420°40′34″ | 360°02′39″ | untrained labours |
| RO4 | Misherfa | 42°52′42″ | 36°11′57″ | untrained labours |

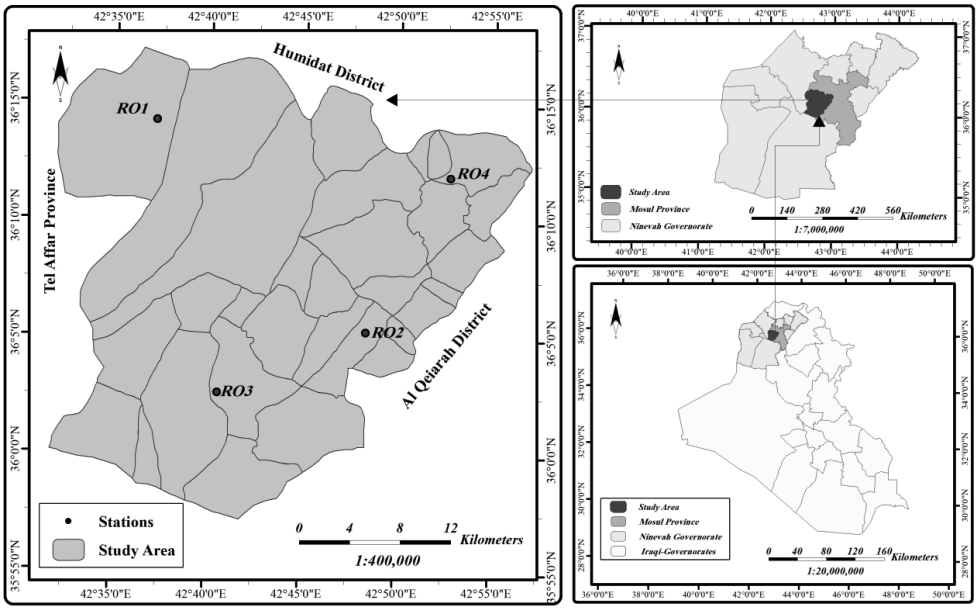


FIGURE 1. The studied area and locations of the operating RO stations

pH gage, TH gage, pH equalization device, in addition to chemical cleaning system. Feed water flow rate capacity is 18 $m^3 \cdot h^{-1}$.

Pretreatment system includes the following components; tanks of reclaimed water, sand filter, activated carbon filter, cartridge 5–10 μm. Permeate capacity is 10 $m^3 \cdot h^{-1}$. Model of RO is Trust CRO-8/12 and the membrane model is AG-8040, noting that all the stations have the same model. The membranes brand name is GE Desal (USA). The diameter and length of the membrane is 8 and 40 inches respectively. The post-treatment system includes the following units: UV unit, in-line storage tanks and ozone unit. Schematic diagram of the studied RO station and the units of the pre and post treatment of groundwater is explained in Figure 2.

## Methodology

### *The studied parameters*

Two groups of samples were taken from feed and permeate water and analysed into two periods: the first is at zero time of operation, while the second period occurred after 10 weeks of operation (this period was the recommended period used by the supplied company).

A number of parameters were laboratory analysed for each sample and then compared with local and international standards and examined according to standard methodology (APHA, 2005) in the laboratory of the college of the Environmental Sciences and Technology, Mosul University – Iraq, as in Table 2. The studied parameters are; TH, $SO_4$, TDS, TA, Mg, Ca, Cl, Na, pH, turbidity and $NO_3$.

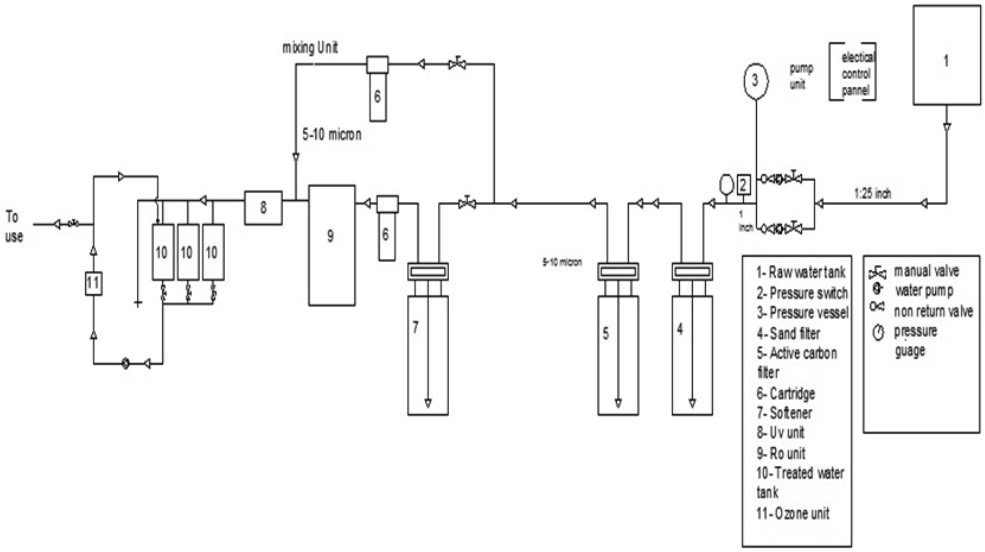


FIGURE 2. Schematic diagram of RO station and its components

TABLE 2. Local and international GWQ standards

| No | Parameter | Unit | Environmental Protection Agency (2004) | World Health Organization (2003) | National standards (IHM, 2001) |
|---|---|---|---|---|---|
| 1 | TH | $mg \cdot l^{-1}$ as $CaCO_3$ | 500 | 100–500 | 100–500 |
| 2 | $SO_4$ | $mg \cdot l^{-1}$ | 400 | – | – |
| 3 | TDS | $mg \cdot l^{-1}$ | 1 000 | 500–1 500 | 500–1 500 |
| 4 | TA | $mg \cdot l^{-1}$ as $CaCO_3$ | 200 | – | 125–200 |
| 5 | Mg | $mg \cdot l^{-1}$ | 150 | 30 | 50–150 |
| 6 | Ca | $mg \cdot l^{-1}$ | 200 | 75 | 75–200 |
| 7 | Cl | $mg \cdot l^{-1}$ | 600 | – | 200–250 |
| 8 | Na | $mg \cdot l^{-1}$ | 200 | 20 | 200 |
| 9 | pH | – | 6.5–8.5 | 6.5-8.5 | 6.5–8.5 |
| 10 | turbidity | NTU | 5 | 5 | 5 |
| 11 | $NO_3$ | $mg \cdot l^{-1}$ | 10 | 10 | 50 |

*Methods used to determine RO stations performance*

Two methods are used to determine RO stations performance: the Simple Additive Weight (SAW) and the Technique for Order of Preference by Similarity to Ideal Solution (TOPSIS). As follows a summary of each method.

The SAW method is firstly used by (McDuffie & Haney, 1973). This method recaps the studied parameters values in one index. A relative weight ($w_i$) is given

to each parameter depending on its importance. Sum of these relative weights must equal 1. The quality rating ($q_i$) is calculated by equation: $q_i = (C_i / S_i) \cdot 100$, where $C_i$ refers to the concentration of a certain parameter, $S_i$ is the depended values limits. Sub-index ($S_{li}$) of a parameter is calculated by multiplying the $w_i$ by $q_i$. Index value is gained from summation of sub-indices which has five ranges: excellent 0–25, good 26–50, poor 51–75, very poor 76–100, and unsuitable > 101 (Afshari, Mojahed & Yusuff, 2010; Al-Ozeer & Ahmed, 2019).

The TOPSIS method is a mathematical method used in ranking the alternatives. It is a goal-based decision making technique for finding the alternative that is closest to the ideal solution (Behzadian, Otaghsara, Yazdani & Ignatius, 2012; Tahyudin, Rosyidi, Ahmar & Haviluddin, 2018). In this study, this method is used to rank the performance of four stations.

The main steps of the TOPSIS method can be summarized as follows (Tsaur, 2011):

Step 1: Input decision matrix as in Table 3, where $X_{i,j}$ represents the feature value, where: $i = 1, ..., M$ and $j = 1, \ldots, 7$.

Step 2: Normalized a decision matrix, as in $R_{i,j} = \dfrac{x_{i,j}}{\sqrt{\sum_{i=1}^{n}\left[(x)_{1,1}\right]^2}}$.

Step 3: $W_j$ (the weights), noting that, the values of the weights which are inserted in the two methods are the same, and these weights are determined according to the importance of each parameter.

Step 4: Construct the weighted normalized matrix ($V_{i,j}$) by multiplying each column by $W_j$.

Step 5: The highest value in the column $V_j^+$.

Step 6: The lowest value in the column $V_j^-$.

Step 7: Determined the $S^+$;

$$S^+ = \sqrt{\sum_{j=1}^{m}(V_{i,j} - v_j^+)^2}$$

Step 8: Determined the $S$;

$$S^- = \sqrt{\sum_{j=1}^{m}(V_{i,j} - v_j^-)^2}$$

Step 9: Calculate closeness to ideal solution ($C_i$); $C_i = S_i^- / (S_i^+ + S_i^-)$.

Step 10: Rank all sites according to the results of Step 9.

## Results

Data of feed and permeate water in two periods and the calculated rejection $R$ efficiency are tabulated in Tables 4, 5, 6 and 7. The rejection $R$ is calculated by the formula $\%R = (1 - P / F) \cdot 100\%$, here $F$ and $P$ represent feed and permeate water concentrations.

TABLE 3. Matrix of parameters and alternatives used in the TOPSIS

| $W_j$ | 0.15 | 0.12 | 0.12 | 0.1 | 0.1 | 0.1 | 0.1 | 0.06 | 0.05 | 0.05 | 0.05 |
|---|---|---|---|---|---|---|---|---|---|---|---|
| Parameter | TDS | Mg | Ca | Cl | $NO_3$ | $SO_4$ | TH | turbidity | pH | Na | TA |
| Site 1 | *X*11 | *X*12 | *X*13 | *X*14 | *X*15 | *X*16 | *X*18 | *X*19 | *X*110 | *X*111 | *X*112 |
| Site 2 | *X*21 | *X*22 | *X*23 | *X*24 | *X*25 | *X*26 | *X*28 | *X*29 | *X*210 | *X*211 | *X*212 |
| Site 3 | *X*31 | *X*32 | *X*33 | *X*34 | *X*35 | *X*36 | *X*38 | *X*39 | *X*310 | *X*311 | *X*312 |
| Site 4 | *X*41 | *X*42 | *X*43 | *X*44 | *X*45 | *X*46 | *X*48 | *X*49 | *X*410 | *X*411 | *X*412 |

TABLE 4. Rejection values of RO1 parameters

| After 10 weeks) | | | At zero time | | | Unit | Parameter |
|---|---|---|---|---|---|---|---|
| *%R* | *P* | *F* | *%R* | *P* | *F* | | |
| 92.3 | 154 | 2 019 | 94.7 | 105 | 2 010 | $mg \cdot l^{-1}$ as $CaCO_3$ | TH |
| 95.7 | 78 | 1 812 | 96.2 | 67 | 1 800 | $mg \cdot l^{-1}$ | $SO_4$ |
| 90.5 | 226 | 2 400 | 91.8 | 228 | 2 800 | $mg \cdot l^{-1}$ | TDS |
| 51.4 | 68 | 140 | 70.1 | 40 | 134 | $mg \cdot l^{-1}$ as $CaCO_3$ | TA |
| 92.3 | 26 | 340 | 92.0 | 26 | 326 | $mg \cdot l^{-1}$ | Mg |
| 90.4 | 24 | 250 | 92.2 | 21 | 269 | $mg \cdot l^{-1}$ | Ca |
| 55.5 | 16 | 36 | 60.0 | 12 | 30 | $mg \cdot l^{-1}$ | Cl |
| 58.6 | 12.4 | 30 | 61.8 | 10.3 | 27 | $mg \cdot l^{-1}$ | Na |
| – | 7.1 | 7.3 | – | 7 | 7.2 | – | pH |
| 90.0 | 0.28 | 2.8 | 95.7 | 0.2 | 4.75 | NTU | turbidity |
| 89.2 | 0.97 | 9.0 | 92.6 | 0.63 | 8.5 | $mg \cdot l^{-1}$ | $NO_3$ |

TABLE 5. Rejection values of RO2 parameters

| After 10 weeks | | | At zero time | | | Unit | Parameter |
|---|---|---|---|---|---|---|---|
| *%R* | *P* | *F* | *%R* | *P* | *F* | | |
| 96.50 | 70 | 1 995 | 96.8 | 66 | 2 086 | $mg \cdot l^{-1}$ as $CaCO_3$ | TH |
| 97.83 | 39 | 1 800 | 98.05 | 35 | 1 800 | $mg \cdot l^{-1}$ | $SO_4$ |
| 95.42 | 96 | 2 100 | 97.5 | 70 | 2 812 | $mg \cdot l^{-1}$ | TDS |
| 72.66 | 41 | 150 | 93.3 | 12 | 180 | $mg \cdot l^{-1}$ as $CaCO_3$ | TA |
| 95.1 | 16.3 | 335 | 97.9 | 7.6 | 365 | $mg \cdot l^{-1}$ | Mg |
| 90.45 | 21 | 220 | 91.06 | 21 | 235 | $mg \cdot l^{-1}$ | Ca |
| 62.14 | 21.2 | 56 | 75.86 | 7 | 29 | $mg \cdot l^{-1}$ | Cl |
| 78.46 | 8.4 | 39 | 83.46 | 4.3 | 26 | $mg \cdot l^{-1}$ | Na |
| – | 7 | 7.3 | – | 6.9 | 7.7 | – | pH |
| 90.00 | 0.2 | 2 | 96.55 | 0.2 | 5.8 | NTU | turbidity |
| 90.1 | 0.8 | 8.9 | 94.4 | 0.53 | 9.5 | $mg \cdot l^{-1}$ | $NO_3$ |

TABLE 6. Rejection values of RO3 parameters

| After 10 weeks | | | At zero time | | | Unit | Parameter |
|---|---|---|---|---|---|---|---|
| *%R* | *P* | *F* | *%R* | *P* | *F* | | |
| 91.3 | 130 | 1 500 | 95.7 | 65 | 1 535 | $mg \cdot l^{-1}$ as $CaCO_3$ | TH |
| 94.7 | 106 | 2 010 | 97.8 | 42 | 1 910 | $mg \cdot l^{-1}$ | $SO_4$ |
| 87.7 | 144 | 1 170 | 91.8 | 90 | 1 100 | $mg \cdot l^{-1}$ | TDS |
| 67.7 | 40 | 124 | 77.0 | 30.8 | 134 | $mg \cdot l^{-1}$ as $CaCO_3$ | TA |
| 89.8 | 28 | 275 | 97.7 | 6 | 265 | $mg \cdot l^{-1}$ | Mg |
| 90.3 | 49 | 507 | 96.8 | 16 | 507 | $mg \cdot l^{-1}$ | Ca |
| 61.1 | 11.7 | 30 | 80 | 6 | 30 | $mg \cdot l^{-1}$ | Cl |
| 58.6 | 8.7 | 21 | 78.2 | 4.5 | 20.7 | $mg \cdot l^{-1}$ | Na |
| – | – | 7.6 | – | 6.6 | 7.6 | – | pH |
| 90.0 | 0.4 | 4 | 93.0 | 0.27 | 3.9 | NTU | turbidity |
| 94.3 | 0.73 | 12.8 | 97.6 | 0.32 | 13.6 | $mg \cdot l^{-1}$ | $NO_3$ |

TABLE 7. Rejection values of RO4 parameters

| After 10 weeks | | | At zero time | | | Unit | Parameter |
|---|---|---|---|---|---|---|---|
| *%R* | *P* | *F* | *%R* | *P* | *F* | | |
| 94.9 | 627 | 1 230 | 97.2 | 30 | 1 100 | $mg \cdot l^{-1}$ as $CaCO_3$ | TH |
| 97.0 | 207 | 690 | 98.4 | 12 | 770 | $mg \cdot l^{-1}$ | $SO_4$ |
| 94.3 | 91.7 | 1 610 | 96.9 | 46 | 1 518 | $mg \cdot l^{-1}$ | TDS |
| 77.3 | 60.3 | 266 | 95.9 | 10 | 245 | $mg \cdot l^{-1}$ as $CaCO_3$ | TA |
| 94.7 | 7.6 | 144 | 97.8 | 2.4 | 112 | $mg \cdot l^{-1}$ | Mg |
| 95.7 | 25.8 | 600 | 98.7 | 8 | 624 | $mg \cdot l^{-1}$ | Ca |
| 65.8 | 45.5 | 133 | 78.3 | 8.2 | 38 | $mg \cdot l^{-1}$ | Cl |
| 78.6 | 16.6 | 77.7 | 88.3 | 6.4 | 55 | $mg \cdot l^{-1}$ | Na |
| – | 7.1 | 7.4 | – | 7 | 7.1 | – | pH |
| 85.4 | 0.55 | 3.8 | 91.2 | 0.35 | 4 | NTU | turbidity |
| 91.2 | 1.1 | 12.6 | 96.0 | 0.47 | 11.8 | $mg \cdot l^{-1}$ | $NO_3$ |

A number of calculations were done to determine the RO stations performance as in Table 8 according to the SAW method. The results show that performance at Ain Alwah RO1, Misherfa Altaha RO2, Ghiziel RO3, and Misherfa RO4 were 98.3, 97.9, 95.3 and 86.3%, respectively.

## Discussion

Figure 3 shows a comparison between the SAW and the TOPSIS results. There is a difference in values between them. And this is due to the principles applied by the two methods themselves, where the SAW occupies

TABLE 8. Ranking of RO stations using the SAW method

| Site | Indices at zero time of operation | | Rejection efficiency [%] | Indices after 10 weeks of operation | | Rejection efficiency [%] | Difference between rejection efficiency [%] | Inverse difference [%] | Rank |
|---|---|---|---|---|---|---|---|---|---|
| | *F* | *P* | | *F* | *P* | | | | |
| Ain Alwah | 228.8 | 20.7 | 90.9 | 215.5 | 23.2 | 89.2 | 1.7 | 98.3 | 1 |
| Misherfa Altaha | 234.6 | 11.7 | 95 | 204 | 14.9 | 92.7 | 2.3 | 97.9 | 2 |
| Ghiziel | 180.6 | 12.4 | 93.1 | 185 | 21.4 | 88.4 | 4.7 | 95.3 | 3 |
| Misherfa | 154.1 | 8.8 | 94.2 | 163.5 | 31.9 | 80.5 | 13.7 | 86.3 | 4 |

The ranking performance resulted from TOPSIS are 99.95, 99.92, 40.2 and 17.99%, respectively as in Table 9.

weighted average, whereas the TOPSIS focuses on maximizing distance from the negative ideal solution, and minimizing

TABLE 9. Ranking of RO stations using the TOPSIS method

| Rank | $P_i$ | Results after 10 weeks of operation | | | Results at zero time of operation | | | Site | No |
|---|---|---|---|---|---|---|---|---|---|
| | % | $P_i$ | $S_i^-$ | $S_i^+$ | $P_i$ | $S_i^-$ | $S_i^+$ | | |
| 1 | 99.95 | 0.9995 | 0.039 | 84.44 | 0.9999 | 0.004 | 143.83 | Ain Alwah | RO1 |
| 2 | 99.92 | 0.9992 | 0.065 | 84.46 | 0.9998 | 0.015 | 143.82 | Misherfa Altaha | RO2 |
| 3 | 40.2 | 0.4020 | 57.76 | 38.83 | 0.1802 | 127.5 | 28.04 | Ghiziel | RO3 |
| 4 | 17.99 | 0.1799 | 80.11 | 17.58 | 0.0036 | 143.6 | 0.529 | Misherfa | RO4 |

After comparing the performance results of the SAW and the TOPSIS methods, it was seen that the stations' performance can be ranked from high to low as follows: RO1: Ain Alwah, RO2: Misherfa Altaha, RO3: Ghiziel, and RO4: Misherfa.

the distance from the positive ideal solution. The SAW gives more convenient values than the TOPSIS method. The result of this study is a good agreement with the findings of the studies of Thor, Ding and Kamaruddin (2013) and Tahyudin et al. (2018).

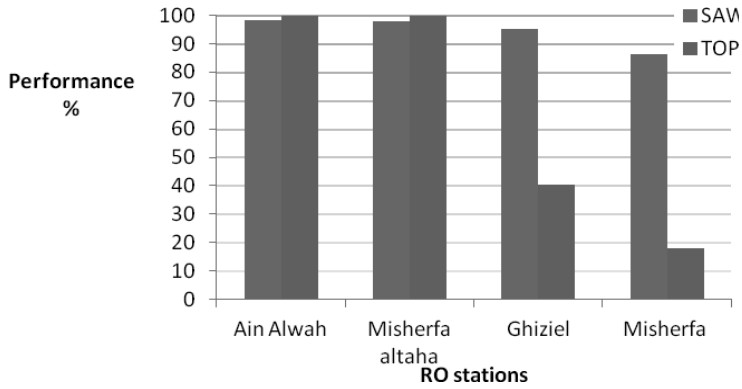


FIGURE 3. A comparison between the SAW and the TOPSIS methods

It was seen that the overall performance shows an excellent rejection efficiency reaching 90% in the following set of parameters; $SO_4$, TDS, Ca, Mg, $NO_3$, Ca, turbidity and TH, however, the other set of parameters CL, and Na show a less rejection efficiency between 60 and 85%, as in Figure 4. It was shown that the divalent cations have higher percentage removal than monovalent anions.

Assessing the performance of RO stations is carried out where RO1 was the best station while RO4 was the worse one. Although the RO system model and the membrane model were the same, the operating conditions of these stations were different. Mismanagement of RO stations (untrained labours) with low maintenance and the lack of frequent washing of the membrane can be considered as the main reason in decreasing (RO3 and RO4) station's performance.

## Conclusions

Total dissolved solids plays a vital role in determining the suitability of the drinking water, where the feed wa-

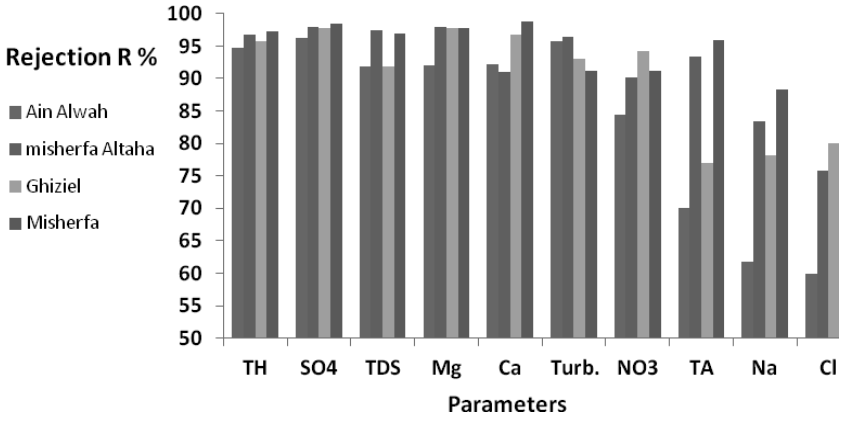


FIGURE 4. Rejection *R* efficiency of the studied parameters at four stations

ter TDS concentrations ranged between 1,100 and 2,800 $mg \cdot l^{-1}$, while the permeate water ranged between 46 and 228 $mg \cdot l^{-1}$ and it was within the permeable standards of drinking water for all stations. The removal efficiency of TDS ranged between 92 and 97%.

It can be observed that the SAW occupies weighted average and its mathematically easier while, the TOPSIS presents a priority of ranks with an optimal station. Therefore, both methods provide an integrated viewpoint of RO stations performance.


### Acknowledgements

The authors are very grateful to the University of Mosul, College of Environmental Sciences and Technology for their provided facilities, which helped to improve the quality of this work.


## References


Abdel-Fatah, M.A., El-Gendi, A. & Ashour, F. (2016). Performance evaluation and design of RO desalination plant: case study. *Journal of Geosciences and Environment Protection*, *4*, 53-63. doi 10.4236/gep.2016.42007

Afshari, A., Mojahed, M. & Yusuff, R. (2010). Simple additive weighting approach to personnel selection problem. *International Journal Environmental Management Technology*, *1*, 511-515.

Al-Bayati, M.A., Salehi, S.A. & Al-Abdraba, W.M. (2015). Evaluation of efficiency of groundwater desalination plants in different hydrogeological conditions in Salahaddin Governorate-Iraq. *Tikrit Journal of Science*, *5*(20), 125-136.

Al-Hotmani, O.M.A., Al-Obaidi, M.A.A., John, Y.M., Patel, R. & Mujtaba, I.M. (2020). An innovative design of an integrated MED-TVC and reverse osmosis system for seawater desalination: process explanation and performance evaluation. *Processes*, *8*(5), 607. doi 10.3390/pr8050607

Al-Jlil, S. (2017). Performance of nano-filtration and reverse osmosis for wastewater treatment. *Journal of Materials and Technology*, *51*(3), 541-548.

Al-Ozeer, A.Z. & Ahmed, M.F. (2019). Groundwater assessment at east side of Mosul City during 2014–2017. *Scientific Review – Engineering and Environmental Sciences*, *28*(1), 35-48. doi 10.22630/PNIKS.2019.28.1.4

American Public Health Association [APHA] (2005). *Standard methods for the examination of water and wastewaters.* 21st ed. Washington DC: American Public Health Association.

Behzadian, M., Otaghsara, S.K., Yazdani, M. & Ignatius, J. (2012). A state-of the-art survey of TOPSIS applications. *Expert Systems with Applications*, *39*(17), 13051-13069.

Bouchareb, A., Metaiche, M., Lounici, H., Khoudja, H.D., Lefkir, A. & Drouiche, N. (2019). Reverse osmosis membrane performance for desalination of Algerian brackish water. *Desalination and Water Treatment Journal*, *151*, 9-19. doi 10.5004/dwt.2019.23912.

El-Harrak, N., Elazhar, F., Zdeg, A., Zouhri, N., Elazhar, M. & Elmidaoui, A. (2013). Performance analysis of the reverse osmosis desalination plant of brackish water used for irrigation: case study. *American Journal of Applied Chemistry*, *1*(3), 43-48. doi 10.11648/j.ajac.20130103.12

Environmental Protection Agency [EPA] (2004). *Guidelines for water reuse. EPA/625/R-04/108*. Washington: Environmental Protection Agency.

Garud, R.M., Kore, S.V., Kore, V.S. & Kulkarni, G.S. (2011). A short review on process and applications of reverse osmosis. *Universal Journal of Environmental Research and Technology*, *1*(3), 233-238.

Haider, H. (2017). Performance assessment framework for groundwater treatment plants in arid environment: a case of Buraydah – Saudi Arabia. *Environmental Monitoring and Assessment*, *189*(11), 189-544. doi 10.1007/s 10661-017-6271-1

Iraqi Health Ministry [IHM] (2001). *Central system for measuring and quality control. Iraqi*

*standards. I.S.S., No 417. ICA:13.060.20.* Baghdad: Health Ministry.
McDuffie, B. & Haney, J.T. (1973). *A proposed River Pollution Index*. Washington: Abstracts of Papers of the American Chemical Society.
Makki, H.F. (2009). Performance evaluation of reverse osmosis process in Al-Dura power station. *Basra Journal for Engineering Sciences*, *9*(1), 122-130.
Metcalf & Eddy Inc., Asano, T., Burton, F. & Leverenz, H. Tsuchihashi, R., Tchobanoglous, G. (2007). *Water reuse. Issues, technologies, and applications*. Los Angeles: AECOM Press.
Tahyudin, I., Rosyidi, R., Ahmar, A.S.H. & Haviluddin, H. (2018). Comparison of the Simple Additive Weighting (SAW) with the Technique for Others Reference by Similarity to Ideal Solution (TOPSIS) methods. *International Journal of Engineering & Technology*, *7*(2.2), 87-89.
Thor, J., Ding, S.H. & Kamaruddin, S. (2013). Comparison of multi criteria decision making methods from the maintenance alternative perspective. *The International Journal of Engineering and Science (IJES)*, *2*(6), 27-34.
Tsaur, R.C. (2011). Decision risk analysis for an Interval TOPSIS Method. *Applied Mathematics and Computation*, *218*(8), 4295-4304.
World Health Organization [WHO] (2003). *Guideline for drinking water quality*. Geneva: World Health Organization.

## Summary

**The performance assessment of reverse osmosis stations at Al-Mahalabea area.** The present study assesses RO stations at four sites in Al-Mahalabea area – Nineveh governorate, Iraq during the summer of 2013. The performance of RO stations are ranked by two methods: the Simple Additive Weight (SAW) and the Technique for Order of Preference by Similarity to Ideal Solution (TOPSIS). Two groups of samples were collected from feed and permeate water for two periods (at zero time of operation and after ten weeks of operation) with eleven parameters for each sample were analysed. The highest overall rejection *R* efficiency appeared with the first set of parameters more than 90% ($SO_4$, TDS, $NO_3$, TH, and turbidity), while the second set was the least (Cl, Na, and total alkalinity – TA) ranged between 65 and 85%. It is observed that both the SAW and the TOPSIS methods are accurate to predict the performance efficiency.

**Author's address:**
Mohammed Fakhraldeen Ahmed
(https://orcid.org/0000-0003-0414-0409)
Mosul University
College of Environmental Sciences
and Technology
Department of Environmental Technology
Mosul, Iraq
e-mail: milhebi@uomosul.edu.iq

Scientific Review – Engineering and Environmental Sciences (2020), 29 (3), 343–354
Sci. Rev. Eng. Env. Sci. (2020), 29 (3)
Przegląd Naukowy – Inżynieria i Kształtowanie Środowiska (2020), 29 (3), 343–354
Prz. Nauk. Inż. Kszt. Środ. (2020), 29 (3)
http://iks.pn.sggw.pl
DOI 10.22630/PNIKS.2020.29.3.29

**Mustafa O. ORIBI[1, 2], Asraa K. ABDULKAREEM[3]**

[1]Iraqi Ministry of Agriculture, Agricultural Meteorological Network
[2]MSc student at the Mustansiriyah University, College of Science
[3]Mustansiriyah University, College of Science

# Scenarios to reduce evaporation from class A evaporation pan by using windbreaks

**Key words:** evaporation basin, windbreaks natural, open water bodies, wind speed

## Introduction

Evaporation refers to the loss of water from the surface of a water body to the atmosphere, that is, the conversion of water from the liquid to the gaseous state (Yao, Zhang, Lemckert, Brook & Schouten, 2010).

Evaporation is way for wasting water around the world. There are various ways to control evaporation from reservoirs such as physical, biological, mechanical, and chemical methods (Hashemi Monfared, Rezapour & Zhian, 2019a).

Evaporation increases with increased air temperatures, high wind speeds and low humidity. Since a large amount of water is wasted every year due to evaporation from storage tanks, evaporation of water from large water bodies affects the hydrological cycle. Among the hydrological cycle, evaporation is the most difficult to estimate due to the complex interactions between the components of the Earth system and atmosphere (Singh & Xu, 1997).

There are many ways to reduce evaporation from lakes and water tanks, and these processes are not new as they started since 1960 when volatile oils were used as a layer covering the surface of the water to protect it from evaporation (Benzaghta & Mohamad, 2009).

The following methods are used to reduce evaporation such as floating lids where act as a lid on the surface of the water to reduce evaporation, such as polymers, foam wax and polystyrene (Cooley & Myers, 1973). Floating objects same principle as floating covers, however rather than a continuous cover multiple individual units are used, often floating freely. This allows for easier installation and maintenance of the cover but reduces the evaporation reduction efficiency (Cooley, 1970). Shadow struc-

tures are used to reduce wind speed and the amount of solar radiation falling on the surface of the water. This technique is suitable for small water tanks (Álvarez, Baille, Martínez & Real, 2006), chemical caps. This method are based on the use of long chain alcohol to form a thin layer on the surface of the water to reduce evaporation. These layers are biodegradable and need to be reapplied every 1 to 4 days. Chemical methods are not effective as the physical methods (Erick, 2007).

Windbreaks using to analyse the factors that cause evaporation, and thus will reduce evaporation from the lakes. This method is the best of all the mentioned methods. The reason in addition to reducing evaporation, the windbreaks also using to protect plants from the influence of winds that cause diseases and pests. It also plays an important role in reducing pollutants (Campi, Palumbo & Mastrorilli, 2009; Hong, Lee & Seo, 2015).

A windbreak is a barrier composed of trees and shrubs that redirects and modifies the force of the wind. Part of the air current is diverted over the topes of the trees and part of it filters through the trees (Manual, 1990).

Windbreaks are barriers used to reduce and redirect wind. They usually consist of trees and shrubs, but may also be perennial or annual crops and grasses, fences, or other materials. The reduction in wind speed behind windbreaks modifies the environmental conditions or microclimate in the sheltered zone. As wind blows against a windbreaks, air pressure builds up on the windward side (the side towards the wind), and large quantities of air move up and over the top or around the ends of the windbreaks. windbreaks structure – height, density, number of rows, species, composition, length, orientation, and continuity – determines the effectiveness of a windbreaks in reducing wind speed and altering the microclimate (Brandle, Hintz & Sturrock, 2012).

Because of the importance of this method, many researchers study research or use theoretical models to calculate the effect of windbreaks on reducing wind speed and evaporation.

Yusaiyin and Tanaka (2009) used wind tunnels and windbreaks to study coefficient of drag for different fenders by Navier–Stokes (RANS) equation, which depends on the width of the fenders, the result showed the width of windbreaks reduce wind velocity from 15 to 20% (Yusaiyin & Tanaka, 2009).

Kim with collaborators used the Fluid Motion Program (CFD) in the design of a windbreak fence simulation to reduce fugitive dust in open areas. This was done by studying the different wind speeds based on climatic data as well as the characteristics of the windbreaks, such as the height and density of the fenders and the distance between the fenders. the importance of this research is to provide a good way to predict and reduce flying dust in open areas (Kim et al., 2018).

Vacek with collaborators studied three types of windbreaks and their effect on high wind speeds. This was done by measuring wind speed for different distances before the fenders, and after the fenders, a station was set as a source of control. The results of the experiment showed that the height and porosity of the fenders play an important and influential role in reducing the wind speed (Vacek et al., 2018).

Hashemi Monfared, Zoraghi, Azhdary Moghaddam, Dehghani Darmian and Abdollahi (2019) in their pilot study focused on the accurate measurement of evaporation and a new approach to reduce this phenomenon in southeastern Iran (Zahedan). After evaluating the experimental results, six relationships were extracted to accurately estimate evaporation in arid regions. The glass lids were used to reduce evaporation. The cover is made of wasted glass, rubber and some floating glue. The results showed a 40% decrease in the evaporation rate.

Hashemi Monfared with collaborators aimed to study the effect of windbreaks on reducing evaporation of lakes and reservoirs in dry areas, identifying the optimum site and planning windbreaks using the FLUENT model. The results showed that winds are the most important factor affecting evaporation in the Shanima region in Sistan, Iran, and that solid windbreaks have a role in effectively reducing evaporation rates (Hashemi Monfared et al., 2019b).

The importance of this research is an applied research which serves society in terms of its applicability to reduce evaporation in environmentally friendly ways, which are natural windbreaks (trees).

## Material and methods

In this section we will look at the study area, climate data and tools used in the experiment.

### Meteorological data

The data used in this study were obtained for the monthly wind speed and direction, from the Meteorological and Seismological Organization (IMOS), other elements, air temperature, solar irradiance, and dew point depending on the climatic stations for the Meteorological Network Iraqi Agricultural.

### Study area

The study area is an experiment that has developed similar conditions to the station conditions, so that the results are more accurate and realistic.

### Experiment

The tools used in the experiment are the class A evaporation pan is a standard device for manual measurement of evaporation (Australian Bureau of Meteorology class A type), diameter 122 cm and height 25 cm, windbreaks from natural trees *Conocarpus* type, number of trees 9, distribution trees in three rows, each row contains three trees, variable height trees 50–100 cm, method of installing windbreaks (parallel and crosses), electric air fan, to direct the air on the evaporation tank and measure the wind speed before and after using the windbreaks, anemometer digital sensor (Banggood, China) to measuring wind speed [$m \cdot s^{-1}$, $km \cdot h^{-1}$, $ft \cdot min^{-1}$, knots, $mi \cdot h^{-1}$] and the finally glass house.

In this paper the researcher depending on modified Penman equation for Iraq conditions to calculate evaporation from open water surfaces such as lakes and rivers (Al-Echrish, 2001).

$$(e_s - e_a) = 33.8639[(0.00738T + + 0.8072)^8 - (0.00738T_d + 0.8072)^8 - - 0.0000342(T - T_d)] \quad (1)$$

$$E = \frac{47.7855726e^{(1.8t-180\cdot 0.1024-0.01066)\ln(R/4.1855)} - 0.0047785 + 0.64(e_s - e_a)(0.028 + 0.00009U)}{0.88153664(0.00738T + 0.8072)^7 + 0.91132775} \quad (2)$$

where:
$E$ – daily evaporation rate [cm],
$R$ – solar radiation [J·cm$^{-2}$],
$e_s - e_a$ – difference of saturated vapour pressure and air vapour pressure [kPa],
$U$ – wind speed at 10 m height above the ground [km·day$^{-1}$].
$T$ – air temperature at 1.5 m above the ground this height is stander in station [°C],
$T_d$ – dew point [°C].

This experiment carried out by using glass house (1.5 × 2 m) with an evaporation basin, to provide organized climatic conditions, then the windbreaks were placed in a direct direction with the wind direction and the measurement of the wind speed and the rate of evaporation twice using a wind gauge and the Benman equation respectively without windbreaks and with bumpers the wind. After that, three basic scenarios were adopted for the weather elements that affect the evaporation process during the summer according to the modified Benman equation for the climatic conditions in Iraq. The main factors are temperature, solar radiation, wind speed, dew point.

- The first scenario (S1) assumes that all climatic factors (air temperature, wind speed, dew point, solar radiation) are maximum.
- The second scenario (S2) assumes that all climatic factors are minimum.
- The third scenario (S3) assumes that all climatic factors are average.

Each of these three scenarios consist of sub-scenario according to the method of windbreaks installation and the number of its rows and height. Windbreaks have installed in parallel way and presented ($\alpha$), and in cross-section ($\beta$), and first row was presented (R1), second row (R2) and third row (R3). Every row has three trees, and the distance between trees and rows is 15 × 15 cm, the trees height is vary from 50 ($A$) to 100 cm ($B$).

## Results and discussion

### Effect windbreak on wind speed

Characteristics of wind velocity reduction behind the windbreak can be expressed by many parameters. The most commonly used are shelter length and width windbreaks. Windbreaks can protect a downwind area whose horizontal length is equal to up to 10 times the trees' height over which wind velocity in the downstream is reduced 20% (Manual, 1990; Yusaiyin & Tanaka, 2009).

Windbreaks reduce average wind speed in three ways. First, the absorb some of the wind energy by means of frictional drag as the moving air passes through and around them. Second, they deflect wind to higher levels. And third, windbreak redirect relatively smooth, horizontal airflow into random directions. That is more turbulence is created (Manual, 1990).

Through the results of the experiment it was found that the increase in the height of the windbreaks (trees) decreases the wind speed in all scenarios for the study period, as showing in Tables 1, 2 and 3.

TABLE 1. Extent of the effect windbreaks on reduce wind speed by experi scenarios in June

| S | Actual wind speed [m·s$^{-1}$] | With using windbreak [m·s$^{-1}$] | | | | | | | | | | | |
|---|---|---|---|---|---|---|---|---|---|---|---|---|---|
| | | $\alpha$ | | | | | | $\beta$ | | | | | |
| | | *A* | | | *B* | | | *A* | | | *B* | | |
| | | R1 | R2 | R3 | R1 | R2 | R3 | R1 | R2 | R3 | R1 | R2 | R3 |
| S1 | 8 | 7.7 | 7.3 | 6.5 | 7.1 | 6.5 | 5.6 | 7.7 | 7.1 | 6.2 | 7.1 | 6.1 | 5.2 |
| S2 | 2 | 1.7 | 1.3 | 0.5 | 1.1 | 0.5 | 0 | 1.7 | 0.9 | 0 | 1.1 | 0.3 | 0 |
| S3 | 5 | 4.7 | 4.4 | 3.6 | 4.1 | 3.5 | 2.6 | 4.7 | 4 | 3.1 | 4.1 | 3.2 | 2.1 |

Actual – measuring wind speed without using windbreaks; $\alpha$ – distributing windbreak in parallel case, $\beta$ – distributing windbreak in intersection case; *A* – windbreaks' height of 50 cm, *B* – windbreaks' height of 100 cm; R1 – one row of trees, R2 – two rows of trees, R3 – three rows of trees.

TABLE 2. Extent of the effect windbreaks on reduce wind speed by experi scenarios in July

| S | Actual wind speed [m·s$^{-1}$] | With using windbreak [m·s$^{-1}$] | | | | | | | | | | | |
|---|---|---|---|---|---|---|---|---|---|---|---|---|---|
| | | $\alpha$ | | | | | | $\beta$ | | | | | |
| | | *A* | | | *B* | | | *A* | | | *B* | | |
| | | R1 | R2 | R3 | R1 | R2 | R3 | R1 | R2 | R3 | R1 | R2 | R3 |
| S1 | 9 | 8.7 | 8.3 | 7.5 | 8.1 | 7.5 | 6.6 | 8.7 | 8.1 | 7.2 | 8.1 | 7.3 | 6.2 |
| S2 | 1.7 | 1.5 | 1.1 | 0.3 | 1 | 0.5 | 0 | 1.5 | 0.6 | 0 | 1 | 0.1 | 0 |
| S3 | 5.3 | 5 | 4.6 | 3.8 | 4.4 | 3.8 | 3 | 5 | 4.2 | 3.2 | 4.4 | 3.5 | 2.3 |

Actual – measuring wind speed without using windbreaks; $\alpha$ – distributing windbreak in parallel case, $\beta$ – distributing windbreak in intersection case; *A* – windbreaks' height of 50 cm, *B* – windbreaks' height of 100 cm; R1 – one row of trees, R2 – two rows of trees, R3 – three rows of trees.

TABLE 3. Extent of the effect windbreaks on reduce wind speed by experi scenarios in August

| S | Actual wind speed [m·s$^{-1}$] | With using windbreak [m·s$^{-1}$] | | | | | | | | | | | |
|---|---|---|---|---|---|---|---|---|---|---|---|---|---|
| | | $\alpha$ | | | | | | $\beta$ | | | | | |
| | | *A* | | | *B* | | | *A* | | | *B* | | |
| | | R1 | R2 | R3 | R1 | R2 | R3 | R1 | R2 | R1 | R1 | R2 | R1 |
| S1 | 12 | 11.7 | 11.3 | 10.3 | 11.1 | 10.3 | 9.6 | 11.7 | 11 | 9.9 | 11.1 | 10.1 | 9.2 |
| S2 | 2.5 | 2.2 | 1.8 | 1 | 1.6 | 1 | 0.1 | 2.2 | 1.5 | 0.6 | 1.6 | 0.7 | 0 |
| S3 | 7.2 | 7 | 6.5 | 5.7 | 6.3 | 5.7 | 4.9 | 7 | 6.3 | 5.2 | 6.3 | 5.5 | 4.3 |

Actual – measuring wind speed without using windbreaks; $\alpha$ – distributing windbreak in parallel case, $\beta$ – distributing windbreak in intersection case; *A* – windbreaks' height of 50 cm, *B* – windbreaks' height of 100 cm; R1 – one row of trees, R2 – two rows of trees, R3 – three rows of trees.

For example, the wind speed for June in S1 is 9 $m \cdot s^{-1}$, decreased to 8.7 $m \cdot s^{-1}$ in the case A while decreased to 8.1 $m \cdot s^{-1}$ in case B. Also, increasing the number of rows reduces the wind speed, as the wind decreases in the R3 more than the R1 and R2. The reason is due to the increased roughness surface.

As for the method of distributing trees in the rows, it appears that the intersection case reduces the winds more than the parallel case in the R2 and R3, but in the R1 no difference occurred because the porosity reduces when the windbreaks installed in crosses case as the porosity is responsible for the air volume increment that passes the windbreaks and this lead to pressure difference between the winds face that responsible for increasing the effective area that encounters the wind direction.

In addition, the number of windbreaks is playing an important role as the air density increases when the number of windbreaks is increased and this lead to affect and obstruct the airflow. The best experiment results in second scenario for the three months (summer season) because the wind velocity in minimum case, were when the height of the fenders was 100 cm, the fenders number of 3, and the method of installing the fenders in cross case [S2βBR3] recorded the highest rate of wind velocity reduction to (100%) of its original value.

**Effect wind speed on evaporation**

According to Equation (1), a direct correlation with temperature, wind speed and relative humidity relationship has been found. This means that the increase in temperature and wind speed increases evaporation rates. As a result, changing one unit of wind speed leads to a clear change in evaporation compared to other factor such as humidity.

Height, density, and orientation are the major factors determining protection provided by windbreaks, but other factors such as width, cross-sectional shape, and composition are also important (Brandle & Finch, 1991).

Low density of windbreaks is responsible for increasing the volume of air passing. This leads to a pressure difference between two sides of the wind, responsible for the increase in an effective area on the side of the wind and the porosity is one of the most effective factors in windbreak structures (Hashemi Monfared et al., 2019).

Through the results of research, it was found that wind speed have an important role in reducing evaporation rate for summer season and showed in Figures 1, 2 and 3. Based on the empiricist relationship, a direct connection has been detected between wind speed and the evaporation, as the evaporation rate increases when wind speed increase, therefore, one unit change of wind velocity creates the clear change in evaporation compared to other factors such as dew point. The experiment proved the significant role of wind speed in evaporation rate limitation. By calculating the actual evaporation of the evaporation basin class A for all scenarios by using Equation (1). Figures 1, 2, and 3 illustrated the gradual decline in the evaporation rate within the summer season.

The following factors have clear effect on the windbreaks; windbreaks height and its number of rows and way of installed it where affect on air density and this is the reason beyond declining

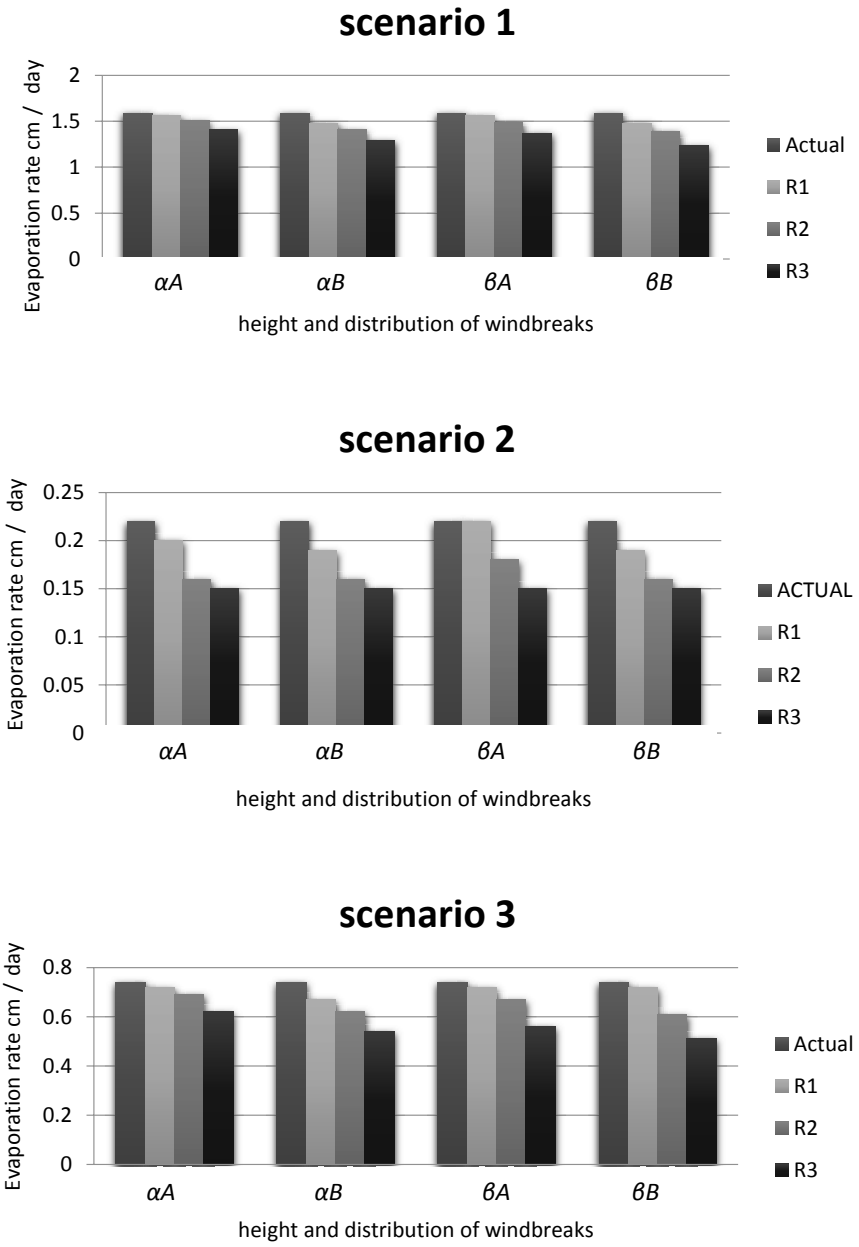


Actual – measuring wind speed without using windbreaks; $\alpha$ – distributing windbreak in parallel case, $\beta$ – distributing windbreak in intersection case, *A* – trees' height of 50 cm, *B* – trees' height of 100 cm; R1 – one row of trees, R2 – two rows of trees, R3 – three rows of trees.

FIGURE 1. Histogram for the effect windbreaks on evaporation rate for three scenarios in June

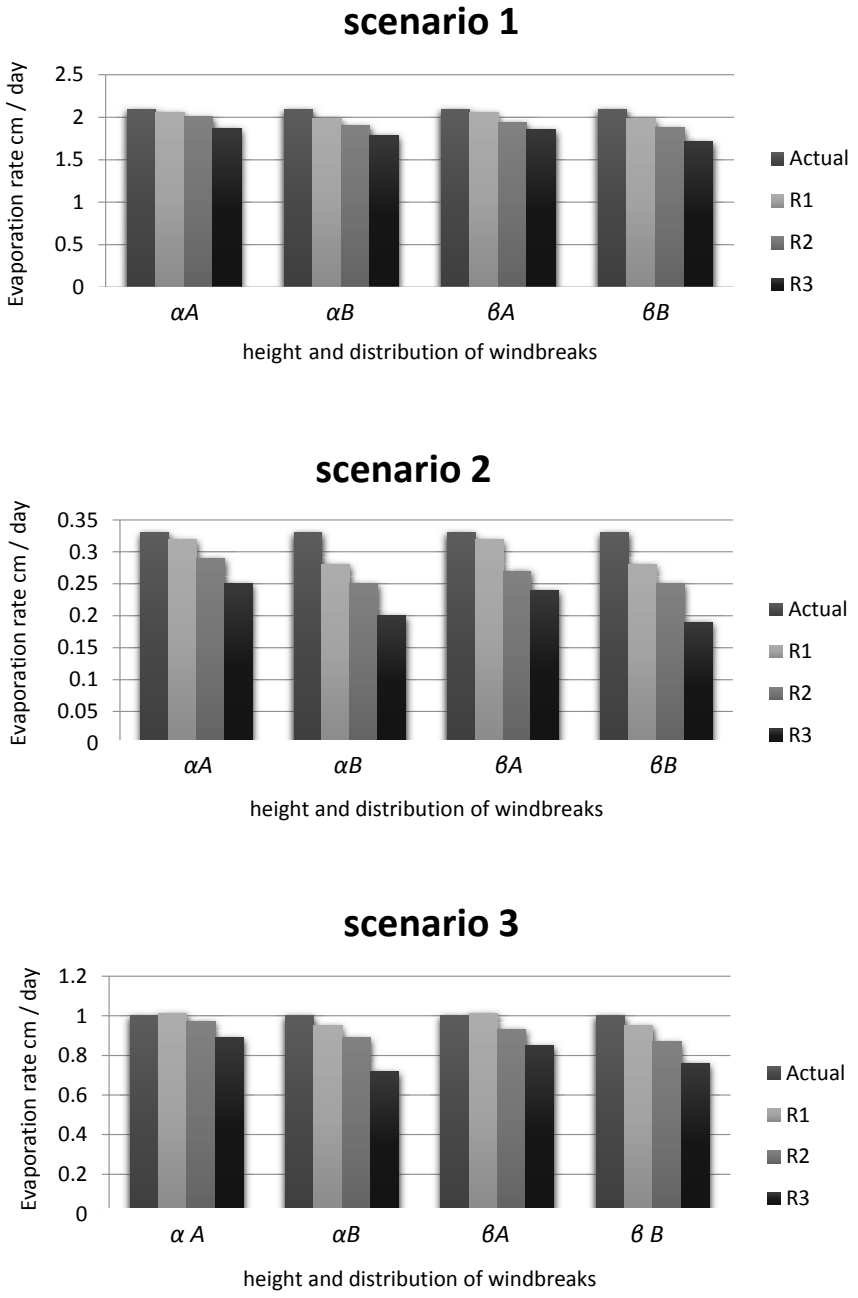


Actual – measuring wind speed without using windbreaks; $\alpha$ – distributing windbreak in parallel case, $\beta$ – distributing windbreak in intersection case, $A$ – trees' height of 50 cm, $B$ – trees' height of 100 cm; R1 – one row of trees, R2 – two rows of trees, R3 – three rows of trees.

FIGURE 2. Histogram for the effect windbreaks on evaporation rate for three scenarios in July

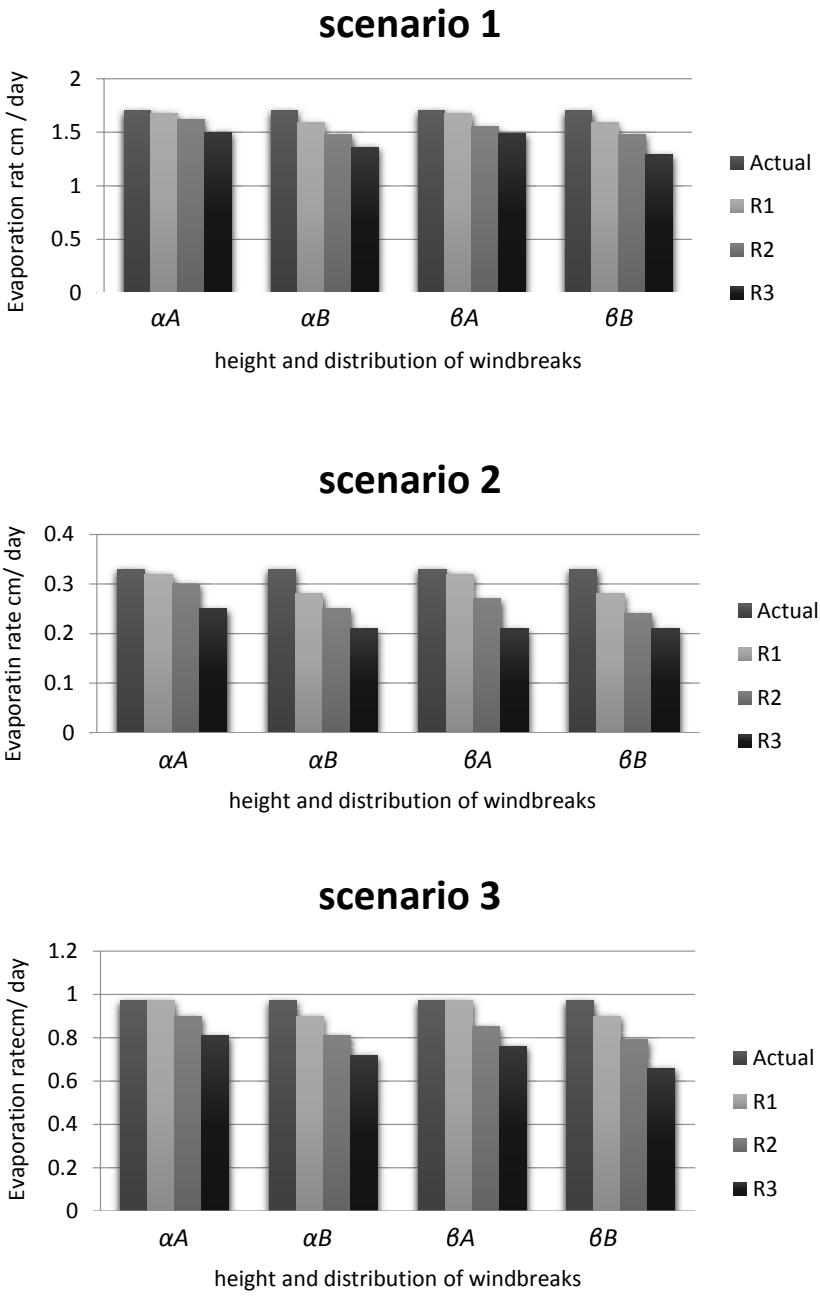


Actual – measuring wind speed without using windbreaks; $\alpha$ – distributing windbreak in parallel case, $\beta$ – distributing windbreak in intersection case, $A$ – trees' height of 50 cm, $B$ – trees' height of 100 cm; R1 – one row of trees, R2 – two rows of trees, R3 – three rows of trees.

FIGURE 3. Histogram for the effect windbreaks on evaporation rate for three scenarios in August

the evaporation rate in the three scenarios as shown in Figures 1, 2 and 3.

The effect of wind on evaporation is evident in different ratio and for all months. As the sub-scenario R3 in the S1 and S3 of the scenario is in all months given the best result of reducing evaporation up 35% to almost but in a scenario S2 there was no clear change because the wind was originally the min value.

The best experiment results were when the height of the fenders was 100 cm, the number of fenders 3, and the method of installing the windbreaks in crosses case [βBR3] recorded the highest rate of evaporation reduction up to 35% of its original value before using windbreaks.

## Conclusions

Through this study it was found that windbreaks have a very important role in reducing wind speed. This depends on the height, density of the trees and number of rows. The best experiment results are when the height of the windbreak was 100 cm, the number of row 3, and the method of installing windbreaks in crosses case [βBR3] recorded the highest rate of evaporation reduction up to 35% of its original value before using windbreaks. Eventually, it can be concluded that the wind is one of the most important factors that have effect on the evaporation rate, it is considered one of the best methods because it is environmentally friendly, unlike chemical methods that affect the environment and living organisms in lakes so the windbreaks can adopted to control the evaporation rate. In addition to this use, the windbreaks can be used to protect from sand dunes and to protect strategic crops from the impact of wind speeds.

## Recommendations

1. Study on the best types of trees that can be used as windbreaks.
2. Study effect trees on wildlife.
3. Applying this study in small lakes.

### Acknowledgements

The authors would like to thank Prof. Dr Monim Hakeem Khalaf Al-Jiboori followed in the Atmospheric Sciences Department, the College of Science, the Mustansiriyah University, for his comments and suggestions in improving the paper and also editing English writing.

## References

Al-Echrish, A.A. (2001). *Modeling of evaporation in Iraq* (master's thesis). Baghdad: Al--Mustansiriyah University.

Álvarez, V.M., Baille, A., Martínez, J.M.M. & Real, M.M.G. (2006). Effect of black polyethylene shade covers on the evaporation rate of agricultural reservoirs. *Spanish Journal of Agricultural Research*, *4*, 280-288.

Benzaghta, M.A. & Mohamad, T.A. (2009). Evaporation from reservoir and reduction methods: an overview and assessment study. *International Engineering Convention.* Domascus, Syria and Medinah, Kingdom of Saudi Arabia, 11-18 May 2009. Domascus, Syria and Medinah, Kingdom of Saudi Arabia: IEC.

Brandle, J.R. & Finch, S. (1991). *EC91-1763-B How windbreaks work*. Lincoln: University of Nebraska-Lincoln.

Brandle, J.R., Hintz, D.L. & Sturrock, J. (2012). *Windbreak technology*. Amsterdam: Elsevier Science.

Campi, P., Palumbo, A. & Mastrorilli, M. (2009). Effects of tree windbreak on microclimate and wheat productivity in a Mediterranean environment. *European Journal of Agronomy*, *30*(3), 220-227.

Cooley, K.R. (1970). Energy relationships in the design of floating covers for evaporation reduction. *Water resources research*, *6*(3), 717-727.

Cooley, K.R. & Myers, L.E. (1973). Evaporation reduction with reflective covers. *Journal of the Irrigation and Drainage Division*, *99*(3), 353-363.

Erick, S. (2007). *Controlling evaporation losses from large storage dams using chemical monolayers. Report*. Toowoomba: University of Southern Queensland, Australia.

Hashemi Monfared, S.A., Rezapour, M. & Zhian, T. (2019a). Using windbreaks for decreasing lake and reservoir evaporation: a case study from Iran. *Polish Journal of Environmental Studies*, *28*(4), 1-10.

Hashemi Monfared, S.A., Zoraghi, K., Azhdary Moghaddam, M., Dehghani Darmian, M. & Abdollahi, A. (2019b). Comparison and measurement of evaporation from water surface of the reservoirs in arid areas and evaluation of a glass cover to reduce evaporation. *Journal of Hydrosciences and Environment*, *3*(5), 14-29.

Hong, S.W., Lee, I.B. & Seo, I.H. (2015). Modelling and predicting wind velocity patterns for windbreak fence design. *Journal of Wind Engineering and Industrial Aerodynamics*, *142*, 53-64.

Kim, R.W., Lee, I.B., Kwon, K.S., Yeo, U.H., Lee, S.Y. & Lee, M.H. (2018). Design of a windbreak fence to reduce fugitive dust in open areas. *Computers and Electronics in Agriculture*, *149*, 150-165.

Manual, A.F. (1990). *Illinois Extension Forestry.* Illinois: Riverside Publishing.

Singh, V. & Xu, C.Y. (1997). Evaluation and generalization of 13 mass-transfer equations for determining free water evaporation. *Hydrological Processes*, *11*(3), 311-323.

Vacek, Z., Řeháček, D., Cukor, J., Vacek, S., Khel, T., Sharma, R.P., Kučera J., Král, J. & Papaj, V. (2018). Windbreak efficiency in agricultural landscape of the Central Europe: multiple approaches to wind erosion control. *Environmental Management*, *62*(5), 942-954.

Yao, X., Zhang, H., Lemckert, C., Brook, A. & Schouten, P. (2010). Evaporation reduction by suspended and floating covers: overview, modelling and efficiency. *Urban Water Security Research Alliance Technical Report*, *28*, 1-13.

Yusaiyin, M. & Tanaka, N. (2009). Effects of windbreak width in wind direction on wind velocity reduction. *Journal of Forestry Research*, *20*(3), 199-204.

## Summary

**Scenarios to reduce evaporation from class A evaporation pan by using windbreaks.** Evaporation from reservoirs and lakes is an important processes frequently occurring in dry, hot regions such as Iraq. In order to preserve the environment and to reduce the amount of evaporation from open water bodies in this study, simulation was performed to reduce evaporation from evaporation basin class A by using windbreaks natural (*Conocarpus* trees). Three basic scenarios were made that depended on the values of the atmospheric elements affecting the evaporation process in summer according to the modified Penman equation for the conditions of Iraq, the climate factors are temperature, solar radiation, wind speed, dew point, and the effect of the number of windbreaks and their height was also introduced in sub- scenario. Experiments have shown that the best sub-scenario for all basic scenarios is when the windbreaks are placed in a direct direction to the wind blowing on the evaporation basin in the form of three rows, each row contains three trees where the windbreaks are in case cross and the height of the trees is 100 cm and the distance between

each tree and another, and between each row and row 15 × 15 cm, the results of this sub-scenario recorded the highest rate of evaporation reduction up to 35% of its original value before using windbreaks.

**Authors' address:**
Mustafa O. Oribi – corresponding author
(https://orcid.org/0000-0003-4414-9328)
Iraqi Ministry of Agriculture
Agricultural Meteorological Network

Mustansiriyah University
College of Science
Department of Atmospheric Sciences
Bagdad, Iraq
e-mail: mustafaudah425@gmail.com

Asraa K. Abdulkareem
(https://orcid.org/0000-0003-2103-0295)
Mustansiriyah University
College of Science
Department of Atmospheric Sciences
Bagdad, Iraq
e-mail: dr.asraa.atmsc@uomustansiriyah.edu.iq

Scientific Review – Engineering and Environmental Sciences (2020), 29 (3), 355–365
Sci. Rev. Eng. Env. Sci. (2020), 29 (3)
Przegląd Naukowy – Inżynieria i Kształtowanie Środowiska (2020), 29 (3), 355–365
Prz. Nauk. Inż. Kszt. Środ. (2020), 29 (3)
http://iks.pn.sggw.pl
DOI 10.22630/PNIKS.2020.29.3.30

**Salwa S. NAIF[1], Najlaa Mohamed HADI[2], Monim H. Al-JIBOOR[1]**

[1]Mustansiriyah University, College of Science
[2]University of Babylon, College of Education for Pure Sciences

# Study of temporal variations of nocturnal and daytime urban heat island in Baghdad

**Key words:** urban heat island, urban impacts, minimum and maximum temperature, temperature trend, Baghdad

## Introduction

The concept of urban heat island (UHI) describes the phenomenon, which takes place in the core of cities or towns, characterized by higher air or surface temperatures, than in surrounding rural areas (Bhargava, Lakmini & Bhargava, 2017). This effect has important implications for energy consumption, environmental pollution and human health and comfort and water use. The warmer urban surface is present at all around the world and has potential impact to local warming (Kalnay & Cai, 2003). It seems with highest intensity basically at nights and inland cities when the sky is free of clouds and the winds are weak. As a result of the rising trend of the urban population, UHI effect emerges due to continued urbanization processes (Nuruzzaman, 2015) that alter the natural land cover to impervious surfaces (Rosenzweig et al., 2005), urban geometry which refers to dimension and spacing of building within a city, and anthropogenic heat activities that include heating, transportation, industry, air condition system that add a waste energy to urban canopy heating (US EPA, 2008).

Nocturnal and daytime UHI can be observed using minimum and maximum air temperature ($T_{min}$ and $T_{max}$) recorded at 2 m during the one day at weather stations (WMO, 2007). There is a discrepancy in difference of UHI intensity between summer and winter. Most studies reported that less UHI was in winter (Oke, 1976; Wilby, 2003; Golroudbary, Zeng, Mannaerts & Su, 2018), while others showed that most winter UHIs were more intense than summer UHIs (Souch & Grimmond, 2006; Sailor, 2006; Schatz & Kucharik, 2014). Thus, this gap in determining which season has most intense UHI requires a careful analysis that will be useful in assessing the

potential implications described above. This study is the first attempt to compare climatically different areas within and outside of Baghdad dependent on real observing. Study of the temporal variations in the UHI over urban areas expresses the modifications in radiation and energy balance at the canopy air layer extending from the ground to below the tops of trees or buildings (Oke, 1976; Bhargava et al., 2017). Buildings, paved roads and other urban substructures tend to store shortwave solar energy during the daytime and then release it back to space as longwave terrestrial radiation after sunset creating increased temperature compared with suburban areas. The ongoing increase in population census in the most world cities (UN, 2018) can be considered an additional factor in intensifying UHI (Oke, 1973).

As the urban landscape transformations associated with land cover changes and increased population continue to grow, the warming effect in densely cities is enhancing the local warming climates as well. This effect has been found in the long-term trends of temperature when the temporal variations of daily, monthly, seasonal and annual mean temperature have been investigated (Huang & Lu, 2015), because of a large portion of the greenhouse gases produced in these environments. Thus, the main aim of this work is to study the nocturnal and daytime UHI in Baghdad on the basis of monthly, seasonal and annual analysis. In addition, the annual trends are also investigated to predict the behaviour of UHI intensities.

## Study area and data

The city of Baghdad, capital of Iraq, is located in inner flat land of the central government which covers 894.3 km$^2$ and has extremely hot, dry summer and damp winter. It is located along Tigris river which divides into two sides Rasafa (east) and Karkh (west), as shown in Figure 1. The urban fabric consists of blocks of low-rise houses (1–3 floors) with 5–12 m high. Several medium-rise buildings up to 20 floors are mostly formal offices and hotels. Baghdad is the commercial, financial and cultural centre of Iraq. The average geography coordinates are of latitude 33.2°N, longitude 44.3°E and 34 m a.m.s.l. After replacing political system in 2003, random urbanization expansion and inner immigration are in particular observed in Baghdad.

The time series of the daily data for minimum ($T_{min}$) and maximum ($T_{max}$) air temperature were acquired from two automatic weather stations (see their photographs in Fig. 1) separated by 20 km distance (Sundus & Al-Jiboori, 2018). Both $T_{min}$ and $T_{max}$ were observed around the dawn (nighttime or nocturnal) and after the noon (daytime), respectively. First station (1) located in the centre of Baghdad on the roof of the Atmospheric Sciences Department building, the Mustansiriyah University with 14 m high above the ground level, which is considered as urban site. Another station (2) belongs to Iraqi Meteorological Organization and Seismology set up in the International Baghdad Airport with height of 2 m. This lies on the border

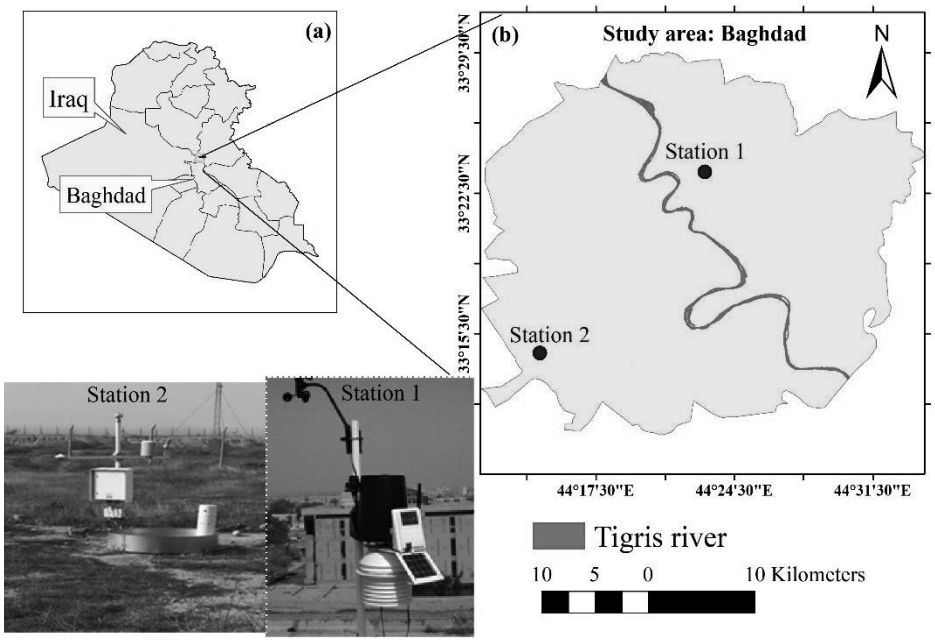


FIGURE 1. Location of Iraq (a) and Baghdad (b) with photographs of two automatic weather stations

of Baghdad with very open area, thus it is considered as rural site. Although the heights of two stations are different, air temperature measurements did not experience significantly differences. This is expected in the canopy of urban area due to theory of constant heat flux in the surface layer of lower atmosphere (Stull, 1989).

The above data collected were analysed for only three years 2008, 2013 and 2019. Fortunately, there were not any missing or gap in the time series because of continuous observation. Three five-year intervals were chosen to show real changes in landscape of Baghdad. To examine the canopy layer UHI and study the dynamic characteristics of the air mass overlying the urban area during the years, these data were chosen to represent middle months of the seasons of the year: January (winter), April (spring), July (summer) and October (autumn). The choice of only one month of each

TABLE 1. Climatic values of air temperature, rainfall and daylight hours for each season

| Season | Temperature range [°C] | Average temperature [°C] | Average rainfall [mm] | Rainfall days | Average daylight [h] |
|---|---|---|---|---|---|
| Winter | 4–16 | 12 | 85 | 18 | 10.5 |
| Spring | 15–29 | 23 | 67 | 15 | 12.4 |
| Summer | 22–44 | 35 | 0 | 0 | 14.2 |
| Autumn | 10–40 | 24 | 25 | 5 | 11.4 |

season is suitable because that the study area is generally cloud-free for most the year, as shown in Table 1 which also displays some climate features for temperature, rainfall and daylight hours at each season.

## Methodology

The main root causes of modification in urban climate are the urbanization process, landscape geometry and thermal properties of building and surface materials (Nuruzzaman, 2015). To confirm the existing UHI in Baghdad, it is important to distinguish the two different areas in the surface characteristics such as urban and rural sites. The comparison of urban versus rural stations is adopted in this study.

Thus, first, daily nocturnal and daytime canopy urban heat islands are usually determined using daily $T_{min}$ and $T_{max}$ measurements taken from these stations, thus UHI intensities were defined as:

$$nocturnal\ UHI = T_{min}(u) - T_{min}(r) = \Delta T(u\text{-}r)_{min} \quad (1)$$

$$daytime\ UHI = T_{max}(u) - T_{max}(r) = \Delta T(u\text{-}r)_{max} \quad (2)$$

The symbols $u$ and $r$ refer to urban and rural conditions.

Second, average values of the resulting daily $\Delta T(u\text{-}r)_{min}$ and $\Delta T(u\text{-}r)_{max}$ were separately calculated for expressing seasonal averages and by the same method, annual averages were computed from seasonal averages.

Third, the three years indicated in the previous section do not experience any extreme climatic means concerning other years (i.e. from 2009–2018, except 2013), but they were in normal conditions. Thus, linear trends were fitted to the annual averages of $\Delta T(u\text{-}r)_{min}$ and $\Delta T(u\text{-}r)_{max}$ by least square method using Origin software (ver. 9.3). This is useful in determining the rate of change by year and to predict the behaviour of UHI intensities in proximity future especially in suggestion the relevant mitigation strategies for adaptation under ongoing global warming. However, the results of nocturnal and daytime UHI were separately fitted to simple linear regression given as

$$UHI(t) = \alpha + \beta \cdot t \quad (3)$$

where
$t$ – independent variable [year],
$\alpha$ – intercept,
$\beta$ – slope (trend).

Fourth, the significance level (t-test, $p < 0.05$) and correlation coefficient ($r$) were determined to explore the potential implications under local climate change.

## Results and discussion

### Daily variation of nocturnal and daytime UHIs

The variations in nocturnal and daytime UHIs, as derived from Equations (1) and (2) respectively, were investigated among 2008, 2013 and 2019. Figures 2 and 3 show daily variations of both nocturnal and daytime UHIs, respectively in four representative months: January, April, July and October. The intra-month variability in all UHI values is obvious due to the air layer adjacent to the sur-

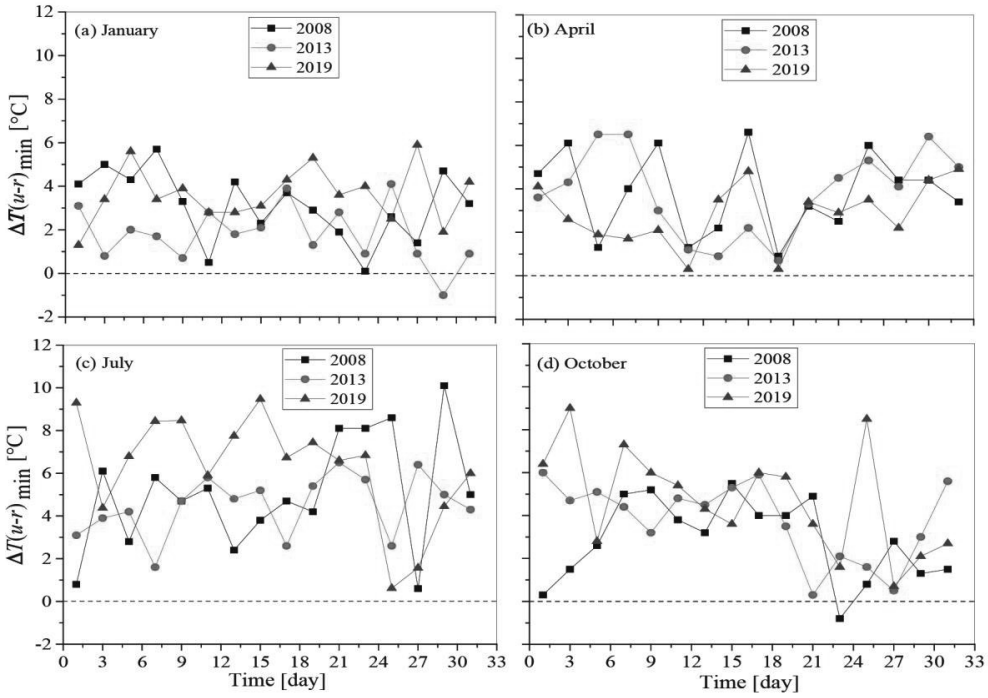


FIGURE 2. Daily variation of nocturnal UHI for three years (2008, 2013 and 2019) in months: January (a), April (b), July (c) and October (d)

face strongly affected by the physical processes as well as the external pressure systems passing the area.

Nocturnal UHI seems to have positive values along the year with its strongest value in summer exceeding 5°C at the above studied years. It can be concluded that at night minimum temperature values in urban area are always larger than those in rural areas. In summer (July) and sometimes autumn (October) months of 2019, UHI intensity reaches the largest positive values beyond 6°C (Figs. 2c and 2d). The positive moderate nocturnal UHI intensity occurred in other seasons (January, April and October) when UHI reached values of about beyond 4°C as illustrated in Figures 2a, 2b and 2d. The least positive value of about 1°C was found in January of 2013.

A different result variation is observed for the daily daytime UHI across all the months of all years. As shown in Figure 3 daily daytime UHI intensity has mostly negative values for both years 2008 and 2013, while in 2019 these values become positive, especially in April (Fig. 3b) and July (Fig. 3c) reaching more than 1°C. It is important to notice that, in Figure 3a across all years, UHI values not only show the increasing trend during the days of January, but also they are approximately close to each other. The reason is that at the last third of January in general the air temperature starts to be warm up and also continuing use with

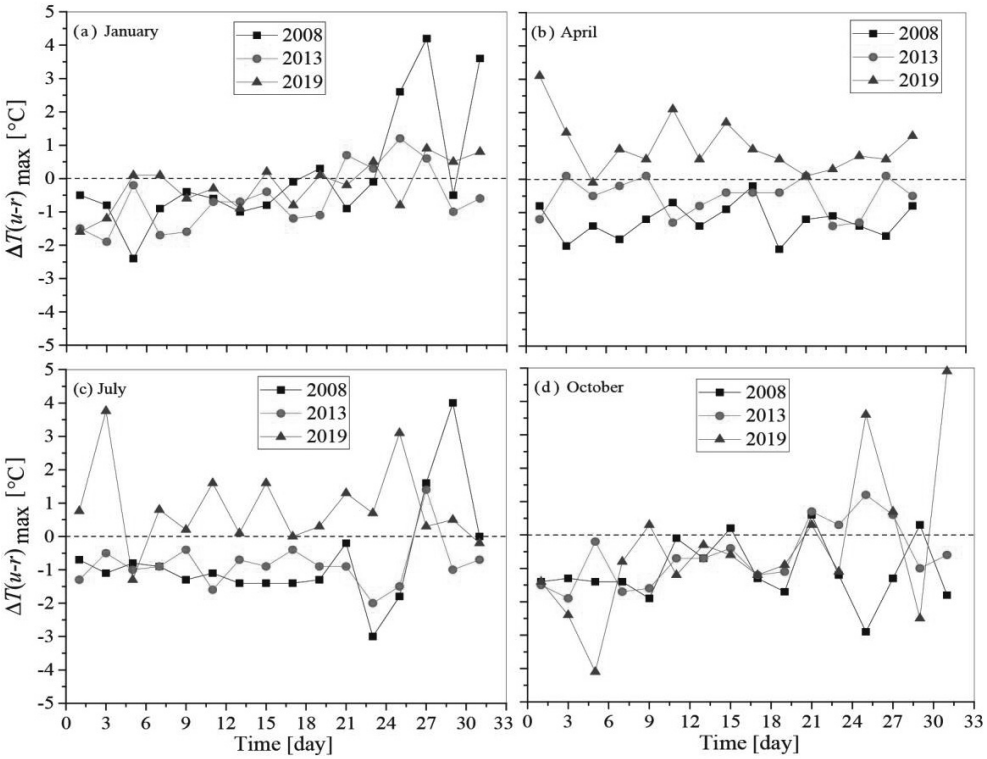


FIGURE 3. Daily variation of daytime UHI for three years (2008, 2013 and 2019) in months: January (a), April (b), July (c) and October (d)

different warming means by dwellers to facing cold winter which, of course, will raise air temperature in urban site. The similar result is nearly also found in October (Fig. 3d), but with more scatter.

## Seasonal variation of nocturnal and daytime UHIs

To reduce high variability in daily nocturnal and daytime UHI, monthly means of January, April, July and October were computed which express winter, spring, summer and autumn and displayed in Figures 4 and 5, respectively. These figures show a distinct seasonal cycle of the $\Delta T(u\text{-}r)_{min}$ and $\Delta T(u\text{-}r)_{max}$. This cycle reveals the weakest and strongest UHI intensities in winter and summer, and different amplitudes in spring and autumn. Absolute positive nocturnal UHI values are found at all seasons and years with average highest during summer and weakest in winter, as shown in Figure 2, which are consistent with the result found in Arnfield (2003) and Schatz and Kucharik (2014). These values are also largest in 2019 except in spring (Fig. 4).

At semiarid environments like Baghdad the summers are characterized by strong solar energy and greater day hours (~14.2 h) with no cloud or rain (Table 1), therefore loss of energy through long wave radiation at nights is

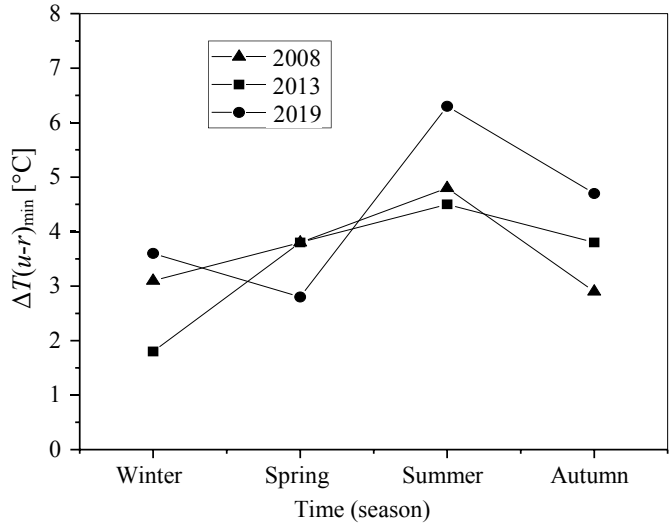


FIGURE 4. Seasonal variation of nocturnal UHI for three years: 2008, 2013 and 2019

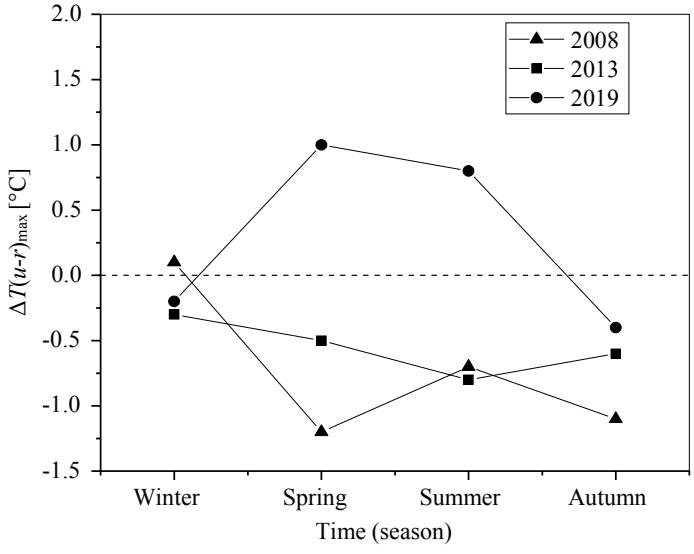


FIGURE 5. Seasonal variation of daytime UHI for three years: 2008, 2013 and 2019

little in urban cities compared to rural areas, so that the well-known effect of the UHI occurs. In general, the inversing result to nocturnal UHI is clear in seasonal variation of daytime UHI, $\Delta T(u\text{-}r)_{max}$, as shown in Figure 5, whereas the cold islands were established well especially in all seasons of two years 2008 and 2013, while in 2019 urban heat island raised in spring and summer (~0.65°C).

As mentioned in the previous discussions that there was more intense UHI in

2019. This belongs to expected several causes: (1) population growth in Baghdad is continuously increasing which reaches 7.9 million in this year (Al-Jiboori, Abu Al-Shear & Ahmed, 2020); (2) the gradual reduction in green areas and their replacement to residential, commercial and industrial are characterized in the city without official approvals (Hussain, 2018); (3) Baghdad is one of the mid-latitude cities whereas the most intensive UHIs have been observed (Wienert & Kuttler, 2005) due to regional and global climate change that might be influenced the ongoing increasing in temperature (Saaroni, Amorim, Hiemstra & Pearlmutter, 2018).

## Annual variation of nocturnal and daytime UHIs

To be more clear in studying nocturnal and daytime UHI, the annual averages are computed using seasonal averages and presented in Figure 6, in which the vertical lines represent the spreading around the annual means, i.e. standard deviation (*SD*). At night time, the similar result of annual thermal differences between urban and rural sites, annual $\Delta T(u\text{-}r)_{\min}$, is also confirmed with high *SD* at three values of the years 2008, 2013 and 2019. Although the values of $\Delta T(u\text{-}r)_{\max}$ are little, it can also clearly see linear increase from 2008 to 2019. The same behaviour is also found in the results of daytime difference with less *SD*.

We now tried to evaluate the annual linear increases in both nocturnal and daytime UHI values during the studied period by calculating the linear trend. Their results were separately fitted using Equation (3). The constants were empirically derived from nocturnal and daytime UHI data which reported in Table 2.

The nocturnal UHI behaviour is more intense (where $\beta = 0.09°C \cdot year^{-1}$ with $r = 0.09$ and $p < 0.001$) than that of day-

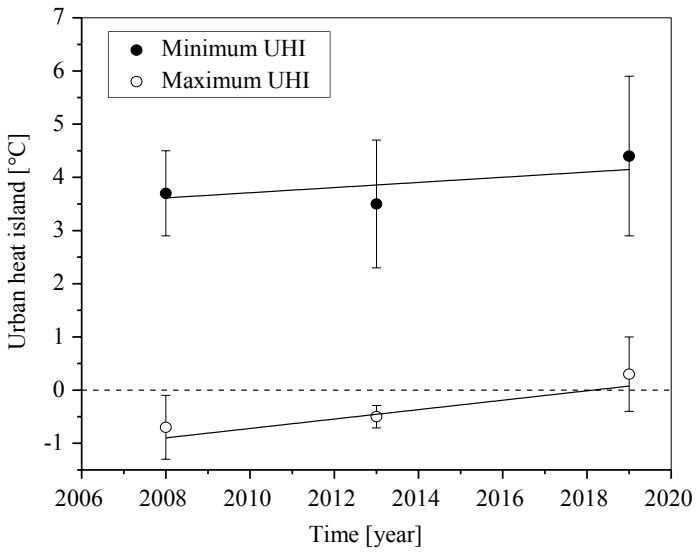


FIGURE 6. Annual variation of both nocturnal and daytime UHIs. Solid lines are for fitting data

TABLE 2. Mean intensities of nocturnal and daytime UHIs in Baghdad

| UHI intensity [°C] | $\alpha$ | $\beta$ [°C·year$^{-1}$] | $r$ | $p$ |
|---|---|---|---|---|
| Nocturnal | –158.3 | 0.09 | 0.79 | < 0.001 |
| Daytime | –63.4 | 0.05 | 0.63 | < 0.005 |

time ($\beta = 0.5$°C·year$^{-1}$ with $r = 0.63$ and $p < 0.005$). Differences between nocturnal and daytime UHI intensities are also apparent from annual trend (Fig. 6, Table 1).

## Conclusions

Daily, seasonal and annual variations are fundamental to the investigation of UHI. Using minimum and maximum temperature data for three five-year period (2008, 2013 and 2019) measured by automatic weather stations located at two different sites with roughness (urban versus rural), nocturnal and daytime UHIs were calculated at four months that represent the four seasons: January (winter), April (spring), July (summer) and October (autumn). Baghdad's UHI is most intensive at the centre of city than at outlying rural site. The intensity of nocturnal UHI has positive signs at all seasons, while daytime UHI shows positive and negative signs across these seasons. In addition, nocturnal UHI intensity in summer has increased to reach maximum 6.5°C in 2019, 4.6°C in 2008 and 2013, while in summer and spring of 2019 daytime UHI reach 0.8°C. This has been attributed to rapid warming in night in the city, possible linked to land cover changes and rapid population growth. Also annual trends of nocturnal and daytime UHIs show linear increase during the studied period. This increase has adverse effects on urban climate, thus several mitigation strategies such as increase vegetated areas, planting shading trees, green roofs using high albedo building materials, etc. are suggested as powerful tools to reduce potential thermal impacts.

### Acknowledgements

The authors are grateful to the Mustansiriyah University and the University of Babylon for acceptance this work. The authors also thank anonymous reviewers for constructive comments, which have improved the quality of this paper.

## References

Al-Jiboori, M.H., Abu Al-Shear, M.J. & Ahmed, M.M. (2020). Impact of land surface changes on air temperatures in Baghdad. *Kuwait Journal of Science*, *47*(4) [in press].

Arnfield, A.J. (2003). Two decades of urban climate research: A review of turbulence, exchanges of energy and water, and the urban heat island. *International Journal of Climatology*, *23*(1), 1-26. doi 10.1002/joc.859

Bhargava, A., Lakmini, S. & Bhargava, S. (2017). Urban heat island effect: It's Relevance in urban planning. *Journal of Biodivversity & Endangered Species*, *5*(1), 1-4. doi 10.4172/2332-2543.1000187

Golroudbary, V.R., Zeng Y., Mannaerts, C.M. & Su, Z. (2018). Urban impacts on air temperature and precipitation over the Netherland. *Climate Research*, *75*(2), 95-109. doi 10.3354/cr01512

Huang, Q. & Lu, Y. (2015). The effect of urban heat island on climate warming in the Yangtze river delta urban agglomeration in China. *International Journal of Environmental Research and Public Health*, *12*(8), 8773-8789. doi 10.3390/ijerph120808773

Hussain, R.Y. (2018). Land use change within the basic design in north of Baghdad. *ARPN Journal of Engineering and Applied Sciences*, *13*(20), 8284-8295.

Kalnay, E. & Cai, M. (2003). Impact of urbanization and land-use change on climate. *Nature*, *423*(6939), 528-531.

Nuruzzaman, M.D. (2015). Urban heat island: Causes, effects and mitigation measures - A review. *International Jourbal of Environmental Monitoring and Analysis*, *3(2)*, 67-73. doi 10.11648/j.ijema.20150302.15

Oke, T.R. (1973). City size and the urban heat island. *Atmospheric Environment Pergamon Press*, *7*(8), 769-779.

Oke, T.R. (1976). The distinction between canopy and boundary-layer urban heat islands. *Atmosphere*, *14*(4), 268-277.

Rosenzweig, C., Solecki, W.D., Parshall, L., Chopping, M., Pope, G. & Goldberg, R. (2005). Characterizing the urban heat island effect in current and future climates in urban New Jersey. *Environmental Hazards*, *6*(1), 51-62.

Saaroni, H., Amorim, J.H., Hiemstra, J.A. & Pearlmutter, D. (2018). Urban green infrastructure as a tool for urban heat mitigation: Survey of research methodologies and findings across different climatic regions. *Urban Climate*, *24*, 94-110. doi 10.1016/j-uclim.2018.02.001

Sailor, D.J. (2006). Mitigation of urban heat islands – Recent progress and future prospects. In *Proceedings of 6th Urban Environment Symposium.* Atlanta, GA. 28 Jan.–2 Feb. 2006. Boston: American Meteorological Society.

Schatz, J. & Kucharik, Ch.J. (2014). Seasonality of the urban heat island effect in Madison, Wisconsin. *Journal of Applied Meteorology and Climatology*, *53*(10), 2371-2386.

Souch, C. & Grimmond, S.B. (2006). Applied climatology: Urban climate. *Progress in Physical Geography*, *30*(2), 270-279.

Stull, R.B. (1989). *An introduction to boundary layer meteorology.* Dordrecht: Kluwer Academic Publisher.

Sundus, H. & Al-Jiboori, M.H. (2018). The study of Refractive-index structure of coefficient behavior derived from two weather stations at Baghdad City. *Al-Mustansiriyah Journal of Science*, *29*(4), 1-6.

United States Environmental Protection Agency [US EPA] (2008). *Heat island compendium.* Retrieved from https://www.epa.gov/heatislands/heat-island-compendium

United Nations [UN] (2018). *World urbanization prospects* (ST/ESA/SER.A/352). New York: Department of Economic and Social Affairs, Population Division.

Wienert, U. & Kuttler, W. (2005). The dependence of urban heat island intensity on latitude – a statistical approach. *Meteorologische Zeitschrift*, *14*(5), 677-686.

Wilby, R.L. (2003). Past and projected trends in London's urban heat island. *Weather*, *58*(7), 251-260.

World Meteorological Organization [WMO] (2007). *Guide to meteorological Iinstruments and methods of observations*. Geneva, Switzerland: World Meteorological Organization.

## Summary

**Study of temporal variations of nocturnal and daytime urban heat island in Baghdad.** Based on daily minimum and maximum air temperature observations for three years: 2008, 2013 and 2019, measured by automatic weather stations located at two sites of Baghdad city were used to compute nocturnal and daytime urban heat island (UHI). First station fixed in campus of the Mustansiriyah University is considered as urban area, and another station followed to Iraqi meteorological organization installed at the International Baghdad Airport was chosen as the rural site. Daily, seasonal and annual averages of nocturnal and daytime UHIs were presented to study the variability and trends.

The results show the evolution of a nocturnal UHI, whose high mean values were recorded in four seasons with largest value found in summer of 2019. Annual trend in nocturnal UHI intensities was found to be larger than that of daytime. Thus, this study propose that maintenance and increase urban parks and planting shading tall trees to mitigate UHI intensity in Baghdad city.

**Authors' address:**
Salwa S. Naif
(https://orcid.org/0000-0002-3793-1162)
Mustansiriyah University
College of Science
Department of Atmospheric Sciences
e-mail: naif.salwa2016@gmail.com

Najlaa Mohamed Hadi
(https://orcid.org/0000-0001-8632-8813)
University of Babylon
College of Education for Pure Sciences
Department of Physics
e-mail: awad_najlaa@yahoo.com

Monim H. Al-Jiboori
(https://orcid.org/0000-0002-0816-3918)
Mustansiriyah University
College of Science
Department of Atmospheric Sciences
e-mail: mhaljiboori@gmail.com

Scientific Review – Engineering and Environmental Sciences (2020), 29 (3), 366–376
Sci. Rev. Eng. Env. Sci. (2020), 29 (3)
Przegląd Naukowy – Inżynieria i Kształtowanie Środowiska (2020), 29 (3), 366–376
Prz. Nauk. Inż. Kszt. Środ. (2020), 29 (3)
http://iks.pn.sggw.pl
DOI 10.22630/PNIKS.2020.29.3.31

**Diana CAR-PUŠIĆ[1], Ksenija TIJANIĆ[1], Ivan MAROVIĆ[1], Marko MLAĐEN[2]**

[1] University of Rijeka, Faculty of Civil Engineering
[2] GT-Trade d.o.o., Split, Croatia

# Predicting buildings construction cost overruns on the basis of cost overruns structure

**Key words:** cost overrun, quantities of works, unforeseen works, additional works, linear regression analysis, soft computing methods

## Introduction

Construction costs are one of the main criteria for decision making in the early stages of the construction process, and therefore their prediction is of interest to all project participants (Ambrule & Bhirud, 2017). Experience has shown that very often there are discrepancies between the estimated costs in relation to the realized costs of the construction project (Peško Trivunić, Cirović & Mučenski, 2013) and discrepancies occur due to lack of data and information in the conceptual phase (Al-Zwainy & Aidan, 2017). The aim is to avoid or minimize cost overruns, which can be achieved by accurate cost estimation during project preparation before signing a construction contract (Car-Pušić & Mlađen, 2020).

In previous studies, various mathematical methods and tools have been used to solve the problem of predicting construction costs and cost overruns in construction projects, such as simple and multiple linear regression, "soft computing" methods, such as: neural networks, machine learning, fuzzy logic, etc. (Plebankiewicz, 2018). It was found that the experience of contractors in previous construction projects is an important element that can help to avoid mistakes and increase the chances of success of future projects in the construction phase. Construction cost data collected from previous projects can be useful for estimating costs in different phases of the project life cycle using linear regression and "soft computing" methods (Tijanić, Car-Pušić & Šperac, 2019).

Researchers have developed several linear regression models to analyse costs and cost estimation depending on different variables, such as construction time (Žujo, Car-Pušić & Brkan-Vejzo-

vić, 2010), structure type, building area, number of floors, floor height (Alshamrani, 2017), geotechnical and construction variables (Petroutsatou, Lambropoulos & Pantouvakis, 2006), etc. Cost estimation models based on linear regression and construction time as an independent variable (predictor) (Žujo et al., 2010) could be considered as an inverse problem compared to the well-known Bromilow time–cost (TC) model (Bromilow, 1969). While this approach can be criticized for its simplicity due to only one independent variable, numerous other studies have been carried out which led to the establishment of country/area specific models with high accuracy (Chan & Kumaraswamy, 1999; Chan, 2001; Car-Pušić, 2004). In some studies, this inverse Bromilow model has been used as a basis for the development of hybrid cost estimation models combining regression and neural networks (Petrusheva, Zileska-Pancovska, Žujo & Brkan-Vejzović, 2017; Petrusheva, Car-Pušić & Zileska-Pancovska, 2019; Car-Pušić & Mlađen, 2020).

The use of artificial neural networks for cost estimation with construction time as an independent variable has been investigated by several authors (Petrusheva et al., 2017; Tijanić & Car-Pušić, 2019; Tijanić et al., 2019). Some other authors (Hegazy & Ayed, 1998; Attala & Hegazy, 2003; El-Kholy, 2015) developed models for predicting the extent of cost overruns in construction projects based on regression analysis and neural networks.

## The main research goal

The main research goal is to identify the discrepancy between realized construction costs and contractually agreed costs for construction projects and to analyse the reasons for the discrepancies, based on the available data for the high-rise buildings (Mlađen, 2017). The discrepancy is usually due to quantity variances compared to the contractually agreed quantities, which are due to unforeseen and sometimes additional work as a result of change orders by the customer. According to the Croatian Chamber of Economy and Croatian Employers Association, "additional works are those which have not been contractually agreed and are not necessary for the performance of the contract, but which are required by the client", and "unforeseen works are urgent works which the contractor has to carry out without the consent of the client in order to maintain the stability and safety of the building, the environment and persons or for the smooth regular execution of the works, and here are other unforeseen works which are necessary for technological and/or functional reasons for the regular execution of the contractually agreed works" (Hrvatska Gospodarska Komora, 2017).

The above definition of unforeseen works emphasizes, inter alia, that unforeseen works are carried out to preserve the environment and the people living in it, which is one of the components of sustainable construction. Construction is an important area for achieving the objectives of sustainability (sustainable development), as it concerns all three aspects of sustainability: economic development, social development, and environmental protection. The first step towards sustainability of buildings is to think about the life cycle of a building, whereby sustainable construction should be seen as a comprehensive process

capable of understanding and meeting the needs and requirements of users while reducing environmental impact and life cycle costs (Vezilić Strmo, Senjak & Štulhofer, 2014; Biolek, Hanak & Marović, 2017).

As construction costs are a significant part of the life cycle of any building, it is very important to plan them properly, avoid overruns and achieve a sustainable project outcome. A sustainable project outcome has positive benefits and long-term social, economic, and environmental impacts. A project is successful if it achieves the objectives or needs defined in the acceptance criteria within an agreed time frame and budget. The main criteria for measuring the success of project implementation methods are cost, quality, time, safety, and how the project ultimately achieves its intended purpose (Fong, Avetisyan & Cui, 2014).

Taking all these aspects into account, the main goal of this work is to model the relationship between the realized and contractually agreed construction costs with the best possible accuracy by applying linear regression and "soft computing" methods, and to contribute in this segment to bringing the construction project to a sustainable level.

## Research hypothesis

According to the available data, the realized construction costs very often exceed the contractually agreed costs. Therefore the following research hypothesis shall be tested: Three types of works cause the cost discrepancy with different effects on them. Further, there is a relationship between realized and contractually agreed construction costs and this can be modelled with acceptable accuracy.

## Methodology

The data for this study were collected by interviewing the site managers responsible for the individual construction projects. The site managers also provided the author with project documentation. By studying and analysing the documentation and the information obtained in interviews, a database was created, which includes 24 public and private high-rise buildings – new construction, renovation and reconstruction – built between 2006 and 2017 in Istria County, Republic of Croatia. The database contains basic data on the constructed buildings, such as the type of intervention, the year of construction and data on the contractually agreed and realized construction costs. Data were also collected on the types of works that caused the cost differences: differences in quantity, additional works, unforeseen works (Mlađen, 2017). Projects of similar or identical nature and complexity were taken into account to make the research result as credible as possible.

A summary of the data collected is presented in Table 1. More detailed information on the projects is available from the authors of this paper and at Mlađen (2017).

For the data collected, the main statistical indicators of total cost overruns and cost overruns caused by differences in quantities, unforeseen works and additional works were calculated. A model was then developed to estimate the reali-

TABLE 1. Summary of the data collected (Mlađen, 2017)

| Project type | Projects number | Average construction year | Contracted construction costs | Realized construction costs | Costs incurred by differences in quantities | Costs incurred by additional works | Costs incurred by unforeseen works |
|---|---|---|---|---|---|---|---|
| | | | average [EUR] | | | | |
| New private investment | 10 | 2014 | 127 164.81 | 149 995.80 | 4 340.57 | 16 514.00 | 1 976.42 |
| Renovation and reconstruction of private investment | 8 | 2014 | 52 752.97 | 57 588.75 | –668.43 | 3 626.03 | 1 878.18 |
| Renovation and reconstruction of public investment | 6 | 2012 | 38 723.57 | 43 189.77 | 2 197.03 | 1 960.05 | 309.12 |

zed construction costs with the lowest error value using linear regression, neural networks, and support vector machine.

A review of the literature has shown that these methods give very good results when applied to similar data sets as in this paper (Attala & Hegazy, 2003; Car-Pušić, 2004; Žujo et al., 2010; El-Kholy, 2015; Petrusheva et al., 2017; Tijanić & Car-Pušić, 2019; Tijanić et al., 2019). In a comparable case, the authors of this paper decided to investigate the applicability of the selected methods in estimating construction costs to obtain models that could be helpful in future cost estimates. Furthermore, the methods proved to be suitable given the amount of data collected.

## Statistical indicators

The basic statistical indicators for the collected database, which are presented in Table 2, are calculated. The average cost overrun of the contractually agreed construction costs is 12.15% with a standard deviation of 11.87%.

According to the relevant Croatian legislation accompanying the construction works, as it said, there are three types of possible differences between contractual and realized works, which may lead to cost differences: differences in quantity, additional works, and unforeseen works. The quantities of work may be larger or smaller, resulting in higher or lower costs ($Q$). They are calculated using the

TABLE 2. Statistical indicators of costs overruns (own studies)

| Specification | *OB%* | *Q(EUR)* | *Q%* | *A(EUR)* | *A%* | *U(EUR)* | *U%* |
|---|---|---|---|---|---|---|---|
| Average | 12.15% | –2 135.02 | –48.36% | 8 579.52 | 97.83% | 1 526.85 | 50.53% |
| Standard deviation | 11.87% | 17 747.40 | 184.70% | 19 537.05 | 112.67% | 2 942.24 | 168.63% |

$A$ – costs incurred by additional works, $U$ – costs incurred by unforeseen works, $OB$ – optimism bias.

same unit prices agreed in the contract as for the contracted quantities. Unforeseen works are important because they are essential for the stability of the structure, safety, and environmental protection. They give rise to additional costs ($U$), especially as they are calculated using the new unit prices which are not laid down in the basic contract. Additional works are not agreed in the basic contract without contractually agreed unit prices. There are works that are required by the client and are not indispensable, which generates additional costs ($A$). There is no doubt that they are all the result of poor preliminary planning.

The "optimism bias" is defined as the tendency for a project's costs to be underestimated and/or benefits to be overestimated. It is expressed as the percentage difference between the estimate at appraisal and the final outturn (MacDonald, 2002). Formula (1) is used for calculation:

$$optimism\ bias \equiv 100 \frac{realized\ value - contracted\ value}{contracted\ value} [\%] \tag{1}$$

The range of optimism bias regarding contracted and realized costs is between 1.6% and 41.5%, which in practice can be regarded as frequent and usual cost overruns. Cost overruns of 50–60% and more, sometimes even 100%, can be considered very high, with negative effects on the quality of the samples and the final model.

Figure 1 shows the structure of the deviations, which indicate that the main cause of cost overruns is additional work that is not necessary but is carried out at the request of the client after the construction contract has been signed. They account for 97.83% of the total cost overrun, with a standard deviation of 112.67%. This shows that the planning of the project budget by the client at the project preparation stage is not appropriate.

Unforeseen work contributes to the exceedance with 50.53% with a standard deviation of 168.63%. This indicates insufficient and inadequate previous investigation work, which can be considered a serious deficit in terms of sustainable construction. In this study, the quantity deviation speaks in favour of quantity differences, i.e. it is negative (–48.36%) with a standard deviation of 184.70%. The contractually agreed quantities are on average higher than the services provided. Although these statistical indicators may seem strange at first glance, the explanation lies in the number of cases in the database, the variety of properties and the type of construction work. These are the reasons for such large standard deviations.

All types of cost overrun sources (Fig. 1), including the negative value of $Q$, indicate poor planning. These negative values simply indicate that the quantities are lower than contractually agreed. Otherwise, this is neither a normal nor a strange situation, but rather one that is present in even larger and more complex construction projects than those considered here (Car-Pušić, 2004). Although this is a better situation than the opposite, it is not an acceptable situation, as such deviations indicate poor planning in the preliminary phase. These analysed indicators prove the first part of research hypothesis.

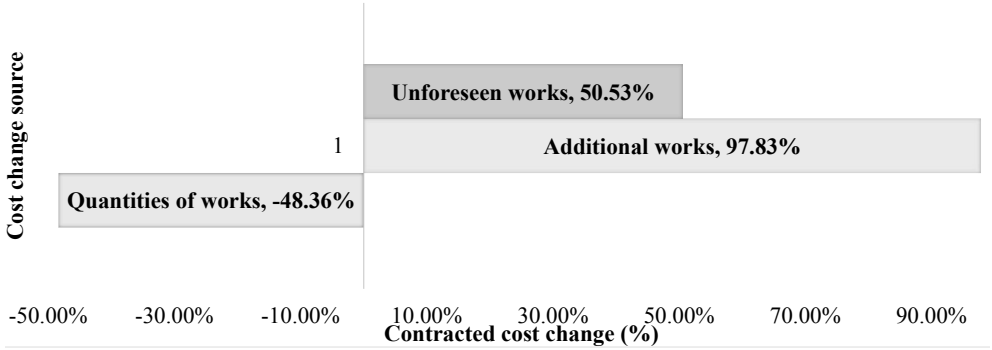


FIGURE 1. Structure of the cost overrun source (own studies)

## Model for predicting the realized construction costs

The modelling of the relationship between realized and contractually agreed costs based on available data was carried out in three steps for two groups of variable cases, as shown in Table 3.

As the statistical indicators show, the largest cost overrun is caused by additional work that is difficult to predict and sometimes unjustified. For this reason, modelling was also carried out for the value of the target variable $C_R - A$. Linear regression was used, as well as the general regression neural network (*GRNN*), the support vector machine (*SVM*) and the radial basic function neural network (*RBF*). A multilayer perceptron (*MLP*), which is very often used for data estimates, was not applicable because the database did not have enough data.

The predictive modelling software the DTREG was used, which is a powerful statistical analysis program that generates neural networks and other techniques (support vector machine, gene expression programming, discriminant analysis, linear and logistic regression model, etc.) that describe data relationships and can be used to predict values for future observations (Sherrod, 2014).

TABLE 3. Steps and groups of variables in modelling the ratio of realized and contracted costs (own studies)

| Step | Data nature | First group of variables pairs | | Second group of variables pairs | |
|---|---|---|---|---|---|
| | | predictor | target | predictor | target |
| 1 | original data | $C_C$ | $C_R$ | $C_C$ | $C_R - A$ |
| 2 | original optimism bias data | $OB$ | $C_R$ | $OB$ | $C_R - A$ |
| 3 | natural logarithms | $\ln C_C$ | $\ln C_R$ | $\ln C_C$ | $\ln(C_R - A)$ |

$C_C$ – contracted cost of construction, $C_R$ – realized cost of construction, $C_R - A$ – realized cost of construction minus costs of additional works, $OB$ – optimism bias, $\ln C_C$ – natural logarithm of contracted cost of construction, $\ln C_R$ – natural logarithm of realized cost of construction, $\ln(C_R - A)$ – natural logarithm of realized cost of construction minus natural logarithm of costs of additional works.

The DTREG software is characterized by the self-optimization of the model parameters to give them the smallest error in the estimation (Tijanić et al., 2019).

The natural logarithms of the variables were modelled based on Bromilow's time–cost model (Bromilow, 1969). In this study the model in formula (2) was assumed as follows:

$$C_R = E \cdot C_C^F \tag{2}$$

where:
$E$ – model parameter that shows the average real price for monetary value of construction,
$F$ – model parameter that shows real cost dependence of contracted cost changes.

Taking the logarithm results in formula (3):

$$\ln C_R = \ln E + \ln C_C \tag{3}$$

By checking the value of t-statistics (62.64 with $p < 0.00001$, $DF = 1$ and $R^2 = 0.993$), it was found that a regression function can be applied (Car-Pušić & Mlađen, 2020).

## Results and discussion

The results for coefficient of determination ($R^2$) and mean absolute percentage error (*MAPE*) are shown below. The *MAPE* and $R^2$ are most often used estimators of the accuracy of the model (Petrusheva, Car-Pušić & Zileska-Pancovska, 2016). The *MAPE* is a measure of prediction accuracy and it is defined by formula (4):

Coefficient of determination indicates how well data points match the approximation function which is obtained from the model – it is a measure of the general match of the model. The value $R^2 = 0.9700$ can be interpreted as: 97% of the variation in the response can be explained by the predictor variables. The remaining 3% can be attributed to unknown variables or inherent variability (Petrusheva et al., 2016).

The results obtained by data processing from Table 3 are given below. Given the nature of the data used, the results are shown in steps 1 to 3. Within each step, cost estimation models are developed by modifying the target variable and the predictor variable, all with the aim of obtaining a model with the lowest possible estimation error.

Step 1. Use of original data:
- Model I: Target variable $C_R$ is function of predictor variable $C_C$ [$C_R = f(C_C)$];
- Model II: Target variable $C_R - A$ is function of predictor variable $C_C$ [$C_R - A = f(C_C)$].

Table 4 shows the results of the mentioned indicators for validation data. The best result for *RBF* is for the original $C_C$ and $C_R$ data, but with a low $R^2$ value. The reduction of additional works did not result in a more accurate model.

Step 2. Use of original optimism bias data:
- Model III: Target variable *OB* for values $C_R$ is function of predictor variable $C_C$ [$OB(C_R) = f(C_C)$];

$$MAPE = \frac{1}{N} \sum \frac{realized\ valus - contracted\ value}{realized\ value} [\%] \tag{4}$$

TABLE 4. Results for linear regression and neural networks for Model I and II (own studies)

| Model | Statistic | *LR* | *GRNN* | *SVM* | *RBF* |
|---|---|---|---|---|---|
| I | $R^2$ | 0.988 | 0.605 | 0.345 | 0.556 |
| | *MAPE%* | 13.824 | 35.130 | 14.814 | 10.976 |
| II | $R^2$ | 0.950 | 0.398 | 0.222 | 0.000 |
| | *MAPE%* | 18.700 | 68.858 | 18.291 | 13.407 |

– Model IV: Target variable *OB* for values $C_R - A$ is function of predictor variable $C_C$ [$OB(C_R - A) = f(C_C)$].

Using these models and selected estimation methods, very poor results were obtained. The highest $R^2$ value obtained is only 0.136 for *SVM*, while all *MAPE* values are extremely high (the lowest value is over 70%).

Step 3. Using data in the form of natural logarithms:

– Model V: Target variable $\ln C_R$ is function of predictor variable $\ln C_C$ [$\ln C_R = f(\ln C_C)$];
– Model VI: Target variable $\ln(C_R - A)$ is function of predictor variable $\ln C_C$ [$\ln(C_R - A) = f(\ln C_C)$].

Using natural logarithms, the highest values of $R^2$ and the lowest values of *MAPE* were obtained, as can be seen from Table 5.

Good results were obtained when $\ln C_C$ and $\ln C_R$ were used as variables instead of the source values using linear regression and *SVM*. The best model accuracy is *MAPE* = 0.522%, with $R^2 = 0.994$. These values indicate a model of acceptable accuracy. This proves the second part of research hypothesis. Again, the accuracy of the model was not improved by excluding the value of the additional work. Nevertheless, it is still claimed that the cost overruns caused by additional work are unreasonably high and indicate poor planning and project management by the client at the design stage of the project. This can be facilitated by the application of a realistic project cost planning model and the commitment of the project manager by the client.

## Conclusions

The experience of construction practice indicates that the construction costs are overrun frequently in construction projects. By analysing the structure of the works that lead to the construction cost overrun, this research has determined that the main cause lies in additional works as the result of client's variation orders, which are not necessarily

TABLE 5. Results for linear regression and neural networks for Model V and VI (own studies)

| Model | Statistic | LR | GRNN | SVM | RBF |
|---|---|---|---|---|---|
| V | $R^2$ | 0.994 | 0.952 | 0.992 | 0.875 |
| | *MAPE%* | 0.522 | 1.268 | 0.529 | 1.267 |
| VI | $R^2$ | 0.990 | 0.928 | 0.992 | 0.963 |
| | *MAPE%* | 0.643 | 1.320 | 0.578 | 1.022 |

needed but are carried out at the request of the investor after signing the construction contract. Additional works account for 97.83% of the total cost overruns, thus confirming the research hypothesis. This is the result of poor planning by the client at the conceptual stage of the project.

Adequate planning of the project budget using the appropriate model will undoubtedly help to reduce construction cost overruns. A more accurate budget estimate contributes to the successful implementation of the project and is one of the construction sustainability criteria. Therefore, it is justified and important to keep exploring the possibilities of the different methods of cost forecasting. In this research, linear regression analysis and several "soft computing" methods have been applied to source data and natural logarithms. The natural logarithms of the variables were modelled on the basis of Bromilow's time–cost model, i.e. by hybrid modelling (by using linear regression and "soft computing" methods). The results of the analysis indicate that better results have been achieved by using hybrid modelling comparing to source data. Despite the small database, the assumption that hybrid models and the use of logarithmic data can provide better indicators of the accuracy of cost prediction models has been confirmed, thus confirming the research hypothesis. Given that it has been affirmed several times (Petrusheva et al., 2016; Petrusheva et al., 2017; Petrusheva et al., 2019), it is recommended to try to model the cost-time relationship in construction projects in the way presented.

Excluding the value of additional work from the total construction costs has not improved the accuracy of the design model. However, this does not mean that these works are justified, but rather that they should be avoided with as much planning as possible in the conceptual phase of the project.

**Acknowledgements**

This work has been fully supported by the University of Rijeka under the project uniri-tehnic-18-125.

## References

Alshamrani, O.S. (2017). Construction cost prediction model for conventional and sustainable college buildings in North America. *Journal of Taibah University for Science*, *11*(2), 315-323.

Al-Zwainy, F.M. & Aidan, I.A.A. (2017). Forecasting the cost of structure of infrastructure projects utilizing artificial neural network model (highway projects as case study). *Indian Journal of Science and Technology*, *10*(20), 1-12.

Ambrule, V.R. & Bhirud, A.N. (2017). Use of artificial neural network for pre design cost estimation of building projects. *Interational Journal on Recent and Innovation Trends in Computing and Communication*, *5*(2), 173-176.

Attala, M. & Hegazy, T. (2003). Predicting cost deviation in reconstruction projects: artificial neural networks versus regression. *Journal of Construction Engineering and Management*, *129*(4), 405-411.

Biolek, V., Hanak, T. & Marović, I. (2017). Data Flow in Relation to Life-Cycle Costing of Construction Projects in the Czech Republic. *IOP Conference Series: Materials Science and Engineering*, *245*, 072032. doi 10.1088/1757-899X/245/7/072032

Bromilow, F.J. (1969). Contract time performance expectations and the reality. *Building Forum*, *1*(3), 70-80.

Car-Pušić, D. & Mlađen, M. (2020). Early stage construction cost prediction in function of project sustainability. In *15th International Conference on Durability of Building Mate-*

*rials and Components* [accepted for publishing].

Car-Pušić, D. (2004). *Metodologija planiranja održivog vremena građenja* [*Planning methodology for sustainable construction time*] (doctoral dissertation). University of Zagreb, Zagreb.

Chan, A.P. (2001). Time-cost relationship of public sector projects in Malaysia. *International Journal of Project Management*, *19*(4), 223-229.

Chan, D.W. & Kumaraswamy, M.M. (1999). Forecasting construction durations for public husing projects. *Hong Kong Perspective Building and Environment*, *34*(5), 633-646.

El-Kholy, A.M. (2015). Predicting cost overrun in construction projects. *International Journal of Construction Engineering and Management*, *4*(4), 95-105.

Fong, C.K., Avetisyan, H.G. & Cui, Q. (2014). Understanding the sustainable outcome of project delivery methods in the built environment. *Organization, Technology & Management in Construction*, *6*(3), 1141-1155.

Hegazy, T. & Ayed, A. (1998). Neural network model for parametric cost estimation of highway projects. *Journal of Construction Engineering and Management*, *124*(3), 210-218.

Hrvatska Gospodarska Komora (2017). *Posebne uzance o građenju* [*Customs business practices on construction – proposal*]. Retrevied from: http://web.hgk.hr/wp-content/uploads/2015/10/Posebne-uzance-o-gradenju-prijedlog.pdf

MacDonald, M. (2002). *Review of Large Public Procurement in the UK*. London: HM Treasury.

Mlađen, M. (2017). *Analiza uzroka i vjerojatnosti troškovnih odstupanja u projektima visokogradnje* [*Causes and probability analysis of cost differences in building projects*] (master's thesis). University of Rijeka, Rijeka.

Peško, I., Trivunić, M., Cirović, G. & Mučenski, V. (2013). A preliminary estimate of time and cost in urban road construction using neural networks. *Technical Gazette*, *20*(3), 563-570.

Petroutsatou, C., Lambropoulos, S. & Pantouvakis, J.P. (2006). Road tunnel early cost estimates using multiple regression analysis. *Operational Research*, *6*(3), 311-322.

Petrusheva, S., Car-Pušić, D. & Zileska-Pancovska, V. (2016). Model for predicting construction time by using general regression neural network. *International Scientific Conference People, Buildings and Environment*, *29*, 33-46.

Petrusheva, S., Car-Pušić, D. & Zileska-Pancovska, V. (2019). Support Vector Machine Based Hybrid Model for Prediction of Road Structures Construction Costs. *IOP Conference Series: Earth and Environmental Science*, *222*, 012010. doi 10.1088/1755--1315/222/1/012010

Petrusheva, S., Zileska-Pancovska, V., Žujo, V. & Brkan-Vejzović, A. (2017). Construction costs forecasting: comparison of the accuracy of linear regression and support vector machine models. *Technical Gazette*, *24*(5), 1431-1438.

Plebankiewicz, E. (2018). Model of Predicting Cost Overrun in Construction Projects. *Sustainability*, *10*(2), 4387. doi 10.3390/su10124387

Sherrod, P.H. (2014). *DTREG Predictive modeling software. Users manual.* Retrieved from: https://www.dtreg.com/uploaded/downloadfile/DownloadFile_5.pdf

Tijanić, K. & Car-Pušić, D. (2019). Procjena operativnih troškova škola primjenom umjetnih neuronskih mreža [The assessment of school operational costs by using artificial neural networks]. In A. Bogdanić et al. (eds.), *Zajednički temelji 2019 – Sedmi skup mladih istraživača iz područja građevinarstva i srodnih tehničkih znanosti* (pp. 126-131). Rijeka: University of Rijeka.

Tijanić, K., Car-Pušić, D. & Šperac, M. (2019). Cost estimation in road construction using artificial neural network. *Neural Computing and Applications*, *2*, 9343-9355.

Vezilić Strmo, N., Senjak, I. & Štulhofer, A. (2014). Sustainability of the existing housing stock and evaluation possibilities. *Prostor*, *22*(1), 122-134.

Žujo, V., Car-Pušić, D. & Brkan-Vejzović, A. (2010). Contracted price overrun as contracted construction time overrun function. *Technical Gazette*, *17*(1), 23-29.

## Summary

**Predicting buildings construction cost overruns on the basis of cost overruns structure.** In construction practice, contractually agreed costs are often exceeded, which interferes with the sustainable realization of construction projects. The research described in this paper covers 24 new construction, renovation and reconstruction projects in the Republic of Croatia realized in the years 2006 to 2017, in order to analyse the occurrence of cost overruns more precisely with regard to the source of the overruns. It was found that additional work is the main source of cost overruns: firstly, additional work as a result of the client's change orders and then unforeseen construction work as a result of unforeseen circumstances. As for the additional works, they are carried out at the client's request and are not necessary for the safety and stability of the building. Using linear regression and "soft computing" methods, the possibility of modelling the relationship between contractually agreed and realized construction costs with satisfactory accuracy was tested. The model with the values of the natural logarithms of the variables, modelled according to the time–cost model of Bromilow, proved to be of the highest accuracy.

**Authors' address:**
Diana Car-Pušić
(https://orcid.org/0000-0003-2555-335X)
University of Rijeka
Faculty of Civil Engineering
Radmile Matejčić, 3, HR51000, Rijeka
Croatia
e-mail: diana.car.pusic@uniri.hr

Scientific Review – Engineering and Environmental Sciences (2020), 29 (3), 377–387
Sci. Rev. Eng. Env. Sci. (2020), 29 (3)
Przegląd Naukowy – Inżynieria i Kształtowanie Środowiska (2020), 29 (3), 377–387
Prz. Nauk. Inż. Kszt. Środ. (2020), 29 (3)
http://iks.pn.sggw.pl
DOI 10.22630/PNIKS.2020.29.3.32

**Elżbieta RADZISZEWSKA-ZIELINA[1], Filip KURAJ[2]**

[1]Cracow University of Technology, Faculty of Civil Engineering
[2]Graduate of the Cracow University of Technology

# Transparent insulation materials market in Europe

**Key words:** survey studies, transparent insulation, market

## Introduction

Over the years, the European Union's energy policy (Directive 2010/31/EU) has been applying increasingly restrictive requirements concerning thermal insulation in buildings. The environmental assessment of residential buildings includes, among others, the environmental load associated with energy consumption and the accompanying atmospheric pollution (Korentz & Nowogońska, 2018). The selection of the appropriate thermal insulation system becomes a critical matter (Fedorczak-Cisak et al., 2019b; Fedorczak-Cisak et al., 2020) due to ecological awareness and the constantly rising costs of heating buildings with conventional energy (Radziszewska-Zielina & Rumin, 2016; Romanska-Zapala et al., 2018; Kisilewicz, Fedorczak-Cisak & Barkanyi, 2019). As a result, solutions that utilise renewable energy sources are sought. These include systems that utilise transparent thermal insulation (Kerschberger, 1994; Buratti & Moretti, 2011).

In Radziszewska-Zielina and Śladowski (2017a, 2017b), Fedorczak-Cisak et al. (2019a), it is suggested to analyse various alternatives of carrying out projects and the associated costs during the initial analysis of a project's feasibility. In Radziszewska-Zielina and Rumin (2016), it was proven that the profitability of a given project depends on the technical solutions used to complete it. Biolek and Hanák (2019) proposed a solution that can aid real estate developers in making decisions in selecting material solutions while accounting for life-cycle costs (LCC). The growing pressure to introduce sustainable building is linked with increasingly rigorous requirements as to the profitability of construction or renovation projects and the occupancy of buildings, in addition to decreasing their impact on the environment. An overview of structural and material solutions of building partitions that account for sustainable development was presented in

Gicala and Sobotka (2017). Radziszewska-Zielina and Kania (2017), Radziszewska-Zielina, Kania and Śladowski (2018) pointed to a range of problems and difficulties in the selection of technologies with which to carry out construction projects. The specificity of cooperation, including communication during the carrying out of construction projects in Ukraine, Poland and Slovakia, was presented by Radziszewska-Zielina (2010, 2011). Communication, coordination and material quality control was presented in the context of client satisfaction with structural system quality by Blaževska-Stoilkovska, Hanák and Žileska-Pančovska (2015).

The subject matter of thermal insulation in buildings is an important and multi-aspect subject. Contrary to traditional thermal insulation systems, wherein thermal insulation is to minimise heat loss from the building's interior, transparent insulation also allows for generating energy from solar radiation. This is performed via the use of transparent materials that can be penetrated by sunlight and that retain high thermal insulation properties. The insulation system in question combines the properties of translucent materials (such as window glazing) which can be easily penetrated by shortwave radiation, with those of materials with high thermal insulation properties, such as mineral wool or polystyrene foam. The combination of these two opposing characteristics has created a partition with a solar radiation penetration rate of around 50% yet with a heat transfer coefficient that is often twice as high as coefficients for typical insulation materials used in construction. In the case of applying transparent insulation to a building's walls, it was possible to create a partition that allows for more heat gain than loss (Fig. 1).

We can obtain two types of partitions when using transparent insulation materials. These are:

– daylight walls – solar radiation enters the building's interiors directly, i.e. the partition is a layer that lets

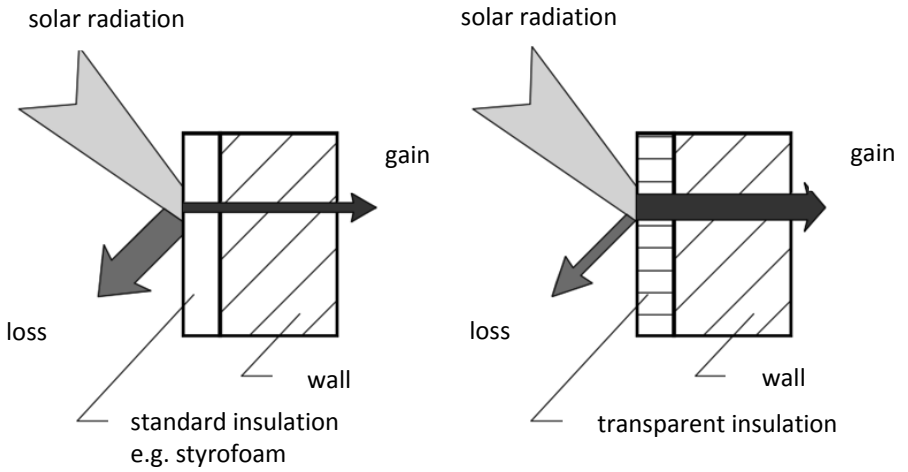


FIGURE 1. Illustration of heat balance for partitions with a typical (traditional) thermal insulation and transparent thermal insulation

though solar radiation and natural light, which allows their absorption by internal partitions and furnishings, in addition to daylighting the interior using scattered light. The partition forms a system that allows direct heat and light gain;

– solid partitions – opaque partitions covered with a layer of transparent insulation. Solar radiation and daylight passes through the insulation layer and enters the accumulation or accumulation–collection layer, which absorbs the radiation energy and indirectly transfers the stream of heat inside. In this case, we are dealing with a system of indirect heat gains.

In both cases we are dealing with heat gain surpassing heat loss. Transparent insulation systems can be designed both for newly erected buildings and those that are to undergo energy retrofitting.

This article presents the transparent thermal insulation market as viewed by its manufacturers. The study was performed using a questionnaire. The authors also referred to the Polish domestic market in the study and its conclusions.

## Method and tools

The objective of the study was to analyse the application of transparent thermal insulation in the European construction sector, determine the popularity of various technologies and materials used in their manufacturing, gauge the competition between transparent insulation manufacturers, and explore investment in the development of new transparent insulation technologies and trends in transparent insulation demand as reported by manufacturers.

The survey questionnaire prepared for the study was shared online through Google Forms in 2019. The research sample was determined via a list of transparent insulation manufacturers active on the European market, as presented by Ujma (2003) and the members of "Fachverband Transparente Wärmedämmung", a German organisation that connects research institutes and manufacturers who develop, produce and sell a range of transparent insulation products. The current member list can be found on the association's website (PATI, 2020). Some of the surveyed companies were featured on both lists. The final survey addressee list comprised twenty companies: fourteen from Germany, five from Switzerland and one from Austria. The respondents were largely composed of experts appointed to fill out the survey on behalf of their respective companies.

## Results

The first question pertained to the popularity of direct and indirect heat gain systems. The use of transparent insulation in direct heat gain systems was the most popular (88.2% of respondents picked this solution). Transparent insulation manufacturers present on the European market were primarily oriented towards new development projects, mostly commercial or public ones, which typically use transparent facades with this system.

The next group of questions concerned the materials used in manufacturing transparent insulation, which

materials had the largest share in manufacturing volume and whether there was ongoing research on implementing new or further developing existing materials.

The percentage share of materials used in the production of transparent insulation by respondents (Fig. 2) demonstrates that glass (82.2%) and synthetic materials were used the most frequently.

The respondents largely indicated that they were working on improving their products at the time of filling out the survey. The greatest share of respondents declared they were working on improving their current products and on combining different transparent insulation systems. The group that aspired to finding new material solutions for their products was the smallest (Fig. 3).

It can be concluded that the current state of the art concerning available materials and their properties enables the pursuit of more advanced solutions and their application in transparent insulation systems, as systems based on new substances are currently being researched.

One of the problems under study was the scale of manufacturing ready-to-use transparent insulation products. To this end, the respondents were asked to report their yearly production volume of insulation products in square metres.

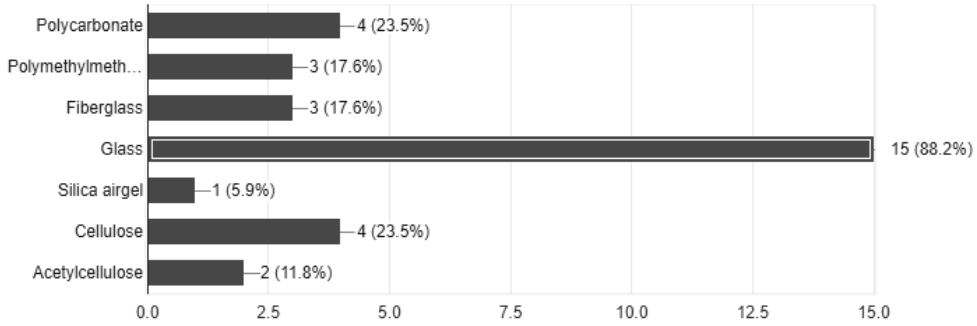


FIGURE 2. Types of materials used by respondents in transparent insulation manufacturing


FIGURE 3. Structure of answers to the question concerning the method of applying improvements to products

Almost half of the respondents (47.1%) reported a yearly production volume exceeding 5,000 $m^2$ of product (Fig. 4). Figure 5 describing the trend in yearly production rate demonstrates that nearly over a half of the respondents (52.9%) reported a stable production rate, while around 40% reported a rise in production rate over the last couple of years. The remaining companies noted a decline in transparent insulation production rate.

Over half (52.9%) of the respondents engaged in transparent insulation manufacturing only, while the remainder also offered the installation of finished insulation products, with the yearly volume of installed insulation reported as shown in Figure 6.

In summary, it can be concluded that there is demand for this type of insulation in Europe and this primarily applies to direct gain transparent insulation systems. The products of the companies who participated in the survey that are dedicated to the European market are largely complete systems that can be installed by construction companies with appropriately trained staff.

The majority of the respondents (52.9%) rated the demand for transparent insulation in Europe as high, while 23.5% rated it as low and a similar number of respondents found it hard to assess.

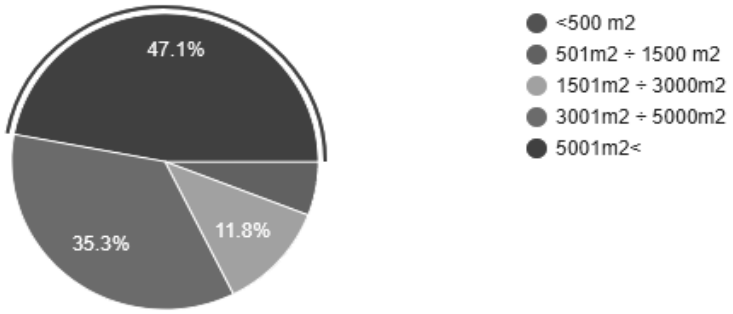


FIGURE 4. Structure of answers to the question concerning the yearly production rate of transparent insulation by surveyed companies

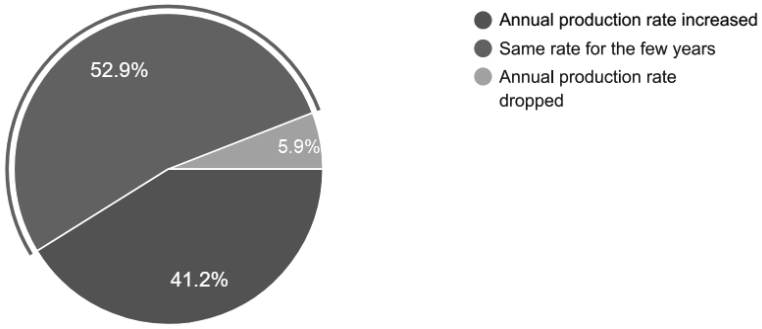


FIGURE 5. Trend in the yearly transparent insulation production rate among surveyed manufacturers

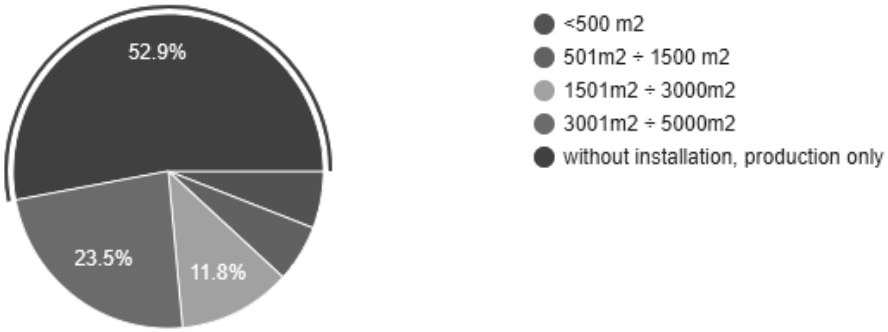


FIGURE 6. Yearly production rate of transparent insulation products reported by manufacturers

It was observed that the country with the largest amount of transparent insulation consumers in Europe was Germany (Fig. 7). All of the companies that took part in the survey reported they had completed at least one order from this country (100%). Great Britain came second (47.1%), while Austria, the Netherlands and Switzerland jointly came in third, with 41.2% each).

The respondents, when asked to identify the country where they had the most orders related to projects applying transparent insulation, pointed to Germany (94.1%) and then to Switzerland (5.9%). When listing the country their company was based in, most respondents reported Germany (82.4% Germany, 11.8% Switzerland, 5.9% Austria).

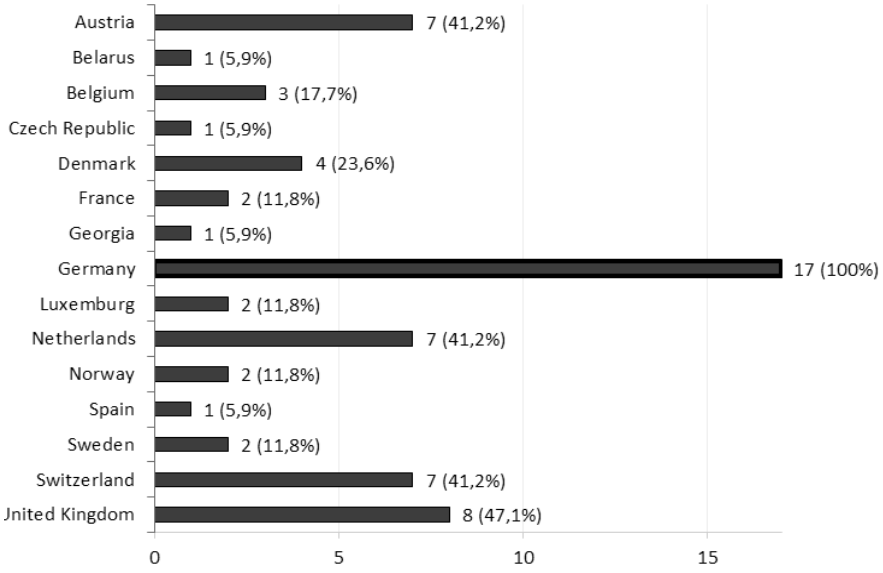


FIGURE 7. Countries in which respondents carried out projects involving transparent insulation

Only one of the companies that took part in the survey had taken part in a construction project in Poland, while the vast majority declared they had no share in the Polish construction market. This was probably affected not only by the higher cost of transparent insulation, but also by difficulty in obtaining subsidies for applying solutions based on renewable energy in development projects. The developer must also go through periodical energy auditing procedures, monitor and document energy consumption data and the savings it brought (2016 Energy Performance Act). Another essential matter are the costs of administrative fees for submitting applications for subsidies, the cost of energy audits and applicable documentation, as well as defining whether the costs do not outweigh the benefits obtained via subsidy. According to a study performed by Go4Energy enterprise in 2014, representatives of the Polish construction sector (Augustyniak & Berezowski, 2014) saw the greatest barriers to energy-efficient buildings in, among others, the low accessibility to subsidies and the low amount of obtainable funds, the lack of a state-operated incentive system, high initial investment costs, complicated procedures and the long wait times associated with obtaining necessary approvals, the lack of political support for energy-efficient building or legislation which does very little to promote this branch of construction. Most respondents were of the opinion that Poland would not become a country where they would be likely to carry out projects and where transparent insulation would be used. Almost half of the respondents did not express a clear opinion on participating in projects in Poland, while only one company declared a willingness to do so. The subject of transparent insulation was discussed at length in Polish publications around ten years ago. There was also one transparent insulation system available on the market at the time. Interest in these solutions was so minuscule in recent years that it is no longer offered. Clients were mostly interested in solutions that had cheap initial investment costs, i.e. traditional thermal insulation systems employing mineral wool or styrofoam. In the opinion of the authors, transparent insulation systems were not presented sufficiently well to potential consumers in terms of their possible benefits.

The respondents, when asked whether they thought there was significant competition on the transparent insulation market, largely gave a negative answer (53%), while 23.5% rated competition as significant and a similar number reported it was hard to assess. The respondents were then asked to report the number of companies with which they competed on the market. The results have been presented in Figure 8. As many as 47.1% of respondents declared they competed with 5–10 companies. It was observed that, in the respondents' opinion, the number of companies they competed with on the transparent insulation market was not high and that the companies that took part in the survey were not hindered in achieving their market goals.

Company representatives were asked to identify the period when their companies entered the transparent insulation market, as presented in Figure 9. Over 70% of the surveyed companies were present on the market for over 25 years.

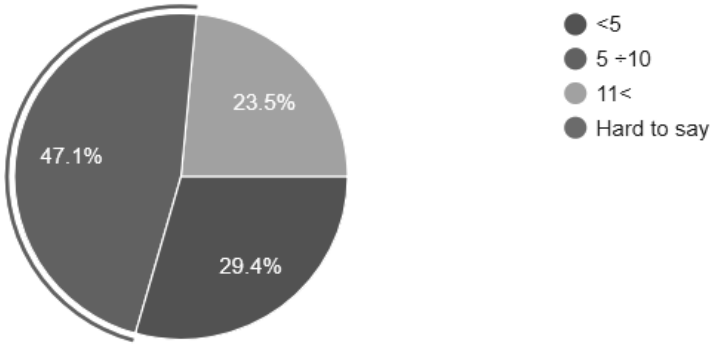


FIGURE 8. Structure of answers to the question concerning the number of companies the respondents competed with

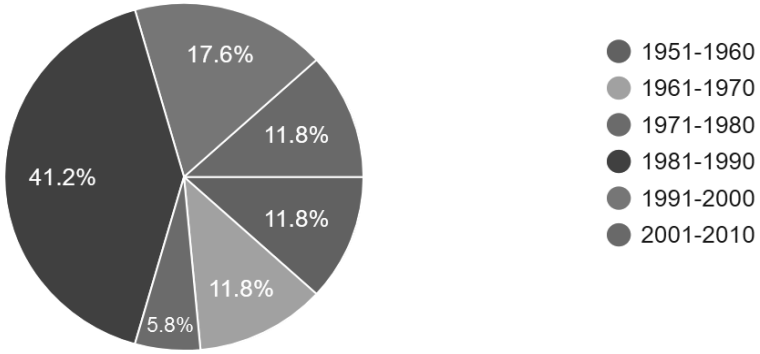


FIGURE 9. Period when the surveyed companies entered the transparent insulation market

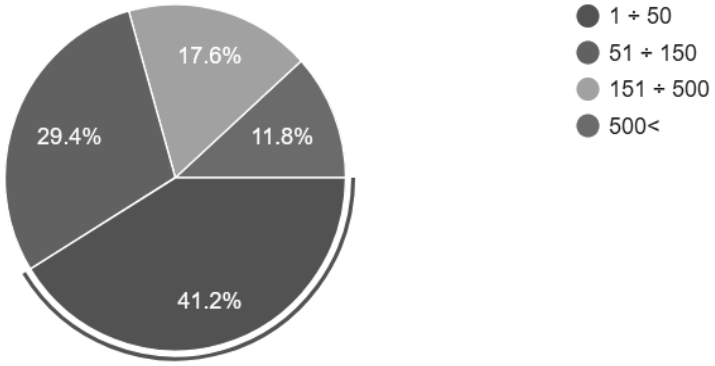


FIGURE 10. Company employee count

Almost 60% of the companies who participated in the survey had an employee count of more than 50 (Fig. 10). Exactly 41.2% of companies employ up to 50 people. Small and medium-sized companies were predominant.

When analysing the information presented above, it can be concluded that the companies which participated in the survey had a confident market position, their many years of experience and employees counts were supported via regular orders, a stable reputation and sufficient demand present in the transparent insulation market in Europe.

The authors are aware that the study results presented herein are one-sided. To have a full picture of the transparent insulation market, one would have to study consumers, study the opinions of potential clients from various countries concerning transparent insulations, and analyse supply and demand. Studies of secondary sources and analyses of documents, reports, statistics and publications would also have to be performed. This will be explored in future studies.

## Conclusions

The application of transparent insulation is associated with higher development costs, yet the potential return on investment in the form of savings during the occupancy stage can convince some developers to invest in it. The appearance of building facades after the application of transparent insulation is also attractive to clients.

Based on the presented survey results, it can be concluded that Europe successively increases its energy effectiveness, while the transparent insulation market can be considered to prosper. However, this prosperity is not equally distributed between countries, as indirect heat gain transparent insulation systems were viewed the most favourably in Germany. Great Britain came second, while Austria, the Netherlands and Switzerland jointly came in third.

Based on an observation of thermal insulation systems used in Poland, it can be observed that interest in transparent insulation is much lower there than in other European countries, particularly Western European ones. Most respondents were of the opinion that Poland would not become a country where they would be likely to carry out projects and where transparent insulation would be used. The main barriers include: an insufficient dissemination of knowledge concerning benefits derived from the use of transparent insulation, the high initial investment cost, potentially complicated assembly systems and a relatively long break-even period. Clients are mostly interested in solutions that have cheap initial investment costs, i.e. traditional thermal insulation systems employing mineral wool or styrofoam.

At present, further measures and programmes focusing on rational energy management are necessary, as developers could be motivated via a system of financial incentives, as well as the liberalisation of current procedures and requirement criteria for obtaining subsidies for newly-designed and modernised buildings.

## References


Augustyniak, T. & Berezowski, M. (2014). *Perspektywy rozwoju budownictwa energooszczędnego w Polsce* [*Prospects for the development of energy-saving construction in Poland*]. Retrieved from: www.g4e.pl/baza-wiedzy/raporty

Biolek, V. & Hanák, T. (2019). LCC Estimation model: a construction material. *Perspective Buildings*, *9*(8), 182. doi 10.3390/buildings9080182

Blaževska-Stoilkovska, B., Hanák, T. & Žileska-Pančovska, V. (2015). Materials supply management in construction projects and satisfaction with the quality of structures. *Tehnicki Vjesnik*, *22*(3), 721-727.

Buratti, C. & Moretti, E. (2011). Transparent insulating materials for buildings energy saving: experimental results and performance evaluation. In *Third International Conference on Applied Energy*. Perugia, 16-18 May 2011 (pp. 1421-1432). Perugia, Italy.

Directive 2010/31/EU of the European Parliament and of the Council of 19 May 2010 on the energy performance of buildings.

Fedorczak-Cisak, M., Kotowicz, A., Radziszewska-Zielina, E., Sroka, B., Tatara, T. & Barnaś, K. (2020). Multi-criteria optimisation of the urban layout of an experimental complex of single-family NZEBs. *Energies*, *13*(7), 1541. doi 10.3390/en13071541

Fedorczak-Cisak, M., Kowalska, A., Radziszewska-Zielina, E., Śladowski, G., Pachla, F. & Tatara, T. (2019a). A multi-criteria approach for selecting the utility function of the historical building "Stara Polana" located in Zakopane. *MATEC Web of Conferences*, *262*, 07002. doi 10.1051/matecconf/201926207002

Fedorczak-Cisak, M., Kowalska-Koczwara, A., Nering, K., Pachla, F., Radziszewska-Zielina, E., Śladowski, G., Tatara, T. & Ziarko, B. (2019b). Evaluation of the criteria for selecting proposed variants of utility functions in the adaptation of historic regional architecture. *Sustainability*, *11*(4), 1094. doi 10.3390/su11041094

Gicala, M. & Sobotka, A. (2017). The analysis of construction and material solutions, taking into account the requirements of sustainable development. *Scientific Review – Engineering and Environmental Sciences*, *26*(2), 159-170.

Kerschberger, A. (1994). Transparente Wärmedämmung zur Gebäudeheizung. Systemausbildung, Wirtschaftlichkeit, Perspektiven [Transparent thermal insulation for heating buildings. System training, profitability, perspectives]. *Bauök-Papiere*, *56*.

Kisilewicz, T., Fedorczak-Cisak, M. & Barkanyi, T. (2019). Active thermal insulation as an element limiting heat loss through external walls. *Energy and Buildings*, *205*, 109541. doi 10.1016/j.enbuild.2019.109541

Korentz, J. & Nowogońska, B. (2018). Assessment of the life cycle of masonry walls in residential buildings. *MATEC Web of Conferences*, *174*, 01025. doi 10.1051/matecconf/201817401025

Professional Association for Transparent Insulation [PATI] (2020). *Members of Professional Association for Transparent Insulation*. Retrieved from: http://www.umwelt-wand.de/ti/about/member.html

Radziszewska-Zielina, E. (2010). Analysis of the partnering relations of Polish, Slovak and Ukrainian construction enterprises. *Technological and Economic Development of Economy*, *16*(3), 432-454.

Radziszewska-Zielina, E. (2011). Assessment methods of partnering relations of Polish, Slovak and Ukrainian construction enterprises with the use of fuzzy logic. *Archives of Civil Engineering*, *1*(57), 87-118.

Radziszewska-Zielina, E. & Kania, E. (2017). Problems in carrying out construction projects in large urban agglomerations on the example of the construction of the axis and High5ive Ooffice buildings in Krakow. *MATEC Web of Conferences*, *117*, 00144. doi 10.1051/matecconf/201711700144

Radziszewska-Zielina, E. & Rumin, R. (2016). Analysis of the profitability of investment in renewable energy sources on the example of a semi-detached house. *E3S Web of Conferences*, *10*, 00079. doi 10.1051/e3sconf/20161000079

Radziszewska-Zielina, E. & Śladowski, G. (2017a). Proposal of the use of a fuzzy stochastic network for the preliminary evaluation of the feasibility of the process of the adaptation of

a historical building to a particular form of use. IOP *Conference Series: Materials Science and Engineering*, *245*(7), 072029. doi 10.1088/1757-899X/245/7/072029

Radziszewska-Zielina, E. & Śladowski, G. (2017b). Supporting the selection of a variant of the adaptation of a historical building with the use of fuzzy modelling and structural analysis. *Journal of Cultural Heritage*, *26*, 53-63.

Radziszewska-Zielina, E., Kania, E. & Śladowski, G. (2018). Problems of the selection of construction technology for structures in the centres of urban agglomerations. *Archives of Civil Engineering*, *64*(1), 55-71.

Romanska-Zapala, A., Bomberg, M., Fedorczak-Cisak, M., Furtak, M., Yarbrough, D. & Dechnik, M. (2018). Buildings with environmental quality management. Part 2: Integration of hydronic heating/cooling with thermal mass. *Journal of Building Physics*, *41*(5), 397-417.

Ujma, A. (2003). Zasady i możliwości stosowania izolacji transparentnych [Principles and possibilities of using transparent insulation]. *Izolacje, 8*(1), 36-45.

Ustawa z dnia 20 maja 2016 r. o efektywności energetycznej. Dz.U. 2016 poz. 831 [Energy performance act of 20 May 2016. Journal of Laws 2016 item 831].

## Summary

**Transparent insulation materials market in Europe.** This paper presents the European market of transparent insulation materials as viewed by manufacturers. The objective of the study was to analyse the application of transparent insulation materials in the construction sector across Europe, determine the popularity of various technologies and materials used to manufacture them, the competition among transparent insulation manufacturers, investment in the development of new transparent insulation technologies, and trends in demand for transparent insulation in Europe. The analysis was performed on the basis of a survey of manufacturers. The use of transparent insulation is associated with high cost, yet the potential return on investment in the form of savings over the course of a building's life-cycle convinces many potential developers to apply these materials. Based on the results of the survey, it can be concluded that European companies follow the increase in energy-efficiency and the transparent insulation market is prosperous, yet differs from country to country. It was observed that the positive perception of indirect heat gain transparent insulation systems was the most prevalent in Germany. The paper also explores the situation on the author's domestic market – the Polish transparent thermal insulation market.

**Authors' address:**
Elżbieta Radziszewska-Zielina
(https://orcid.org/0000-0002-3237-4360)
Politechnika Krakowska im. Tadeusza Kościuszki
Wydział Inżynierii Lądowej
ul. Warszawska 24, 31-155 Kraków
Poland
e-mail: eradzisz@L7.pk.edu.pl

Scientific Review – Engineering and Environmental Sciences (2020), 29 (3), 388–396
Sci. Rev. Eng. Env. Sci. (2020), 29 (3)
Przegląd Naukowy – Inżynieria i Kształtowanie Środowiska (2020), 29 (3), 388–396
Prz. Nauk. Inż. Kszt. Środ. (2020), 29 (3)
http://iks.pn.sggw.pl
DOI 10.22630/PNIKS.2020.29.3.33

**Roman TRACH[1], Sergey BUSHUYEV[2]**

[1]Warsaw University of Life Sciences – SGGW, Institute of Civil Engineering
[2]Kyiv National University of Construction and Architecture

# Analysis communication network of construction project participants

**Key words:** social network analysis, centrality measures of nodes, construction project**,** communication, knowledge

## Introduction

Construction projects delivery was characterized by Ochieng and Price (2009), as a complex process taking place in a turbulent environment with unpredictable work patterns, especial work and temporarily organized teams. In addition, the construction industry is characterized by limited resources and a high level of competition. Limited resources and a competitive environment determine knowledge and information as a particularly important resource for the development of the construction industry.

After the concept of knowledge management was first applied in construction projects, scientists began a discussion on how to manage knowledge and information in specific projects, taking into account the problems associated with the specifics of the construction industry. A significant part of the work was aimed at the analysis of knowledge management in one organization, in which knowledge is considered as a valuable resource or intellectual asset (Pryke, 2005; Ochieng & Price, 2009; Trach, Pawluk & Lendo-Siwicka, 2020). A study of knowledge management between project participants will provide researchers with an improved understanding of the processes and will further improve the construction projects efficiency. Recently, the integration of the general knowledge of participants in a construction project has been gaining importance.

The integration of knowledge is a process in which people who have previously gained experience in specialized fields of knowledge share it in order to achieve a common result. The knowledge integration brings together project participants and can mitigate the short-

comings that arise due to the fragmentation of the construction project stages. The knowledge integration between organizations involved in the construction project delivery has already attracted researcher's attention. Baiden, Price and Dainty (2006) supposed that a joint project team can be very effective, as team members from different organizations create a pool of different skills and knowledge. Nicolini, Holti and Smalley (2001) indicated that when managing a construction project, not only material resources and information should be integrated, but also the knowledge and participants experience. Briscoe and Dainty (2005) also studied topical issues construction project integration and came to the conclusion that the knowledge in the project is as important as the issues of communication and information exchange.

A communication network is one of the elements of a knowledge management system in projects and serves to organize and maintain information links between project participants. Pryke (2012) defined the construction project as a network of organizations connected by information flows and relationship communication networks. Successful project management very often depends on the effectiveness of relationships between project team members (PMI, 2001; Trach & Lendo-Siwicka, 2018). The communication of project teams includes individuals, information flows (knowledge, information), tools for processing information flows and barriers that arise in the way of information.

Scientists often use social network analysis (SNA) to identify key elements in social, biological, physical, communication, transport and other networks (Marsden & Lin, 1982). Recently, network analysis has been used in studies directly related to construction, in particular for the analysis of projects structure. One of the first articles was devoted to communication problems between the project main participants: client, project manager, architect and contractor (Loosemore, 1998). Madani, Daim and Weng (2017) used network analysis to study intelligent buildings, to find the most effective technologies and new innovative opportunities. Abbsaian-Hosseini, Liu and Hsiang (2017) analysed the relationship between the degree centrality and effectiveness in the implementation of joint work by construction teams. Chinowsky and Songer (2011) diagnosed the networks that arise in construction projects, and noticed that there are social and informational connections between the project participants. They argue that successful teams demonstrate a high level of communication between team members and a high cooperation degree. Pryke, Badi, Almadhoob, Soundararaj and Addyman (2018) analysed the self-organizing networks that emerged from the infrastructure project delivery. The data obtained show that these networks exhibit a high degree of sparseness, short paths and high clustering in dense communities around participants with many links. Among recent studies, two articles should be pointed out in which the authors analyse the relationship among participants in self-organizing networks of construction project. Using SNA allowed them to understand and identify some problems and shortcomings of projects (Śladowski, Radziszewska-Zielina & Kania, 2019).

Later, they discovered an anomaly in communication between the participants and proposed an optimization method to increase the effectiveness of using network communication (Radziszewska-Zielina, Śladowski, Kania, Sroka & Szewczyk, 2019).

Social network analysis tools allow you to explore various indicators of networks that can be classified depending on the direction of analysis:

1. Indicators for analysing the network (graph) characteristics: density, average degree of the network, average path length, clustering coefficient, which shows how fully all project teams participants are involved in the communication structure.
2. Indicators for the analysis of network participants (nodes and edges): centrality measures, indicating the discontinuity degree of the project participants and the relationships between them.
3. Indicators for the analysis of communities in the network, which indicate the degree to which the nodes in the graph tend to group into communities (clusters).

The purpose of this work is the calculation and analysis centrality measures for participants in the construction project delivery. Centrality measures can answer the following questions:

– whether the node is influential or central to the network,
– whether the node is critical for the flow of information in the network.

## Material and methods

Social network analysis has based on methods and tools of graph theory. Mathematically, the links network in the project can be represented in the form of an undirected graph $G = (V, E)$, where $V$ is non-empty set of nodes, and $E$ is the set of pairs of the form $e = (u, v)$, $u, v \in V$, which are called edges, and the nodes $u$ and $v$ are the ends of the edges. If we consider the project as a graph, then its participants will be represented by nodes of the graph, and the connections between them are the edges of the graph.

In this study, a graph is undirected weighted type of graph whose nodes (network participants) are connected by edges. The link strength between network participants is displayed using the measure "weight of edge". The edge sets in this case consists of unordered pairs of nodes $(u, v) = (v, u)$ (Bornholdt & Schuster, 2003).

To investigate the communication network between the project participants, centrality measures of nodes were analysed: degree centrality, betweenness centrality, eigenvector centrality and measure of importance PageRank. For an undirected graph, degree centrality of nodes can be written as the adjacency matrix (Freeman, 1978). The adjacency matrix of the graph $G = (V, E)$ with the number of nodes $n$ is a square matrix $A$ of size $n$ in which the value of $a_{ij}$ is equal to the number of edges from node $i$ to node $j$. Thus, degree centrality of node $i$ can be calculated by the formula:

$$Cd(i) = \frac{\sum_{j=1}^{n} a_{ij}}{n-1} \tag{1}$$

The logical continuation in the evolution of degree centrality is eigenvector centrality. The significant difference between these two metrics is that when

calculating of degree centrality, only the number of neighbouring nodes is used, without taking the level of their influence in network. Obviously, not all neighbour nodes are equal. In many cases, the importance of a node increases due to the presence of links with nodes that have a high level of influence in network. This means that nodes with a few very important neighbours in their influence can surpass nodes with many links connecting them to unimportant nodes.

Eigenvector centrality of node $i$ is proportional to the sum of the centrality neighbouring nodes $i$ can be calculated by the formula (Bonacich, 1987)

$$Ce(i) = k_1^{-1} \sum_j a_{ij} x_j \quad (2)$$

where:
$k_j$ – eigenvalues of adjacency matrix $A$,
$k_i$ – the largest of them,
$a_{ij}$ – adjacency matrix element,
$x_j$ – eigenvector centrality of node $j$.

The measure eigenvector centrality of node $i$, which was obtained due to the high level of prestige of node $j$, can distort the real influence of node $i$ in network.

This problem was taken into account when calculating the measure of centrality PageRank (Page, Brin, Motwani & Winograd, 1999). The measure of node PageRank is calculated using the formula

$$Cpr_{(i)} = \alpha \sum_j a_{ij} \frac{x_j}{k_j^{out}} + \beta \quad (3)$$

where:
$\alpha, \beta$ – constants,
$a_{ij}$ – adjacency matrix element,
$x_j$ – eigenvector centrality of node $j$,
$k_j^{out}$ – number of edges out coming from node $j$.

If the node $j$ does not have out coming edges, then $k_j^{out}$ is equated to one in order to avoid division by zero.

Measure betweeness centrality shows how paths connecting other participants pass through a network member. In other words, this measure indicates how much this participant acts as a broker for connections between other network participants. A network participant can influence its other participants, supporting, delaying or disrupting the process of transmitting knowledge and information. In any case, it has the potential to carry out such actions.

Measure betweeness centrality is calculated as the ratio of the shortest paths running through a given node to the total number of all shortest (Freeman, 1977)

$$Cb(i) = \sum \frac{g_{kj}(i)}{g_{kj}} \quad (4)$$

where:
$g_{kj}(i)$ – number of shortest paths from node $k$ to node $j$ that pass through $i$,
$g_{kj}$ – number of shortest paths from node $k$ to node $j$.

## Results and discussion

We have analysed the communication network between project participants for residential building construction located in Rivne, Ukraine. Construction began in February 2019, and its completion is scheduled for September 2021. The study was conducted from June to July 2019, at the stage design completion and

beginning of construction work. Since communication is considered the central mechanism of iterative interaction (Mahmud, 2009), the initial stage of the study was identification of relationships between participants in construction project delivery. Each of its participants needed to determine persons with whom he communicated. Communication in the project takes place by phone, email or verbal form.

At the second stage of the study, communication strength between the network participants was calculated, that is, each graph edges were assigned a weight. Communication strength was calculated based on the method presented in Pryke et al. (2018) as a function of two variables: frequency and quality of communication. The frequency and quality of communications were calculated based on data collected from 17 project participants. An analysis of communication frequency was carried out using a five-point rating (less than once a week, once a week, several times a week, once a day, more than once a day, with an estimate of 1 to 5 points, respectively). To analyse communication quality, we used a three-point rating scale (low, medium, high) and three indicators – importance, accuracy and timeliness.

Then value of communication strength between nodes $i$ and $j$ can be determined by the formula

$$E_{ij} = F_{ij} \cdot Q_{ij} \tag{5}$$

where:

$F_{ij}$ – communication frequency, which is calculated as $f_{ij}$ / 5,

$Q_{ij}$ – communication quality, which is calculated as $q_{ij}$ / 9.

The node weight is calculated as the sum of the weights of all the edges (communication strength) related with this node. An adjacency matrix of size 17 × 17 was formed based on value of communication strength between all the participants (edge weight).

The data from the matrix were used to calculate centrality measures (the table) and visualize communication network (Figs. 1–3).

Centrality measures calculation and visualization were implemented using NetworkX library in Python programming language. The positioning of graph nodes was implemented using Fruchterman–Reingold force algorithm (SpringLayout). In Figures 1–3, the abbreviation was used to Installation Design Office, IDO.

The analysis degree centrality of nodes (Fig. 1) observed a high value measure in network participants: “Project manager”, “Architect” and “Construction site manager”, which directly correlates with number of connections with other network participants.

The calculation of PageRank algorithm showed the same results of nodes importance in network as calculation degree centrality.

The analysis eigenvector centrality showed the highest values of measure were among participants “Project manager”, “Design office” and “Construction site manager” (Fig. 2). At the same time, nodes “Project manager” and “Construction site manager” received a high value due to that they have many neighbouring nodes with a low level of impact in network. Node “Design office” got a high value due to that it had few

TABLE. The centrality measures of the participants in construction project network

| Specification | Number of links | Degree centrality | Betweeness centrality | Eigenvector centrality | PageRank |
|---|---|---|---|---|---|
| General construction supervision | 7 | 89.26 | 0 | 0.264 | 0.061 |
| Project manager | 16 | 180.47 | 0.392 | 0.42 | 0.119 |
| Construction site manager | 11 | 124.65 | 0.025 | 0.303 | 0.085 |
| Construction works manager | 9 | 99.39 | 0 | 0.257 | 0.069 |
| Construction engineer | 5 | 54.98 | 0 | 0.17 | 0.041 |
| Architect | 12 | 131.05 | 0.142 | 0.301 | 0.091 |
| Chief engineer | 7 | 87.73 | 0.008 | 0.271 | 0.06 |
| Design office | 9 | 106.15 | 0.083 | 0.308 | 0.071 |
| Chief mechanical engineer | 6 | 68.82 | 0 | 0.193 | 0.05 |
| Surveyor department | 3 | 36.54 | 0 | 0.122 | 0.03 |
| Safety engineer | 5 | 44.20 | 0 | 0.134 | 0.035 |
| Delivery manager | 5 | 67.95 | 0 | 0.204 | 0.049 |
| Estimate department | 3 | 28.61 | 0.025 | 0.091 | 0.026 |
| Construction engineer | 5 | 64.24 | 0.025 | 0.177 | 0.048 |
| Electrical installation design office | 6 | 82.21 | 0.008 | 0.236 | 0.057 |
| Plumbing installation design office | 5 | 70.91 | 0 | 0.211 | 0.05 |
| Gas installation design office | 6 | 84.52 | 0 | 0.238 | 0.059 |

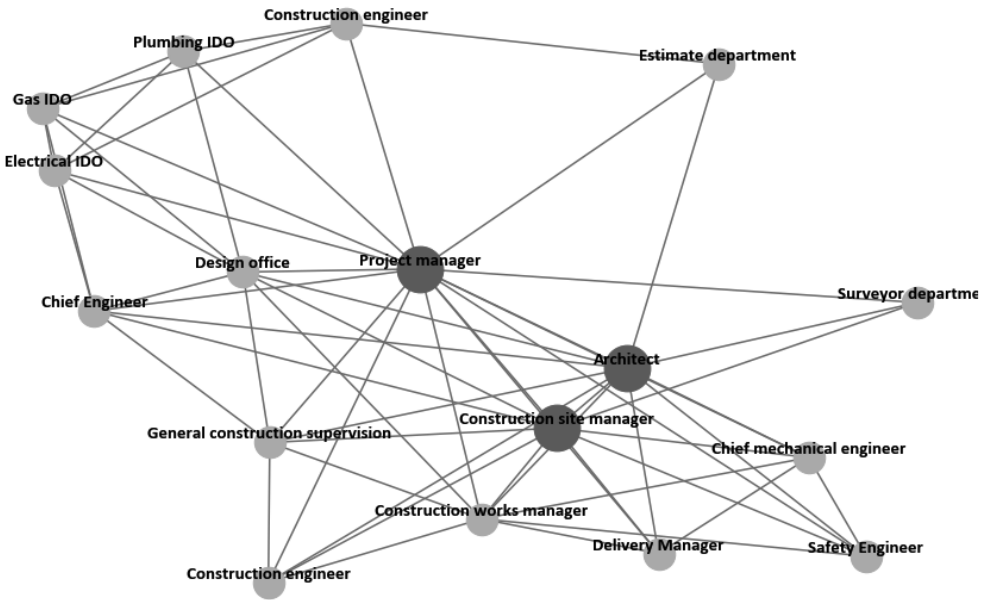


FIGURE 1. Degree centrality of nodes

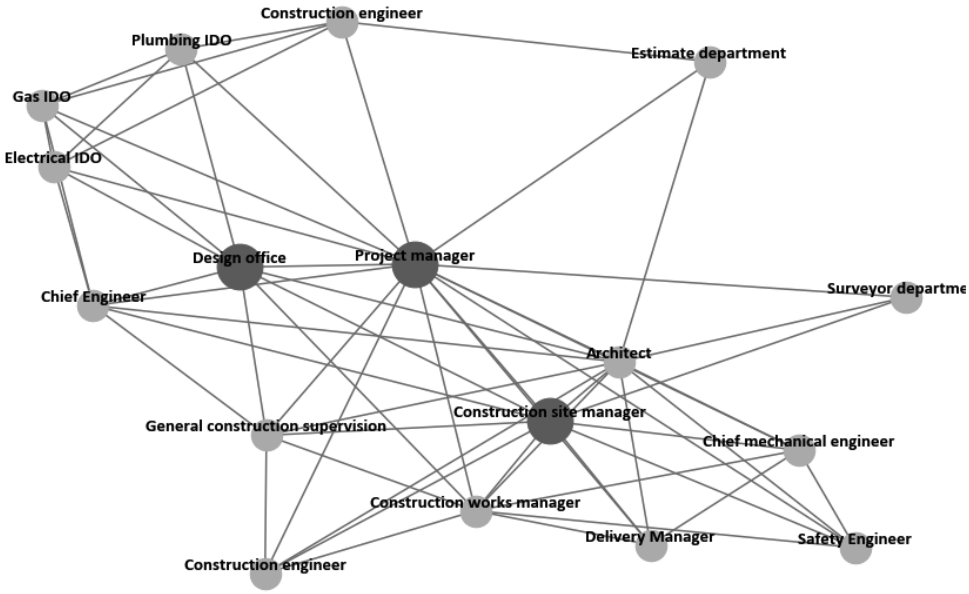


FIGURE 2. Eigenvector centrality and measure PageRank of nodes

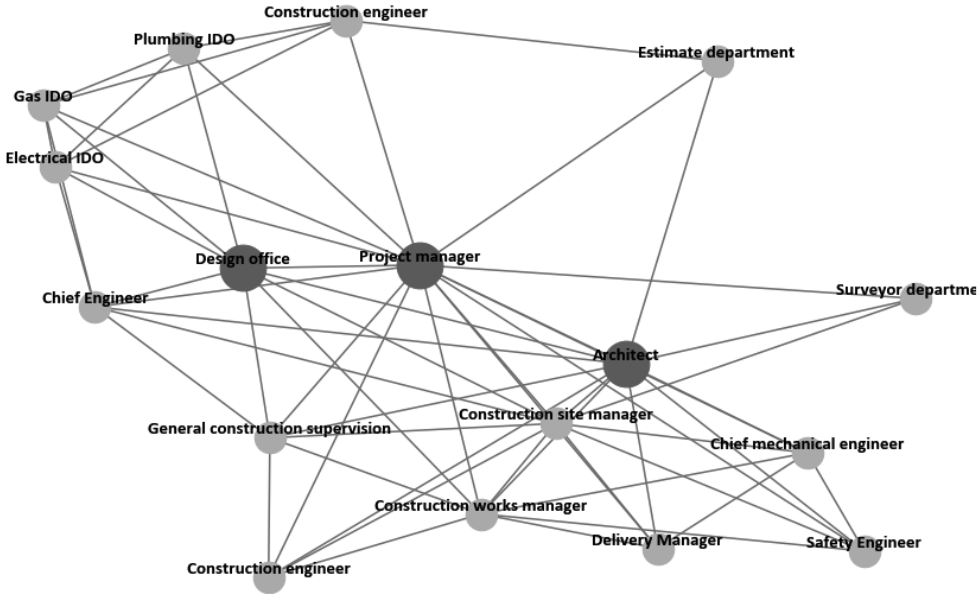


FIGURE 3. Betweeness centrality of nodes

neighbours, but with a high level of influence in network.

The analysis betweeness centrality indicated the highest values of the measure were among the participants "Project manager", "Architect" and "Design office", which indicates them as the main brokers for knowledge and information sharing in this network (Fig. 3).

## Conclusions

Project managers often want to understand how the interaction in the project occurs, how strong are the connections between team members, who is the key person, which information is transmitted efficiently and which is not. Use of SNA and calculation of centrality measures of network participants can help in solving these problems. Having analysed the centrality measures that were calculated for construction project network, we can conclude:

- high ratings of participants "Project manager", "Design office", "Architect" and "Construction site manager" can be assessed as normal for this project stage, since during the study of network there was a transition from design stage to start of construction works;
- the highest rating among all network participants for the calculated centrality measures had "Project manager". This is a positive fact since its main task is to coordinate and integrate project participants;
- the high impact of participant "Design office" in terms of eigenvector centrality and betweeness centrality indicates his importance for network communication, as he acts as broker and itself has connections with important project participants.

Further research will focus on continuing to analyse the project's communications network in the next stages of its delivery.

## References


Abbsaian-Hosseini, A., Liu, S.M. & Hsiang, S.M. (2017). Social network analysis for construction crews. *International Journal of Construction Management*, *19*(2), 1-15.

Baiden, B.K., Price, A.D.F. & Dainty, A.R.J. (2006). The extent of team integration within construction projects. *International Journal of Project Management*, *24*(1), 13-23.

Bonacich, O.F. (1987). Power and centrality: a family of measures. *American Journal of Sociology*, *92*(5), 1170-1182.

Bornholdt, S. & Schuster, H. (eds.). (2003). *Handbook of graphs and networks: From the genome to the Internet*. Weinheim: Wiley-VCH Verlag.

Briscoe, G. & Dainty, A.R.J. (2005). Construction supply chain integration: an elusive goal? *Supply Chain Management: An International Journal*, *10*(4), 319-326.

Chinowsky, P. & Songer, A. (2011). *Organizational management in construction*. New York: Spon Press.

Freeman, L.C. (1977). A set of measures of centrality based on betweenness. *Sociometry*, *40*, 35-41.

Freeman, L.C. (1978). Centrality in social networks conceptual clarification. *Social Networks*, *1*(3), 215-239.

Loosemore, M. (1998). Social network analysis: using a quantitative tool within an interpretative context to explore the management of construction crises. *Engineering, Construction and Architectural Management*, *5*(4), 315-326.

Madani, F., Daim, T. & Weng, C. (2017). Smart building technology network analysis: applying core–periphery structure analysis. *International Journal of Management Science and Engineering Management*, *12*(1), 1-11.

Mahmud, S. (2009). Framework for the role of self-organization in the handling of adaptive challenges. *Emergence: Complexity and Organization*, *11*(2), 1-14.

Marsden, P. & Lin, Y.N. (1982). *Social structure and network analysis.* Beverly Hills: Sage Publishing.

Nicolini, D., Holti, R. & Smalley, M. (2001). Integrating project activities: the theory and practice of managing the supply chain through clusters. *Construction Management and Economics*, *19*(1), 37-47.

Ochieng, E.G. & Price, A.D.F. (2009). Framework for managing multicultural project teams. *Engineering, Construction and Architectural Management*, *16*(6), 527-543.

Page, L., Brin, S., Motwani, R. & Winograd, T. (1999). *The PageRank citation ranking: Bringing order to the web. Technical report 1999-66.* Stanford: Stanford InfoLab, Stanford University.

Project Management Institute [PMI] (2000). *A Guide to the Project Management Body of Knowledge (PMBOK Guide). Edition 2000.* Newtown Square, PA: Project Management Institute.

Pryke, S. (2005). Towards a social network theory of project governance. *Construction Management Economics*, *23*(9), 927-939.

Pryke, S. (2012). *Social network analysis in construction*. Oxford: Wiley and Sons.

Pryke, S., Badi, S., Almadhoob, H., Soundararaj, B. & Addyman, S. (2018). Self-organizing networks in complex infrastructure projects. *Project Management Journal*, *49*(2), 18-41.

Radziszewska-Zielina, E., Śladowski, G., Kania, E., Sroka, B. & Szewczyk, B. (2019). Managing information flow in self-organising networks of communication between construction project participants. *Archives of Civil Engineering*, *65*(2), 133-148.

Śladowski, G., Radziszewska-Zielina, E. & Kania, E. (2019). Analysis of self-organising networks of communication between the participants of a housing complex construction project. *Archives of Civil Engineering*, *65*(1), 181-195.

Trach, R. & Lendo-Siwicka, M. (2018). Zastosowanie sieciowej struktury organizacyjnej w zintegrowanej realizacji przedsięwzięcia budowlanego [Network organizational structure ap-plication in integrated project delivery]. *Scientific Review – Engineering and Environmental Sciences*, *27*(1), 82-90.

Trach, R., Pawluk, K. & Lendo-Siwicka, M. (2020). The assessment of the effect of BIM and IPD on construction projects in Ukraine. *International Journal of Construction Management*, 1-8.

## Summary

**Analysis of communication network of the construction project participants.** The construction industry is characterized by limited resources and a high level of competition. Limited resources and a competitive environment determine knowledge and information as a particularly important resource for the development of the construction industry. A communication network is one of the elements of a knowledge management system in projects and serves to organize and maintain information links between project participants. We have analysed the communication network between project participants for residential building construction using social network analysis (SNA). The purpose of this work is the calculation and analysis centrality measures for participants in the construction project delivery. Centrality measures can answer the following questions whether the node is influential or central to the network and whether the node is critical for the flow of information in the network.

**Authors' address:**
Roman Trach
(https://orcid.org/0000-0001-6654-9870)
Szkoła Główna Gospodarstwa Wiejskiego
w Warszawie
Instytut Inżynierii Lądowej
ul. Nowoursynowska 159, 02-776 Warszawa
Poland
e-mail: roman_trach@sggw.edu.pl

Sergey Bushuyev
(https://orcid.org/0000-0002-7815-8129)

## Informacje dla autorów

Na łamach *Przeglądu Naukowego – Inżynieria i Kształtowanie Środowiska* zamieszczane są **oryginalne prace naukowe w języku polskim lub angielskim, niepublikowane** w innych czasopismach. Prawa autorskie tekstów przyjętych do druku udzielone są Wydawnictwu SGGW, a artykuły są udostępniane na warunkach Open Access na zasadach licencji Creative Commons CC BY-NC (patrz oświadczenie autorów na stronie http://iks.pn.sggw.pl).

**Wymagania techniczne dotyczące przygotowania prac:**

1. Tekst i tabele należy złożyć w formie elektronicznej, w plikach o formacie MS Office, a rysunki – wstawione do tekstu i w oddzielnych plikach graficznych, w programach pracujących w środowisku Windows (Excel, Photoshop itp.) w wersji czarno-białej. Rysunki i zdjęcia w wersji papierowej są drukowane w skali szarości, a na stronie internetowej czasopisma wygenerowane w wersji kolorowej.
2. Objętość artykułu wraz z ilustracjami nie może przekraczać 10 stron formatu A-4, interlinia – 1,5 wiersza, marginesy – 2,5 cm, czcionka TNR 12 pkt., tekst w układzie jednokolumnowym.

**Układ pracy** (zgodnie z szablonem: http://iks.pn.sggw.pl/do_autorow.html):

1. Imię i nazwisko autora(-ów) – u góry z lewej strony.
2. Pod nazwiskiem – miejsce pracy w polskim i angielskim języku.
3. Tytuł pracy – w polskim i angielskim języku.
4. Słowa kluczowe (*Key words*) – w polskim i angielskim języku.
5. Tekst pracy (w języku polskim lub angielskim) powinien obejmować: **wprowadzenie, materiał i metody, wyniki, podsumowanie i dyskusję, wnioski, literaturę, streszczenie w języku angielskim (Summary), streszczenie w języku polskim, adres autora(-ów).**
6. Tytuły tabel i rysunków, opisy główki pionowej i poziomej tabel oraz wszystkie napisy na ilustracjach muszą być w polskim i angielskim języku w wersji czarno-białej.
7. W tekstach w języku polskim do oznaczania pozycji dziesiętnej liczb należy używać przecinka, a w języku angielskim – kropki.
8. Przy powoływaniu się w artykułach angielskojęzycznych na publikacje w *Przeglądzie Naukowym* autorzy proszeni są o używanie jego angielskiej nazwy.
9. Wykaz piśmiennictwa i powołania należy sporządzić według międzynarodowego formatu APA i zestawić w porządku alfabetycznym. Bliższe informacje, przykłady formatowania i program do tworzenia opisów bibliograficznych w wymaganym formacie znajdują się na stronie *Przeglądu Naukowego* (http://iks.pn.sggw.pl/do_autorow.html), np.:
   Kowalski, J. i Nowak, P. (2009). *Analiza regresji stosowana.* Warszawa: Wydawnictwo Naukowe PWN.
   Kowalski, J., Nowak, P. i Bartnik, Z. (2009). Suspended sediment sources in two small lowland agricultural catchments in the UK. *Journal of Hydrology*, *252*(1-4), 1–24. doi:10.1016/s0022-1694(01)00388-2
   *Procedura recenzowania.* (2014). Pobrano z lokalizacji Przegląd Naukowy Inżynieria i Kształtowanie Środowiska: http://iks.pn.sggw.pl/recenzje.html.
10. Przy pierwszym powoływaniu się w tekście na innych autorów podaje się np.: „zdaniem Kowalskiego (2002)" lub „(Kowalski, 2002)". Przy większej liczbie autorów „(Kowalski, Malinowski i Witkowski, 2002)".
11. Streszczenia powinny zawierać ok. 500 znaków.
12. Author's address:
    Jan Kowalski
    Nazwa miejsca pracy w języku polskim (uczelnia, wydział, katedra)
    ulica, kod pocztowy miejscowość, Poland
    e-mail
13. Oświadczenie o oryginalności pracy (http://iks.pn.sggw.pl/oswiadczenie.doc).